



UNIVERSITAT DE  
BARCELONA

## Study of extracellular matrix remodeling and the role of periostin b during zebrafish heart regeneration

Anna Garcia Puig

**ADVERTIMENT.** La consulta d'aquesta tesi queda condicionada a l'acceptació de les següents condicions d'ús: La difusió d'aquesta tesi per mitjà del servei TDX ([www.tdx.cat](http://www.tdx.cat)) i a través del Dipòsit Digital de la UB ([diposit.ub.edu](http://diposit.ub.edu)) ha estat autoritzada pels titulars dels drets de propietat intel·lectual únicament per a usos privats emmarcats en activitats d'investigació i docència. No s'autoritza la seva reproducció amb finalitats de lucre ni la seva difusió i posada a disposició des d'un lloc aliè al servei TDX ni al Dipòsit Digital de la UB. No s'autoritza la presentació del seu contingut en una finestra o marc aliè a TDX o al Dipòsit Digital de la UB (framing). Aquesta reserva de drets afecta tant al resum de presentació de la tesi com als seus continguts. En la utilització o cita de parts de la tesi és obligat indicar el nom de la persona autora.

**ADVERTENCIA.** La consulta de esta tesis queda condicionada a la aceptación de las siguientes condiciones de uso: La difusión de esta tesis por medio del servicio TDR ([www.tdx.cat](http://www.tdx.cat)) y a través del Repositorio Digital de la UB ([diposit.ub.edu](http://diposit.ub.edu)) ha sido autorizada por los titulares de los derechos de propiedad intelectual únicamente para usos privados enmarcados en actividades de investigación y docencia. No se autoriza su reproducción con finalidades de lucro ni su difusión y puesta a disposición desde un sitio ajeno al servicio TDR o al Repositorio Digital de la UB. No se autoriza la presentación de su contenido en una ventana o marco ajeno a TDR o al Repositorio Digital de la UB (framing). Esta reserva de derechos afecta tanto al resumen de presentación de la tesis como a sus contenidos. En la utilización o cita de partes de la tesis es obligado indicar el nombre de la persona autora.

**WARNING.** On having consulted this thesis you're accepting the following use conditions: Spreading this thesis by the TDX ([www.tdx.cat](http://www.tdx.cat)) service and by the UB Digital Repository ([diposit.ub.edu](http://diposit.ub.edu)) has been authorized by the titular of the intellectual property rights only for private uses placed in investigation and teaching activities. Reproduction with lucrative aims is not authorized nor its spreading and availability from a site foreign to the TDX service or to the UB Digital Repository. Introducing its content in a window or frame foreign to the TDX service or to the UB Digital Repository is not authorized (framing). Those rights affect to the presentation summary of the thesis as well as to its contents. In the using or citation of parts of the thesis it's obliged to indicate the name of the author.

# Study of extracellular matrix remodeling and the role of periostin B during zebrafish heart regeneration

TESI DOCTORAL

Anna Garcia Puig





UNIVERSITAT DE  
BARCELONA

FACULTAT DE FARMÀCIA I CIÈNCIES DE L'ALIMENTACIÓ

PROGRAMA DE DOCTORAT EN BIOMEDICINA

2019

TESI DOCTORAL

**Study of extracellular matrix remodeling and the role of  
periostin b during zebrafish heart regeneration**

Memòria presentada per  
**Anna Garcia Puig**

per optar al títol de  
**Doctora**

per la Universitat de Barcelona

Tesi doctoral realitzada sota la direcció del Dr. Ángel Raya Chamorro al Centre de  
Medicina Regenerativa de Barcelona (CMRB).

Signat,

El director:

Dr. Ángel Raya Chamorro

El Tutor:

Dr. José Antonio del  
Río Fernández

La Doctoranda:

Anna Garcia Puig



# CONTENTS

<b>ABSTRACT.....</b>	<b>vii</b>
<b>List of figures.....</b>	<b>ix</b>
<b>List of tables... ..</b>	<b>xi</b>
<b>List of abbreviations .....</b>	<b>xiii</b>
<b>1. INTRODUCTION.....</b>	<b>1</b>
1.1. Regeneration overview .....	3
1.1.1. Types of regeneration .....	6
1.2. Regeneration in vertebrates and mammals .....	9
1.3. Heart regeneration .....	10
1.3.1. Heart regeneration in urodeles.....	12
1.3.2. Heart regeneration in mice .....	14
1.3.3. Limitations of heart regeneration in humans .....	16
1.4. Heart regeneration in zebrafish .....	18
1.4.1. Zebrafish as a model organism .....	18
1.4.1.1. Molecular tools in zebrafish .....	20
1.4.1.2. CRISPR/Cas9 .....	22
1.4.2. Zebrafish heart .....	23
1.4.3. Zebrafish heart regeneration and injury models .....	25
1.4.3.1. Amputation .....	25
1.4.3.2. Cryoinjury.....	26

## CONTENTS

1.4.3.3. Genetic ablation.....	27
1.4.3.4. Hypoxia/reoxygenation .....	28
1.4.4. Cellular and molecular mechanisms of zebrafish heart regeneration	30
1.4.4.1. Myocardial contribution .....	30
1.4.4.2. Epicardial contribution .....	32
1.4.4.3. Endocardial contribution .....	33
1.4.4.4. Immune cell contribution .....	34
1.5. Extracellular matrix in zebrafish heart regeneration.....	35
1.5.1. Periostin .....	37
1.5.1.1. Periostin in myocardial infarction.....	39
1.5.1.2. Homology between species.....	40
<b>2. OBJECTIVES.....</b>	<b>43</b>
<b>3. MATERIALS AND METHODS.....</b>	<b>47</b>
3.1. Zebrafish breeding and husbandry .....	49
3.2. Ventricular amputation surgery.....	49
3.3. EdU labelling .....	50
3.4. Cardiac tissue collection .....	51
3.5. Sample processing .....	52
3.6. Immunohistochemistry.....	52
3.6.1. EdU signal development .....	54
3.6.2. TUNEL staining .....	54
3.7. Hematoxinilin and Eosin staining.....	56
3.8. Masson’s Trichrome staining .....	56
3.9. Probe synthesis for in situ hybridization .....	57

## CONTENTS

3.10. <i>In situ</i> hybridization in cryosections .....	58
3.11. Genomic DNA extraction from embryos or finclips.....	60
3.12. RNA extraction .....	60
3.13. cDNA synthesis.....	61
3.14. qRT-PCR primer design and efficiency test.....	61
3.15. qRT-PCR.....	61
3.15.1. qPCR data processing.....	62
3.16. Generation of a <i>postnb</i> conditional KD zebrafish transgenic line with Tol2 system .....	62
3.16.1. Generation of the construct.....	62
3.16.2. $\mu$ Needles and injection plates for zebrafish embryo injection .....	65
3.16.3. <i>In vitro</i> transcription of Cre-nls mRNA .....	65
3.16.4. Embryonic injection of Tol2-construct and transposase mRNA .....	66
3.16.5. Founder, F1 and F2 screening .....	66
3.17. Embryonic tamoxifen treatment .....	67
3.18. Embryonic CRE-nls injection .....	67
3.19. Adult tamoxifen treatment.....	67
3.20. CRISPR-Cas9 <i>postnb</i> biallelic KO zebrafish transgenic line .....	68
3.20.1. sgRNA design and synthesis .....	68
3.20.2. Cas9 and sgRNA injection.....	69
3.20.3. Fluorescence PCR .....	70
3.20.4. Founder, F1 and F2 screening .....	70
3.20.5. KO stable line generation .....	71
3.21. <i>In situ</i> zymography .....	72
3.22. Ventricle decellularization .....	72
3.23. ECM processing and staining .....	73

## CONTENTS

3.24. Genomic DNA extraction from zebrafish ventricles .....	73
3.25. Protein extraction and quantification.....	74
3.25.1. Deyolking embryos in batches .....	74
3.26. Western Blot .....	75
3.27. Liquid chromatography-Mass spectrometric analyses.....	76
3.27.1. Proteomic data Availability .....	79
3.28. Criteria for protein identification.....	79
3.29. Label-free Protein Quantification .....	80
3.30. Analysis and validation of proteomic data on regeneration .....	81
3.31. Atomic force microscopy (AFM) for the measurement of the extracellular matrix stiffness.....	82
3.32. Statistical analysis .....	83
<b>4. RESULTS.....</b>	<b>85</b>
CHAPTER 1: Study of the ECM protein dynamic changes in zebrafish heart regeneration.....	87
4.1.1. Development and characterization of a decellularization protocol for zebrafish ventricles .....	87
4.1.2. Profile of ECM proteins in adult zebrafish hearts.....	89
4.1.3. Changes in ECM protein composition during zebrafish heart regeneration.....	90
4.1.4. Changes in ECM biomechanical properties during zebrafish heart regeneration.....	93
CHAPTER 2: Role of <i>postnb</i> during zebrafish heart regeneration.....	99
4.1.5. Characterization of <i>postnb</i> in zebrafish cardiac injury .....	99



## CONTENTS

4.1.6. Generation of a conditional shRNA expressing knock-down zebrafish line for <i>postnb</i> to study cardiac regeneration .....	102
4.1.7. Generation of a knock-out <i>postnb</i> line using CRISPR-Cas9 technology to study cardiac regeneration .....	110
4.1.8. Macrophage recruitment, matrix metalloproteinase activity and revascularization are not affected in <i>postnb</i> <sup>-/-</sup> regenerating zebrafish .....	113
4.1.9. <i>postnb</i> <sup>-/-</sup> had decreased collagen cross-linking and a softer ECM... ..	115
<b>5. DISCUSSION .....</b>	<b>119</b>
<b>6. CONCLUSIONS.....</b>	<b>129</b>
<b>References.....</b>	<b>133</b>
<b>Appendix I. qRT-PCR primers .....</b>	<b>153</b>
<b>Appendix II. Supplementary material from chapter 1 .....</b>	<b>155</b>
<b>Appendix III. Supplementary material from chapter 2 .....</b>	<b>159</b>
<b>Appendix IV. Publications .....</b>	<b>163</b>
<b>Agraiments.....</b>	<b>165</b>



# ABSTRACT

Adult zebrafish (*Danio rerio*), in contrast to mammals, are able to regenerate their hearts in response to injury or experimental amputation. Our understanding of the cellular and molecular bases that underlie this process, although fragmentary, has increased significantly over the last years. However, the role of the extracellular matrix (ECM) during zebrafish heart regeneration has been comparatively rarely explored. A better understanding of all the mechanisms underlying this complex process would help developing strategies to regenerate the human heart. With this aim, here, we set out to characterize the ECM protein composition in adult zebrafish hearts, whether it changed during the regenerative response, and the role of the matricellular protein periostin b.

For this purpose, in the first part of the current thesis, we established a decellularization protocol of adult zebrafish ventricles that significantly enriched the yield of ECM proteins. We then performed proteomic analyses of decellularized control hearts and at different times of regeneration. Our results show a dynamic change in ECM protein composition, most evident at the earliest (7 days post-amputation) time-point analyzed. Regeneration associated with sharp increases in specific ECM proteins, and with an overall decrease in collagens and cytoskeletal proteins. We finally tested by atomic force microscopy that the changes in ECM composition translated to decreased ECM stiffness. Our cumulative results identify changes in the protein composition and mechanical properties of the zebrafish heart ECM during regeneration.

In the second part of the current thesis, we have examined the role of periostin b (*postnb*) during zebrafish heart regeneration. We found that *postnb* was abundant in the injury of amputated zebrafish ventricles, and we designed two strategies to suppress

## ABSTRACT

*postnb* during regeneration: 1) a shRNA transgenic knock-down, and 2) a CRISPR/Cas9 *postnb*<sup>-/-</sup> zebrafish. Knock-down and knock-out fishes did not exhibit any evident developmental defects, but showed a lack complete cardiac regeneration after amputation. The absence of *postnb* did not have any effect on leukocyte recruitment, matrix metalloproteinase activation or revascularization after amputation. However, *postnb*<sup>-/-</sup> zebrafish developed a softer cardiac ECM due to a reduction of collagen cross-linking, and showed an increase of cardiomyocyte proliferation and a decrease on cardiomyocyte cell death after amputation. The stiffness control by *postnb* seem to be important to correctly modulate stiffness for a complete cardiac regeneration. Stiffness analysis together with proliferation analysis suggest that *postnb* is needed to increase the stiffness in the injury border to instruct cardiomyocytes to stop proliferating and migrate to the injury site.

# LIST OF FIGURES

Figure I 1   Regeneration at different levels of biological organization. ....	3
Figure I 2   Phylogenetic distribution of regeneration across the Metazoa and the Chordata. ....	5
Figure I 3   Types of regeneration. ....	8
Figure I 4   Heart regenerative capacity in warm- or cold-blooded animals. ....	11
Figure I 5   Different approaches used to study cardiac regeneration in vertebrates. ...	13
Figure I 6   Causes and consequences of myocardial infarction in humans. ....	18
Figure I 7   Zebrafish adults and larvae. ....	19
Figure I 8   Guided designed endonucleases used in zebrafish. ....	22
Figure I 9   Anatomy and morphology of the zebrafish heart. ....	24
Figure I 10   The zebrafish heart and injury models. ....	27
Figure I 11   Summary of events during zebrafish heart regeneration. ....	32
Figure I 12   Periostin interacts with multiple extracellular proteins. ....	38
Figure I 13   Periostin and associated diseases. ....	40
Figure I 14   Periostin A expression during development. ....	41
Figure I 15   Periostin B expression during development. ....	42
Figure MM 1   Workflow to generate the shRNA <sup>postnb</sup> knock-down line. ....	68
Figure MM 2   Workflow to generate the CRISPR/Cas9 knock-out transgenic line. ....	71
Figure R 1   Decellularization protocol for zebrafish hearts. ....	88
Figure R 2   Preservation and enrichment of ECM proteins after decellularization. ....	89
Figure R 3   Decellularization increases ECM protein detection. ....	91

## List of figures

Figure R 4   Changes in ECM protein composition during heart regeneration. ....	92
Figure R 5   mRNA expression changes of ECM proteins significantly changed during zebrafish heart regeneration.....	93
Figure R 6   Stiffness of the extracellular matrix of regenerating hearts. ....	94
Figure R 7   Periostin is dynamically expressed during cardiac regeneration. ....	99
Figure R 8   Periostin is expressed in the injury site. ....	100
Figure R 9   Periostin colocalization with vimentin. ....	102
Figure R 10   Constructs of the conditional shRNA expressing knock-down transgenic zebrafish line for <i>postnb</i> . ....	103
Figure R 11   Localization of the designed shRNAs. ....	104
Figure R 12   shRNA construct injection and founders. ....	105
Figure R 13   Functionality assessment of the best shRNA lines. ....	106
Figure R 14   Embryonic <i>postnb</i> protein expression in the shRNA line and after recombination. ....	107
Figure R 15   Adult <i>postnb</i> reduction by shRNA at 7dpa. ....	108
Figure R 16   Cardiac regeneration difficulty by <i>postnb</i> knock-down. ....	109
Figure R 17   <i>postnb</i> <sup>-/-</sup> line by CRISPR/Cas9. ....	111
Figure R 18   Cardiac regeneration is impaired in <i>postnb</i> <sup>-/-</sup> zebrafish. ....	112
Figure R 19   <i>postnb</i> does not have any effect on macrophage recruitment, MMPs activation or revascularization of coronary vasculature. ....	114
Figure R 20   Collagen cross-linking and ECM stiffness are reduced in <i>postnb</i> <sup>-/-</sup> zebrafish while cardiomyocyte proliferation increases. ....	116
Supplementary Figure 1   Biological Process GO enrichment analysis on the differentially-expressed proteins during cardiac regeneration. ....	157
Supplementary Figure 2   Map of the construct bactin2:loxP-RFP-STOP-loxP-bactin2-miR30-shRNA-GFP. ....	159
Supplementary Figure 3   Adult tamoxifen treatments of the shRNA lines. ....	160
Supplementary Figure 4   Adult tamoxifen treatment of dTg (( <i>eab2</i> :loxP-GFP-loxP-RFP)( <i>bactin2</i> :Cre-Ert2)). ....	161

## LIST OF TABLES

Table I 1   Comparison between different injury models for studying zebrafish heart regeneration.....	29
Table MM 1   List of primary antibodies.....	53
Table MM 2   List of secondary antibodies.....	53
Table MM 3   Primers to amplify a <i>postna</i> and <i>postnb</i> region to generate the RNA probes .....	58
Table MM 4   <i>postnb</i> sequences targeted .....	62
Table MM 5   Primers used to generate the <i>postnb</i> KD conditional line .....	64
Table MM 6   Primers for sgRNA <i>in vitro</i> synthesis .....	69
Table MM 7   Primers to amplify a <i>postnb</i> genomic region for fluorescence PCR and T7 assay .....	70
Table R 1   Proteome of decellularized zebrafish ventricles. ....	95
Supplementary Table 1   qRT-PCR primer sequences. ....	153
Supplementary Table 2   Proteins identified during the decellularization process. ....	155
Supplementary Table 3   Peptides identified in the decellularized samples. ....	155
Supplementary Table 4   List of proteins represented with an overall of >5 spectral counts. ....	155
Supplementary Table 5   List of proteins represented with an overall of >5 spectral counts, normalized by VSN method. ....	155
Supplementary Table 6   List of proteins differentially expressed during heart regeneration.....	156
Supplementary Table 7   List of the peptide identification in LC-MS/MS analysis. ....	156
Supplementary Table 8   List of protein identifications. ....	156





# LIST OF ABBREVIATIONS

<b><sup>14</sup>C</b>	Carbon-14 isotope
<b>4OH-Tamoxifen</b>	4-Hydroxy-Tamoxifen
<b>AFM</b>	Atomic Force Microscopy
<b>At</b>	Atrium
<b>BA</b>	Bulbus arteriosus
<b>BMP</b>	Bone morphogenetic protein
<b>bp</b>	Base pair
<b>BrdU</b>	5-bromo-2'-deoxyuridine
<b>Cas9</b>	CRISPR associated protein-9
<b>cDNA</b>	Complementary DNA
<b>CM</b>	Cardiomyocytes
<b><i>col</i></b>	Collagen
<b><i>col1a2</i></b>	Collagen type 1, alpha 2
<b><i>col4a2</i></b>	Collagen type 4, alpha 2
<b><i>col5a1</i></b>	Collagen type 5, alpha 1
<b><i>col5a2a</i></b>	Collagen type 5, alpha 2a
<b>Cre</b>	Cyclic recombinase
<b>Cre-ER</b>	Cre recombinase fused to a mutated estrogen receptor domain
<b>Cre-nls</b>	CRE recombinase fused a nuclear transporting signal
<b>CRISPR</b>	Clustered Regularly Interspaced Short Palindromic Repeats
<b>crRNA</b>	CRISPR RNA
<b>Ct</b>	Cycle threshold value

## List of abbreviations

<b>CTD</b>	carboxyl-terminal domain
<b>cxcr4a</b>	Chemokine (C-X-C motif) receptor 4a
<b>DAPI</b>	4',6-diamidino-2-phenylindole
<b>dH<sub>2</sub>O</b>	Distilled water
<b>DNA</b>	Deoxyribonucleic acid
<b>Dnmt3ab</b>	DNA (cytosine-5-)-methyltransferase 3 alpha b
<b>dpa</b>	Days post-amputation
<b>dpf</b>	Days post-fertilization
<b>dpi</b>	Days post-injury
<b>DSB</b>	Double strand break
<b>DsRed</b>	Discosoma red fluorescent protein
<b>DTA</b>	Diphtheria toxin chain A
<b>EC</b>	Endocardium
<b>ECM</b>	Extracellular matrix
<b>EdU</b>	5-ethynyl-2'-deoxyuridine
<b>EGFP</b>	Enhanced green fluorescent protein
<b>EMI</b>	Emilin
<b>ENU</b>	N-ethyl-N-nitrosourea
<b>EP</b>	Epicardium
<b>EPDC</b>	Epicardial derived cell
<b>EPDC</b>	Epicardial derived cells
<b>ER</b>	Endoplasmic reticulum
<b>F0</b>	Filial generation 0, also known as founder.
<b>F1</b>	Filial generation 1. Subsequent generations are called F2, F3, etc.
<b>FAS1</b>	fascilin-like-1
<b>fbn2b</b>	Fibrillin 2b
<b>FDR</b>	False Discovery Rate
<b>fn</b>	Fibronectin
<b>fn1b</b>	Fibronectin 1b
<b><i>foxp3a</i></b>	Forkhead box P3a
<b><i>gata4</i></b>	Transcription factor gata4

<b>GFP</b>	Green fluorescent protein
<b>GO</b>	Gene Ontology
<b>h</b>	Hour / hours
<b>HA</b>	Hyaluronic acid
<b><i>hand2</i></b>	Heart and neural crest derivatives expressed 2
<b>HDR</b>	Homology directed repair
<b>hpa</b>	Hours post-amputation
<b>hpf</b>	Hours post-fertilization
<b>HSC</b>	Hematopoietic stem cells
<b>igf</b>	Insulin-like growth factor
<b>IL-13</b>	Interleukin 13
<b>IL-4</b>	Interleukin 4
<b>Indel</b>	Insertion or deletion of base pairs in the DNA
<b>ISH</b>	<i>In situ</i> hybridization
<b>Kb</b>	Kilobase
<b>KD</b>	Knock-Down
<b>kDa</b>	Kilo Dalton
<b>KO</b>	Knock-Out
<b>LAD</b>	Left anterior descending coronary artery
<b>LC-MS/MS</b>	Liquid Chromatography – Tandem Mass Spectrometry
<b>LOX</b>	Lysyl-oxidase
<b>M</b>	Myocardium
<b>MI</b>	Myocardial infarction
<b>min</b>	Minute / minutes
<b><i>mlc2a</i></b>	Myosin light chain a (officially called <i>myl7</i> )
<b>MMP / mmp</b>	Matrix metalloproteinase
<b>MQ-H<sub>2</sub>O</b>	MiliQ water
<b>mRNA</b>	Messenger RNA
<b>Mtz</b>	Metronidazole
<b>MW</b>	Molecular weight
<b><i>myl7</i></b>	Myosin light polypeptide 7

## List of abbreviations

<b>NHEJ</b>	Non-homologous end joining
<b><i>nkx2.5</i></b>	NK2 homeobox 5
<b>Nrg1</b>	Neuregulin 1
<b>NTR</b>	Nitroreductase
<b>°C</b>	Centigrade grades
<b>PAM</b>	Protospaced adjacent motif
<b>PBS</b>	Phosphate buffered saline
<b>PCR</b>	Polymerase Chain Reaction
<b>Pdgf</b>	Platelet-derived growth factor
<b>PFA</b>	Paraformaldehyde
<b>PK</b>	Proteinase K
<b><i>postn</i></b>	Periostin
<b><i>postna</i></b>	Periostin A
<b><i>postnb</i></b>	Periostin B
<b>pre-crRNA</b>	Precursor CRISPR RNA
<b>qRT-PCR</b>	Quantitative real time polymerase chain reaction
<b>RA</b>	Retinoic acid
<b><i>raldh2</i></b>	Retinaldehyde dehydrogenase 2
<b>RFP</b>	Red fluorescent protein
<b>RNA</b>	Ribonucleic acid
<b>RT</b>	Room temperature
<b>SDS</b>	Sodium-dodecyl disulfate
<b>sec</b>	Second / seconds
<b>SEM</b>	Standard Error of the Mean
<b>sgRNA</b>	Single guide RNA
<b>shh</b>	Sonic hedgehog
<b>shRNA</b>	Short-hairpin RNA
<b>ssDNA</b>	Single stranded DNA
<b>TALEN</b>	Transcription activator-like effector nucleases
<b><i>tbx18</i></b>	T-box transcription factor encoding gene 18
<b><i>tbx20</i></b>	T-box transcription factor encoding gene 20

<b><i>tbx5</i></b>	T-box transcription factor encoding gene 5
<b><i>tcf21</i></b>	Transcription factor 21
<b><i>tgfβ</i></b>	Transforming growth factor beta
<b><i>tnc</i></b>	Tenascin C
<b><i>tracrRNA</i></b>	Trans-activating CRISPR RNA
<b><i>T<sub>reg</sub></i></b>	Regulatory T cell
<b>TUNEL</b>	Terminal deoxynucleotidyl transferase dUTP nick end labeling
<b>V</b>	Ventricle
<b><i>vegfaa</i></b>	Vascular endothelial growth factor Aa
<b><i>wpf</i></b>	Weeks post-fertilization
<b>WT</b>	Wildtype
<b>ZFN</b>	Zinc finger nuclease



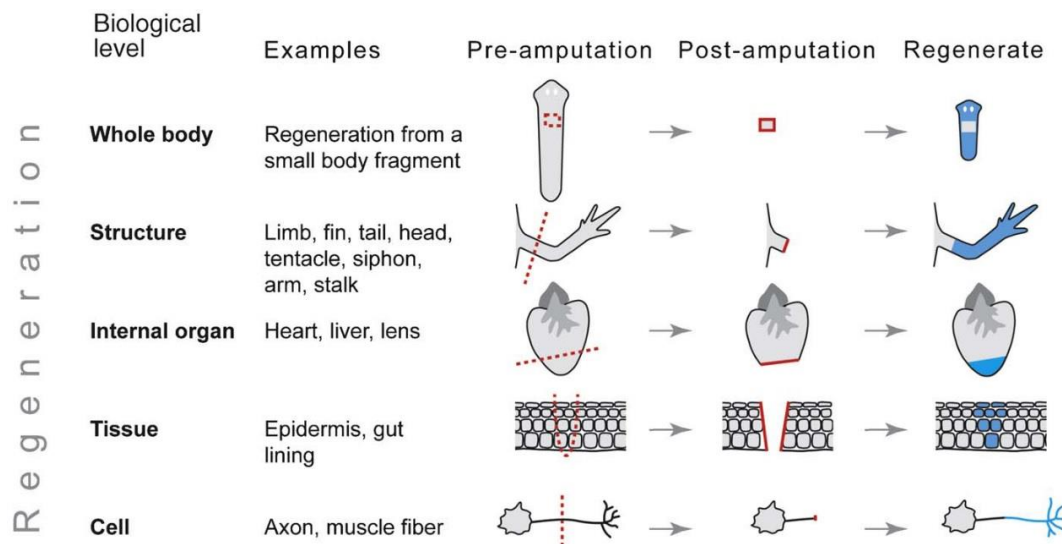
# **1. INTRODUCTION**





### 1.1. REGENERATION OVERVIEW

Regeneration is one of the oldest fields in biology and has always captivated human’s attention (Dinsmor, 1991; Vrontosova et al., 1960). Scientists such as Réamur and Trembley started to study this phenomenon as early as the 18<sup>th</sup> century observing models such as crayfish and hydra, respectively. By the early 19<sup>th</sup> century, regeneration in many kinds of animals was already described but confined to gross observations. Charles Darwin did also regeneration studies on planarian, and, today, regeneration is discussed in terms of evolutionary theory. These scientists provided the first regeneration knowledge. Although we have learned a lot from these first discoveries, there are lots of mechanisms that are yet not fully understood.



**Figure I 1| Regeneration at different levels of biological organization.** A particular species might regenerate at all, none, or just a subset of these levels. Functional links between regenerative processes at successive levels are probable, but it remains unclear which aspects of regeneration are homologous across levels. Dashed red lines indicate amputation planes; solid red lines indicate wound surfaces; and blue fill indicates regenerated body parts. From Bely and Nyberg, 2010.

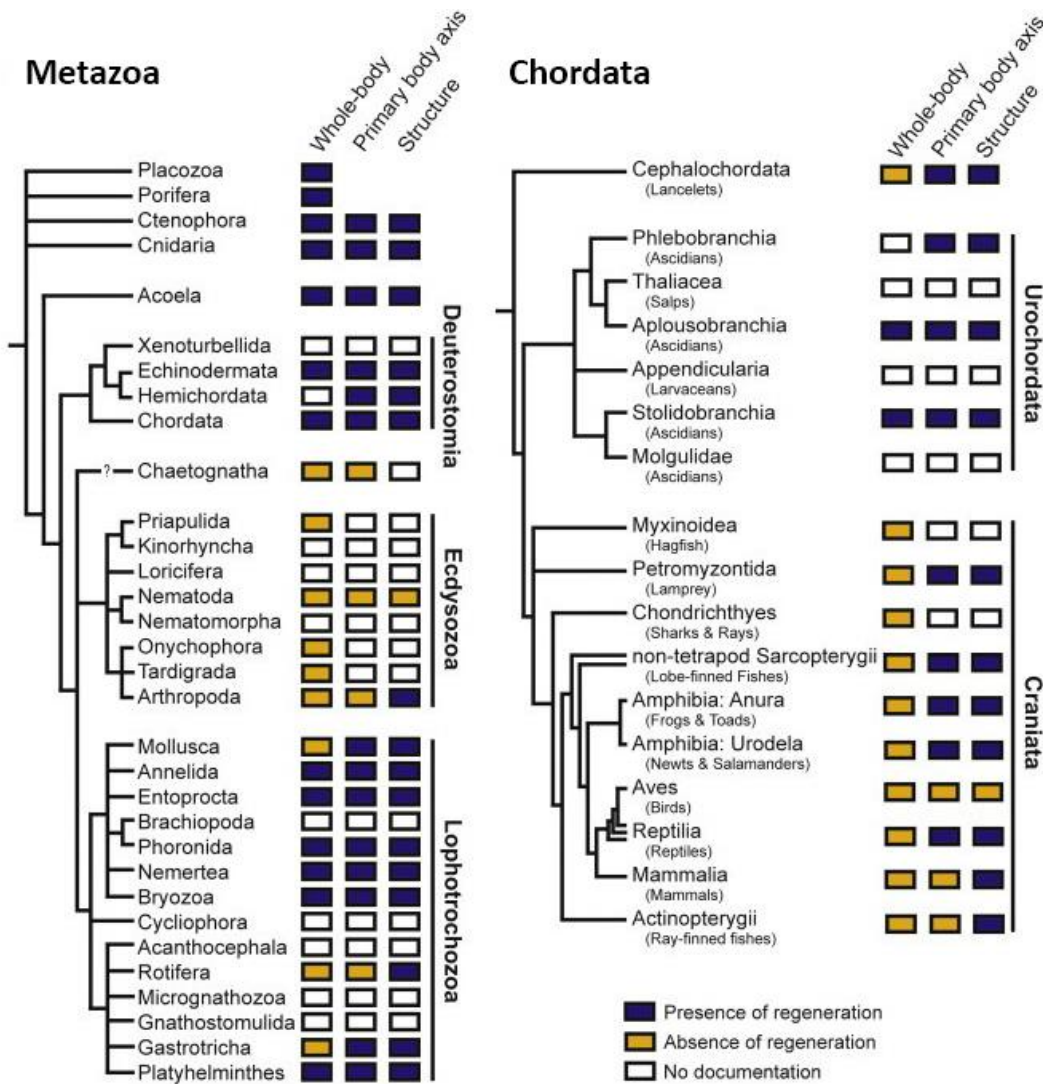
But, what is regeneration? According to Stedman’s Medical Dictionary, *regeneration* is the “reproduction or reconstitution of a lost or injured part” (Bely and Nyberg, 2010; *Stedman’s medical dictionary*, 2005). However, regeneration is a complex term that comprises multiple levels of biological organization (Figure I 1). It can be unleashed by diverse causes taking place through different stages of the life cycle. The

## 1. INTRODUCTION

progression of regeneration may be via different developmental processes and originate structures with a variable similarity to the original. Thus, regeneration is fascinating, comprising many different processes carried out by different mechanisms. First, there has to be recognition of tissue loss or injury, followed by mechanisms that have to reconstruct the damaged structure. Getting to know which and how these mechanisms are initiated, regulated, and ended will have an enormous impact for regenerative medicine in humans. Many research centers around the world have invested many resources in regenerative medicine research units.

The ability to regenerate is widespread in the animal kingdom, with representatives from most animal phyla (Figure 1 2) (Brockes and Gates, 2014; Sánchez Alvarado, 2000). Classical examples include cnidarians such as hydra, annelids, mollusks, nemertean worms, platyhelminthes such as planarians, and chordates including vertebrates such as zebrafish. Whereas some animals, such as many cnidarians and flatworms, can regenerate an entire individual from a small body fragment, others, such as birds, nematodes and leeches, are largely or completely incapable of regenerating any structure (Gross, 1969; Vrontosova et al., 1960). Regenerative capacity can vary considerably even in a given order or among parts of the same organism. Many lizards, for example, can easily replace a tail but not a limb, and many annelid worms can regenerate a tail but not a head (Alibardi and Toni, 2005; Bely, 2006). Furthermore, regenerative capacity is restricted in many mammals. Whether regeneration represents an evolutionary adaptation acquired by regeneration-competent species, or a common ancestral trait lost during evolution is still subject to debate (Bely and Nyberg, 2010; Brockes et al., 2001; Tanaka and Ferretti, 2009).

In the animal kingdom, the regenerative phenomenon involves different number of cell types: from a single cell type (such as salamander lens regeneration) to all the cells within a region (such as planarian regeneration). In case of the salamander, the dorsal iris is restricted and unipotent, and give rise to the missing lens (Tsonis et al., 2004). By contrast, a small piece of planarian tissue (1/200 of its body mass) regenerates



**Figure I 2| Phylogenetic distribution of regeneration across the Metazoa and the Chordata.** ‘Presence of regeneration’ (blue box) indicates that at least one well-substantiated report exists for regeneration in that taxon and does not imply that all species in that taxon can regenerate. ‘Absence of regeneration’ (yellow box) indicates that there is at least one well- substantiated report for the lack of regeneration in that taxon (and none indicating the presence of regeneration). ‘Whole-body regeneration’ is defined as the potential to regenerate every part of the body (although not necessarily simultaneously or from a tiny fragment). The ability to regenerate the primary body axis is scored independently for each taxon and does not assume homology of body axes across or within phyla. Adapted from Bely and Nyberg, 2010.

all the cell types of the entire organism, considering it pluripotent (Figure I 1) (Reddien and Alvarado, 2004). The new cells needed for the regenerative processes can be produced by resident **stem cells** or through different mechanisms such as **dedifferentiation** or **transdifferentiation** (Tanaka and Reddien, 2011). In the dedifferentiation mechanism, cells lose their differentiated state to be able to divide, and in the transdifferentiation mechanism, differentiated cells change into a different

## 1. INTRODUCTION

differentiated cell type (Jopling et al., 2011). In the case of stem cells, asymmetric division clonally produces both, more stem cells of the same type (thus maintaining the stem cell population), and a differentiated progeny (Weissman et al., 2001). These three mechanisms for cell production can act simultaneously in regeneration of complex tissues.

### 1.1.1. Types of regeneration

Since regeneration comprises multiple biological processes, there are described many types of regeneration. Sometimes is difficult to assign the category to a known regenerative process due to the poor understanding of some of them. These categories are summarized in Figure I 3 and will be explained below.

The natural replacement of worn-out body parts is known as **physiological regeneration** (Figure I 3). It is often studied as cellular turnover being just a way to maintain the organism homeostasis. Then, it may not be considered as a true regenerative process (Carlson, 2007). Some examples would be the replacement of blood cells, or the shedding cycles of crustacean exoskeletons and snakeskin. An important characteristic is that many physiological regeneration processes can be regulated upon the organism needs. For example, if an athlete goes to high altitudes, its body will generate more erythrocytes to be able to face the lower oxygen levels. As it can be appreciated by the examples given, the physiological regeneration does not have a global specific regeneration mechanism.

On the contrary, there is the **reparative regeneration** (Figure I 3) that has been typically applied to the post-traumatic regeneration (Carlson, 2007). It is based as the replacement of a lost or damaged body part, and it can occur at single cell or body part level. Some of the most known examples are the regeneration of the amputated limb or tail of a salamander or newt, or the reconstitution of the whole body from a small fragment of its original mass of planarian.

The reparative regeneration can, in turn, be classified in different regeneration mechanisms. The first mechanism would be the replacement of complex structures by dedifferentiation of the adult structure. An undifferentiated mass, called blastema, is formed that finally differentiates and specifies again (Carlson, 2007). This is known as **epimorphic regeneration** (Figure I 3) and the typical example is the regenerating amphibian limb.

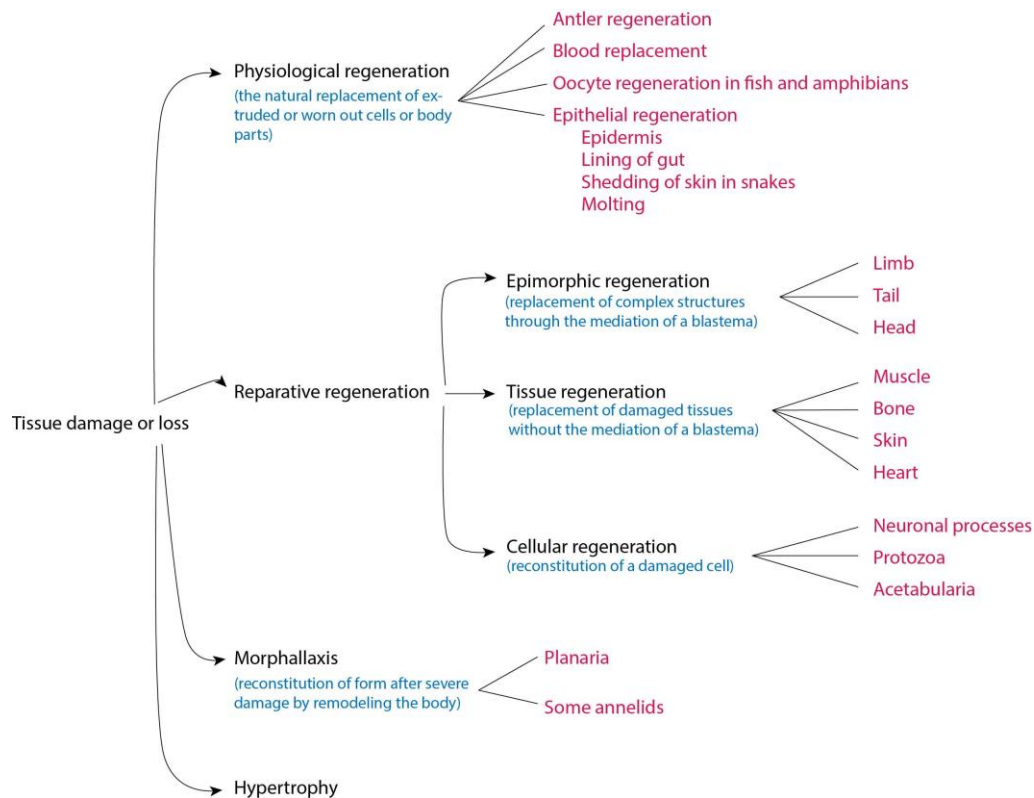
The second mechanism of reparative regeneration would be the repair of a damaged tissue after a traumatic event without a blastema formation, and is known as **tissue regeneration** (Figure I 3). It can be initiated by different traumatic events such as mechanical trauma (the most common one), extreme heat or cold, or toxins (Carlson, 2007). Some examples of this mechanism would be skeletal muscle and bone regeneration. To undergo the complete process, tissue regeneration does not only involve the main cellular precursors of each particular tissue, but also additional cells types. Thus, the regeneration of the local microvasculature and the remodeling or reconstitution of the connective tissue stroma or extracellular matrix also occur. Cardiac muscle regeneration in zebrafish or amphibians would be considered as tissue regeneration, and involve the dedifferentiation and proliferation of the remaining cardiomyocytes to undergo the process (Jopling et al., 2010; Oberpriller, John O.; Oberpriller, Jean C.; Mauro, 1991; Poss et al., 2002).

And last but not least, **cellular regeneration** would be the last reparative regeneration mechanism (Figure I 3). This mechanism is based on the regeneration of a single cell that suffered a trauma (Carlson, 2007). Classic examples are the reconstitution of protozoa after natural fission or resection, and the regeneration of damaged axons of peripheral nerves.

Contrary, there is another regenerative process that is based on the repatterning of the existing tissue with little new growth. It is known as **morphallaxis** (Figure I 3) and it is defined by two main characteristics: 1) the “part is transformed directly into a new organism, or a part of an organism,” and 2) there is no “proliferation at the cut surfaces”

## 1. INTRODUCTION

(Morgan, 1901). Classical morphallaxis is a phenomenon that is confined mostly to invertebrate regenerating systems, but it is a striking phenomenon that is poorly understood at the mechanistic level. One example of organism that undergoes morphallaxis would be the hydra. When cut in half, the half containing the head regenerates a new basal disc, and the part containing the basal disc regenerates a new head.



**Figure I 3| Types of regeneration.** Diagram depicting the major types of the named regenerative phenomena. Adapted from Carlson, 2007.

Another way to face damage is hypertrophy (Figure I 3), but it is important not to confuse it with regeneration. **Hypertrophy** is the increase of mass after a damage or partial removal, and sometimes organs do not need to be damaged to hypertrophy, but increase their mass after an increased functional demand (Carlson, 2007). This leads to two types of hypertrophy: the *compensatory*, which increases a paired organ size after its pair has been damaged or lost (ex. kidneys and lungs); and the *regenerative*, which restores the mass of damaged internal organs (ex. liver and pancreas). The mass can be

increased due to an increase in cell number (*hyperplasia*) or an increase in cell size (*hypertrophy*) or both (Goss, 1966).

## **1.2. REGENERATION IN VERTEBRATES AND MAMMALS**

Urodele amphibians, the par-excellence regenerative model, and teleost fish, with some species-specific restrictions, can regenerate many complex structures and organs including their retina, lens, limbs/fins, tail, jaws, spinal cord, optic nerves, intestine, lateral line and heart (Tsonis, 2000). There are some differences on how regeneration is accomplished in different structures/organs and species, but there are also commonalities.

On the other hand, mammalian species cannot regenerate as extensively as invertebrates or lower vertebrates; however, they maintain the capacity to replace lost cells from different tissues to maintain organism homeostasis (physiologic regeneration). The two main mechanisms for this cell replacement are cell duplication such as beta cells (Dor et al., 2004) and hepatocytes (Yanger et al., 2014), or stem cell proliferation and differentiation in intestinal epithelium, skin or blood cells (Wagers and Weissman, 2004). It is important though not to confuse physiologic regeneration with epimorphic regeneration (Raya et al., 2004). However, these mechanisms are not enough to counterbalance the tissue loss after a significant injury, and cannot be the base to remodel a complex structure. This leads to an inability of adult mammalian species to regenerate or replace a damaged or missing organ.

Arguably, some scientists have described two regeneration events in mammals, closure of excisioned tissues in ears and digit tips. The ears of some mammals are able to undergo scar-free regeneration after the removal of a cylindrical mass of ear tissue including epidermis, dermis, muscle and cartilage. This response was first characterized in rabbit ears, and after some years it was described that different mouse strains regenerate in a variable manner (Gawriluk et al., 2016; Williams-Boyce and Daniel, 1980). Referring to the digit tip regeneration, it has been observed in mouse (Borgens, 1982; Neufeld and Zhao, 1995) and other species including humans (Illingworth, 1974).

## 1. INTRODUCTION

Although not free from controversy, fingertip regeneration in humans is reported to be restricted to the distal most or terminal phalangeal element.

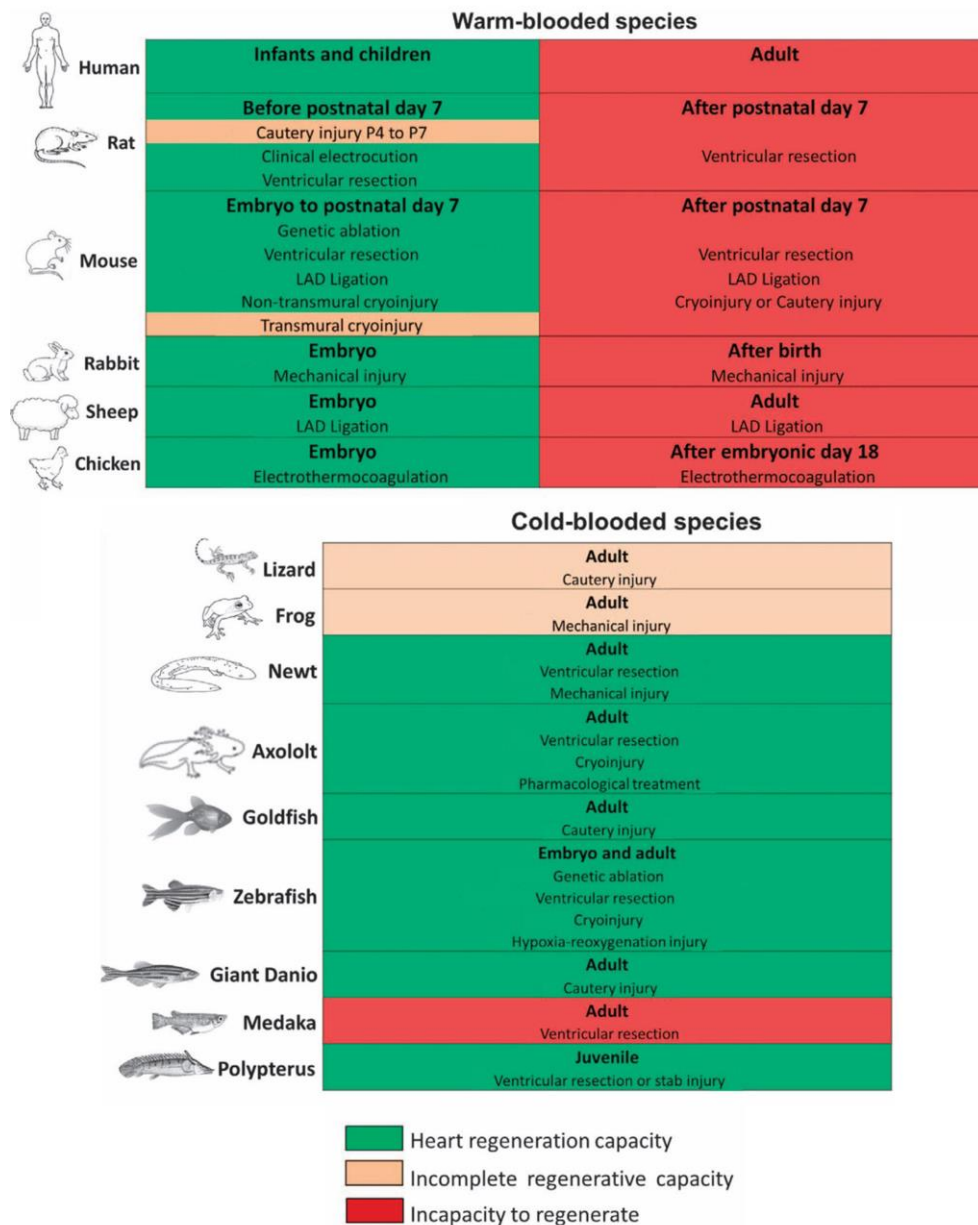
### **1.3. HEART REGENERATION**

Being able to regenerate the human heart has emerged as a worldwide challenge in recent years, especially since heart failure remains the major cause of morbidity and mortality in the westernized world (Mozaffarian et al., 2016). According to the World Health Organization (WHO), 7.5 million people die annually due to cardiovascular diseases, and this represents almost 1/3 of all global deaths (Mendis et al., 2011). This is mainly due to the fact that human heart, as the majority of adult mammals, has limited capacity to recover and regenerate after a major cardiac injury (Laflamme and Murry, 2011). Currently, the existing pharmacological treatments have been designed to target the mechanical characteristics of the cardiovascular system, including the reduction of blood pressure (angiotensin converting enzyme inhibitors, angiotensin receptor blockers, beta-blockers, isosorbide dinitrate, and hydralazine hydrochloride), the reduction of blood volume (aldosterone antagonists, diuretics) and the increase of the cardiac contractile force (digoxin) (Leach and Martin, 2018). However, none of these available drugs aims to reverse the damage caused by the cardiovascular diseases.

In order to tackle this concern, the only solution would be to find a treatment that replaces the damaged myocardium for a functional one; or that induces the regeneration potential of human myocardium by activating key genes that have demonstrated to be key players in heart regeneration of other species. Different therapeutic strategies have been studied involving stimulation of cardiomyocyte proliferation, cardiac progenitor or stem cells, cell therapy, reprogramming, and tissue engineering which compiles all of them (Amado et al., 2005; Chimenti et al., 2010; Hou et al., 2013; Leach and Martin, 2018; Tsifaki et al., 2018). However, none of them have succeeded in complete heart regeneration so far. Currently, the only viable treatment when heart failure is established is heart transplantation, which is limited by organ donor availability and complicated by the lifelong immune suppression needed (Benjamin et al., 2018). Therefore, the study of natural heart regeneration that occurs in other



organisms (Figure I 4 and Figure I 5) and the understanding of the underlying mechanisms stands out as an alternative approach to develop successful clinical therapies to regenerate the human heart.



**Figure I 4 | Heart regenerative capacity in warm- or cold-blooded animals.** For each species, cardiac regenerative ability is indicated in green (ability to regenerate), orange (incomplete capacity to regenerate) or red (incapacity to regenerate). In each case, the approach used to induce cardiac damage is indicated. In warm-blooded species, cardiac regeneration appears to be restricted to a defined early-developmental period during embryonic and early-neonatal life. In cold-blooded animals, six out of nine species have the ability to regenerate their heart during adult life, whereas three out of nine species show an incomplete capacity or incapacity to undergo heart regeneration. Adapted from Vivien et al., 2016.




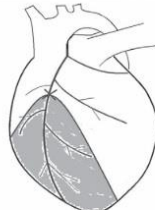
### 1.3.1. Heart regeneration in urodeles

Amphibians can be separated into three orders, urodele (newt, salamander and axolotl), anuran (frogs and toads), and apoda (caecilians). Urodele amphibians have a functional tail in adult life, whereas anuran amphibians lose their tail after metamorphosis, and apoda are limbless with a worm-like form. Anuran and urodele amphibians are able to regenerate several tissues and organs such as limbs, retina and nerve tissue (Vivien et al., 2016). Therefore, urodele and anuran amphibians are useful models to explore the mechanisms of cardiac regeneration in aquatic and terrestrial tetrapod vertebrates.

The first studies describing the proliferative potential of newt cardiomyocytes in injured myocardium were conducted by John Oberpriller and Jean C. Oberpriller at the beginning of 1970s (Oberpriller and Oberpriller, 1971, 1974). Although the newt's heart proliferative capacity, authors concluded that newts were not able to completely regenerate upon amputation of the ventricular apex, due to the presence of fibrotic tissue after injury (Oberpriller and Oberpriller, 1971, 1974). Yet, recent studies provided evidence that adult newt heart has the ability to regenerate after the resection of the 20% of the apex, or the removal of the lateral portion of the ventricle (5-10%) (Mercer et al., 2013, 2012; Witman et al., 2011). Newts have also proved to regenerate after mechanical injury by repeated crushing of the ventricle with forceps (Borchardt and Braun, 2007; Laube et al., 2006). To date, more physiologically injury models such as cryoinjury or ischemic injury have not been reported in the newt (Figure 4 and Figure 5). The timing needed to complete the cardiac regeneration depends on the injury method, but typically occurs within 60-90 days.

Despite the pioneering role as a heart regeneration experimental model, newt is not the most studied organism due to the lack of genetic tools and the limitation of molecular and genetic analysis. Sequencing its enormous genome, estimated to be 1,010 bases or ~10 times the size of the human genome, have been a big challenge (Looso et al., 2013). Despite, novel transcriptional and proteomic studies helped to unveil the mechanisms involved in newt cardiac regeneration (Looso et al., 2013; Witman et

al., 2011). Interestingly, the most significant transcriptional changes in newt cardiac regeneration are associated with ECM, which indicates its importance in the regenerative process (Mercer et al., 2013).

			
<b>Genetic ablation</b>	<b>Cryoinjury Cautery injury Mechanical injury</b>	<b>Ventricular resection</b>	<b>LAD ligation</b>
<b>TYPE OF DAMAGE</b>			
CM specific death	Cardiac damage by freezing, burning, squeezing or electrical shock	Removal of ventricular tissue	Ligation of the left anterior descending coronary artery
<b>EXTENT OF TISSUE REMOVAL</b>			
60 % CMs in the global myocardium	10 to 30 % of the ventricle	10 to 20 % of the ventricle	75 % CMs are lost below the ligation
<b>INFLAMMATION and ECM DEPOSITION</b>			
No	Variable	Yes	Yes
<b>HEART REGENERATIVE CAPACITY</b>			
<b>YES</b> zebrafish larvae <b>YES</b> adult zebrafish <b>YES</b> embryonic mouse <b>YES</b> neonatal mouse	<b>YES</b> newt <b>YES</b> axolotl <b>YES</b> adult zebrafish <b>YES</b> giant danio <b>YES</b> goldfish <b>YES</b> polypertus <b>YES</b> neonatal rat <b>YES</b> embryonic rabbit <b>YES</b> neonatal mouse (NTC) <b>NO</b> neonatal mouse (TC) <b>NO</b> adult mouse <b>NO</b> adult rabbit	<b>YES</b> newt <b>YES</b> axolotl <b>YES</b> adult zebrafish <b>YES</b> neonatal mouse <b>YES</b> neonatal rat <b>NO</b> medaka <b>NO</b> adult mouse <b>NO</b> adult rat	<b>YES</b> embryonic sheep <b>YES</b> neonatal mouse <b>NO</b> adult mouse <b>NO</b> adult sheep <b>NO</b> adult rabbit <b>NO</b> adult rat

**Figure I 5 | Different approaches used to study cardiac regeneration in vertebrates.** The four main methodological approaches used in the literature to induce cardiac damage are indicated. For each approach, the type of injury induced, the extent of tissue removal and the extent of inflammation and ECM deposition after injury are indicated. The ability to regenerate the myocardium after the defined type of injury is indicated for the vertebrate species analyzed. NTC, non-transmural cryoinjury; TC, transmural cryoinjury. Adapted from Vivien et al., 2016.

In addition, axolotls (*Ambystoma mexicanum* and *A. dumerilii*) have also been studied in terms of cardiac regeneration. They have proven to regenerate after ventricular resection, cryoinjury and pharmacological heart failure caused by isoproterenol (Figure I 4 and Figure I 5) (Cano-Martínez et al., 2010, 2007; Lauridsen and

## 1. INTRODUCTION

Pedersen, 2014). Following cryoinjury or ventricular resection axolotl can regenerate within 60-90 days (Lauridsen and Pedersen, 2014).

To date, there is no study analyzing the heart regeneration capacity in terrestrial urodeles such as salamanders or post-metamorphic axolotls. Nevertheless, it is known that land-phase amphibians have worst limb regeneration compared to their water-based forms (Vivien et al., 2016), suggesting a worse cardiac regeneration. In addition, heart regeneration has not been deeply studied in anuran amphibians. There are two studies more than 50 years ago, that report adult frog incomplete heart regeneration after mechanical injury induced by apex crushing (Figure I 4) (Rumyantsev, 1973, 1961).

### **1.3.2. Heart regeneration in mice**

Currently, it is accepted that cardiomyocyte turnover in adult mice is very low (~1% per year) (Senyo et al., 2013). This allows the heart to partially replace some cardiomyocytes during normal aging. On the other hand, this limited renewal is not enough to cope with massive cardiomyocyte loss after myocardial infarction. Cardiomyocyte turnover after myocardial infarction reaches the ~3% within and adjacent the injured area compared to sham-operated mice (Senyo et al., 2013), but is also insufficient to completely renew the damaged myocardium. The origin of the newly formed cardiomyocytes is not still fully known, since genetic lineage tracing studies have determined that they come from existing cardiomyocytes and from progenitors (Beltrami et al., 2003; Hsieh et al., 2007; Senyo et al., 2013; Van Berlo et al., 2014).

Contrary, embryonic and neonatal mice have cardiac regeneration abilities. Sturzu et al. proved, by cardiomyocyte genetic ablation, that mice embryonic myocardium is able to regenerate without marks of cardiac dysfunction or hypertrophy (Figure I 4 and Figure I 5) (Sturzu et al., 2015). They studied different degrees of cardiomyocyte death and determined that, after a cardiomyocyte loss of 50-60%, there was a significant proliferation increase of the remaining cardiomyocytes and that these were the responsible for the cellular replacement (Sturzu et al., 2015). Thus far, the contribution of non-cardiomyocyte cells in this process has not been investigated.

When it comes to neonatal mice, several studies have reported cardiac regeneration during a brief post-natal developmental window. This has been proved through resection of the ventricular apex, ligation of the left anterior descending coronary artery (LAD ligation), cryoinjury and genetic ablation (Figure 4 and Figure 5) (Darehzereshki et al., 2015; Haubner et al., 2012; Hsieh et al., 2007; Jesty et al., 2012; Lavine et al., 2014; Notari et al., 2018; Porrello et al., 2013, 2011). After apical resection and LAD ligation of 1-day-old mice a blood clot is formed and inflammatory cells are recruited to the injury. Later on, ECM is remodeled and cardiomyocyte proliferation is globally activated in the heart (Haubner et al., 2012; Porrello et al., 2013, 2011). Furthermore, in the LAD ligation model, extensive angiogenesis and revascularization are associated with the regeneration process (Aurora et al., 2014; Porrello et al., 2013). In the cryoinjury model, epicardial activation has been detected as well (Darehzereshki et al., 2015). When it comes to the origin of the new cardiomyocytes, it has been demonstrated that the majority of them derive from pre-existing ones (Porrello et al., 2011). However, in cryoinjury, c-kit<sup>+</sup> cardiac progenitors have also been implicated in the generation of new myocardium (Jesty et al., 2012). In all of the injury methodologies assessed, it has been proved that neonatal cardiac regeneration is limited to a window of 7 days after birth (Porrello et al., 2013, 2011). Even so, a recent study may suggest that the cardiac regenerative potential may be even more limited in time, and that the neonatal ability to regenerate the heart is lost by post-natal day 2 (Notari et al., 2018).

As seen, the cardiac regenerative potential of neonatal mice has been reproduced by multiple studies, but this biological process was under some controversy. Andersen et al. reported in 2014 that neonatal mice were not able to regenerate their hearts after apical resection, failing to detect proliferating cardiomyocytes (Andersen et al., 2014). This controversial findings lead to discussion, and others determined several technical issues, being the method of injury performed in a different way (Sadek et al., 2014; Sen and Sadek, 2015). In addition, a systematic analysis by Bryant et al. observed that the major determinant of the neonatal regenerative response after apical resection is the size of resection (Bryant et al., 2015). Something similar happens with cryosection, since structural recovery of the myocardium is described after non-transmural

## 1. INTRODUCTION

cryoinjury in P1 heart, but is incomplete after transmural injury (Figure 1 5) (Darehzereshki et al., 2015; Jesty et al., 2012; Strungs et al., 2013).

### **1.3.3. Limitations of heart regeneration in humans**

For a long time, it was believed that human cardiomyocytes were terminally differentiated and post-mitotic, being cardiomyocyte hypertrophy the postnatal heart growth mode. Several investigators have tried to measure the number of cardiomyocytes in the human heart at normal and pathological conditions, but it is complicated and needs many assumptions to be done (Burton et al., 1999; Goldstein et al., 1974; Li et al., 1996). Even so, there are two studies that have tried more direct approaches to measure DNA synthesis in adult human hearts. The first one, by Bergmann et al., took advantage of the worldwide pulse of atmospheric  $^{14}\text{C}$  that took place during the testing of nuclear weapons during the cold war (Bergmann et al., 2009). The  $^{14}\text{C}$  entered the human food chain, labelling the newly formed cells. The Limited Nuclear Test Ban Treaty of 1963, caused a reduction of the  $^{14}\text{C}$  levels and provided researchers with pulse-chase conditions. As predicted, cardiomyocytes and non-cardiomyocyte cardiac cells were found to have incorporated  $^{14}\text{C}$ , thus being substantially younger than the patient. Mathematical modelling suggested that cardiomyocyte turnover was age dependent, with ~1% cardiomyocyte/year renewal at age of 20, and 0.4% at age 75. Following this basis, the ~45% of cardiomyocytes would be renewed through a normal human lifespan. Further studies of this data, have reported that most human cardiomyocytes stop proliferating after the first year of life (Bergmann et al., 2015).

The second study, by Kajstura et al., studied post mortem hearts from patients with cancer that were treated with the thymidine analogue iododeoxyuridine (IdU) (Kajstura et al., 2010). This agent intercalates in the synthesizing DNA and can be detected by immunohistochemistry. Cardiomyocyte labelling rates were identified to be from 2.5% to 46%. Mathematical modelling suggested a cardiomyocyte turnover of 22% per year. Taken together, this studies show evidence from adult human heart plasticity although some findings are hard to reconcile.

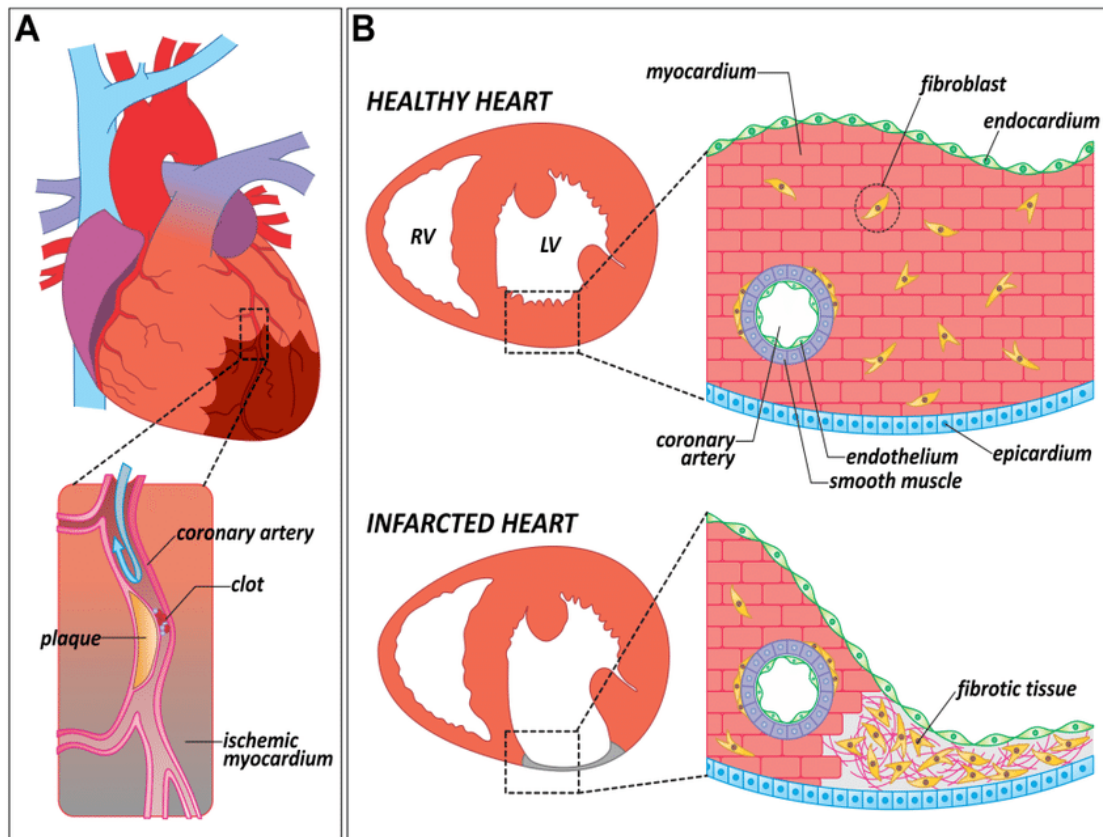
In contrast to the low regenerative potential of adult human heart, there are case studies that reveal cardiac regeneration in children and infants (Figure I 4). There is evidence of little or absent myocardial scarring of children undergone corrective cardiac surgery, or complete recovery of a new-born patient after a severe myocardial infarction (Fratz et al., 2011; Haubner et al., 2016).

A possible reason for this insufficient proliferation of mammalian cardiomyocytes might be their DNA content. After birth, human and rodent cardiomyocytes undergo a period of physiologic growth that is difficult to support with a diploid genome. Different approaches have been identified to cope with this problem. Almost all rodent cardiomyocytes, experience a final round of DNA replication and nuclear division without cytokinesis, generating a ~75% of binucleated cardiomyocytes with a diploid ( $2n$ ) DNA content (Li et al., 1996). By contrast, humans and other primates experience a final round of DNA replication without karyokinesis or cytokinesis, giving rise to mononucleated cells but with tetraploid ( $4n$ ) or higher ploidy (Adler and Costabel, 1975; Bergmann et al., 2015; Olivetti et al., 1996). Although some evidence shown for the proliferation of binucleated cardiomyocytes (Naqvi et al., 2014), it is possible that mononucleated diploid cardiomyocytes are less differentiated than polynucleated and polyploid cardiomyocytes. Thus, they will be able to reenter cell cycle easier, being more ready to contribute to myocardial regeneration. Indeed, most of the zebrafish cardiomyocytes are mononucleated (Poss, 2007), and this could explain their high proliferative capacity.

Thus, the scarce capacity of cardiomyocyte regeneration makes human heart one of the least regenerative organs in the body. Consequently, heart failure is an increasing health problem, being predicted to reach epidemic proportions as our population ages (Mendis et al., 2011). The human ventricle is comprised of 2-4 billion cardiomyocytes, and after a myocardial infarction 1 billion cardiomyocytes (~25%) can be eradicated in few hours (Murry et al., 2006). Most myocardial infarctions are caused by an occlusion of a coronary artery by an atheromatous plaque, and the resulted damaged myocardium is replaced by a non-contractile fibrous scar tissue (Figure I 6)

## 1. INTRODUCTION

(Frangogiannis, 2006). But, not only cardiac diseases are responsible for cardiomyocyte loss, but also aging itself is associated with the loss of about 20 million cardiomyocytes per year in absence of specific heart disease (Olivetti et al., 1991).



**Figure 1.6 | Causes and consequences of myocardial infarction in humans. (A)** Schematic representation of a human heart in which one of the coronary arteries is occluded by an atheromatous plaque (magnified area). When blood flow is interrupted, a region of the myocardium becomes ischemic (brown shade). Ischemic myocardium eventually dies and is replaced by fibrotic tissue. **(B)** Anatomical and histological differences between a healthy and an infarcted heart. In contrast to a healthy heart, the infarcted ventricle shows a thinning of the affected wall, in which the cardiac muscle has been replaced by fibrotic tissue. LV, left ventricle; RV, right ventricle. Adapted from González-Rosa et al., 2017.

## 1.4. HEART REGENERATION IN ZEBRAFISH

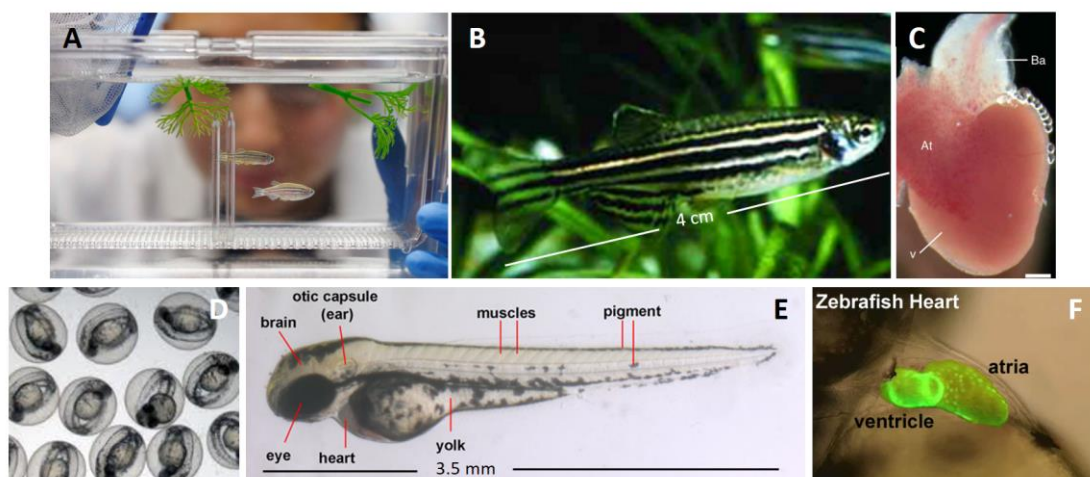
### 1.4.1. Zebrafish as a model organism

Zebrafish (*Danio rerio*, Hamilton 1822) is a small, freshwater, teleost fish (family Cyprinidae, order Cypriniformes) native to small rivers, streams, paddy fields, and channels in south-eastern Asia, including India, Myanmar, Bangladesh and Nepal



(Holtzman et al., 2016). As well as being found in any pet store as ornamental fish, it has become widespread as a vertebrate model in research. The advantageous features that have given zebrafish such good position in the research world are: 1) a maintenance remarkably simpler and cheaper than mammals, 2) a short generation time, 3) large number of eggs in one lay, 4) and the ability to follow-up *in vivo* the development thanks to the external fertilization and the transparency of larvae until 72hpf (Figure 1 7). It has also been of great research interest due to its ability to regenerate numerous organs, including all seven fins (Poss et al., 2003), the retina (Vihtelic and Hyde, 2000), optic nerve (Becker and Becker, 2000), the spinal cord (Thomas et al., 1998), the telencephalon (Kroehne et al., 2011), kidney (Diep et al., 2011), pancreas (Beer et al., 2016) and heart (Poss et al., 2002; Raya et al., 2003).

Zebrafish was, by the 1920s, recommended as a potential genetic and embryologic model (Goodrich, 1929), and was used for the first time in embryologic research by Craser (1934) (Creaser, 1934). However, the actual position as an organism model started with George Streisinger, who was the first researcher to use the zebrafish as a genetic model (Streisinger et al., 1981), and Charles Kimmel, who defined the key stages of embryogenesis and characterized the first zebrafish mutants (Kimmel, 1993; Kimmel et al., 1989).



**Figure 1 7 | Zebrafish adults and larvae.** (A) Female and male adult zebrafish are put in a crossing tank to obtain eggs. The size of (B) an adult zebrafish is around 4cm long, and (C) the adult heart is 1-2mm. (D) Zebrafish eggs remain in their chorion until 48-72hpf. (E) At 72hpf, larvae have already developed many organs, including the heart (F).

## 1. INTRODUCTION

About 71% of human genes have at least one corresponding gene in zebrafish genome, known as ortholog (Howe et al., 2013). Due to the teleost genome duplication event, there may be two orthologs in the zebrafish genome for one given human gene (Glasauer and Neuhauss, 2014). In addition, the zebrafish genome has several unique genes with no corresponding ortholog in mammalian genome. Besides, 84% of genes associated with human disease have a zebrafish counterpart. All these genomic similarities makes zebrafish a great animal model to study biological processes and human diseases (Howe et al., 2013).

### 1.4.1.1. Molecular tools in zebrafish

Another aspect that favoured zebrafish to develop as a great research model was the numerous molecular tools that were initially developed for studies in developmental biology. The first strategy used to identify genes responsible for development was the generation of developmental and behavioral mutants through random chemical mutagenesis with N-ethyl-N-nitrosourea (**ENU**), an alkylating agent that modifies single DNA bases resulting in randomly distributed point mutations (Solnica-Krezel et al., 1994). However, the principal drawback of this technique is intensive screening, by sequencing, needed to identify the point mutation.

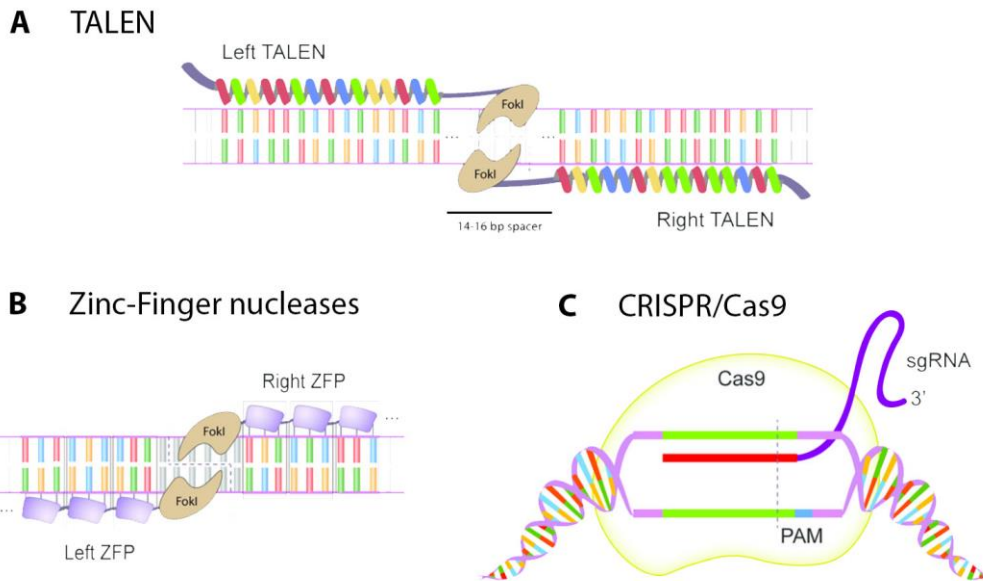
Nowadays, the almost full annotation of the zebrafish genome is available (Howe et al., 2013), and it has facilitated the use of zebrafish in research allowing the precise selection of any genomic sequence of interest. One of the alternative approaches to ENU, that benefited from the zebrafish genome annotation, is the random integration of exogenous DNA, also called **insertional mutagenesis** (Kettleborough et al., 2013). This strategy relies on transposon- or viral-based methods to introduce a desired DNA fragment into the zebrafish genome. The most known transposon based mutagenesis system used in zebrafish is the Tol2 system (Kwan et al., 2007). This system uses flanking sequences to integrate a DNA construct within transposon sites with the help of a transposase. So, by injecting the DNA construct and the mRNA of the transposase into a single cell embryo, transgenic zebrafish can be easily generated. Depending on the strategy used, reporter, knock-down or conditional transgenic lines can be generated.

Thousands of transgenic zebrafish lines available (at [zfin.org](http://zfin.org)) have been generated with this method.

Another classical way of knocking down genes is **morpholino** injection. Morpholinos are stable, modified oligonucleotides (the deoxyribose ring has been replaced with a morpholine ring) designed to block translation or splicing of targeted genes by complementary binding to sequences at gene's transcription or splicing sites (Summerton and Weller, 1997). Although it is efficient until 2dpf when injected into one-cell stage embryos, the principal drawback of this technology is its transience effect. In addition, since it is a strategy directed to block mRNA and not to disrupt the DNA sequence, and off-target effects are commonly present, sometimes the resulting phenotypes are difficult to interpret. Therefore, these characteristics make the use of morpholinos not really suitable for adult purposes. Nevertheless, different approaches have attempted to use morpholinos in adult tissues, such as vivo-morpholinos (Hyde et al., 2012; Thummel et al., 2011), cerebro-ventricular microinjection (Kizil et al., 2013) or morpholino-loaded beads (Becker and Becker, 2014).

Today, generating knock-down phenotypes by using morpholinos has largely been replaced by **targeted genome editing techniques** (TILLING, targeting induced local lesions in genomes). This strategy can produce heritable changes in the genome leading total ablation of gene products and the generation of mutant lines with relative ease. TILLING techniques include Zinc finger nucleases (ZFNs), transcription activator-like effector nucleases (TALENs), and clustered regularly interspaced short palindromic repeats (CRISPRs)/Cas9 (Figure 1 8) (Bibikova et al., 2001; Simone et al., 2018; Wyatt et al., 2015). All these techniques are based in the induction of double strand breaks (DSB) in the DNA, which are fixed by endogenous DNA repair pathways that can cause stochastic insertion or deletion (indel) mutations, and lead to disruption of the open reading frame and the subsequent protein structure. The DSBs induced by these technologies are frequently repaired by the error-prone non-homologous end joining (NHEJ), and less frequently by homology directed repair (HDR).

## 1. INTRODUCTION



**Figure I 8| Guided designed endonucleases used in zebrafish. (A)** The fused FokI functions as a homodimer that binds both sides of the target DNA and cleaves upon dimerization with the TALEN pairs. TALENs are normally used as dimers with 15–20 TALE repeats binding on one strand separated by a spacer region of 15–20nt followed by another 15–20 TALE repeats binding the opposite strand; consequently, the DSB occurs at around the halfway point of the spacer where the fused FokI domains have the greatest probability of dimerization and subsequent DNA cleavage. **(B)** Zinc-finger nucleases fuse, in site-specific manner, 3–6 zinc finger recognition domains to the either side of the DNA and catalyze the DNA cleavage by a FokI enzyme that dimerizes with the zinc-finger/DNA hybridization. **(C)** SpCas9 recognizes the target sequence with the assistance of the sgRNA next to the 3' PAM sequence and induces a DSB 3bp 5' from the PAM. Adapted from Simone et al., 2018.

### 1.4.1.2. CRISPR/Cas9

The genome editing field has changed enormously thanks to the CRISPR and CRISPR associated protein-9 (Cas9), which reduced price and design complexity, and increased the versatility of genome editing. In the commonly used CRISPR-Cas9 system derived from the human pathogen *Streptococcus pyogenes* (SpCas9), a native NGG 3' PAM (protospacer adjacent motif) sequence is required for an efficient cleavage activity (Figure I 8C) (Cong et al., 2013). This system needs a Cas9 protein as well as two CRISPR RNAs (crRNAs): trans-activating crRNA (tracrRNA) and a precursor crRNA (pre-crRNA). The pre-crRNA contains a spacer to target a desired 20bp site (protospacer) of the genome that precedes an NGG trinucleotide, the requisite PAM. These two RNAs generate a chimera in order to form the single guide RNA (sgRNA).

The Cas9 can be used as a protein or mRNA. To generate the mRNA, the Cas9 can be cloned into vectors that facilitate the synthesis of capped and polyadenylated

Cas9 mRNA via *in vitro* transcription from either SP6 or T3 promoters (Jao et al., 2013). On the other hand, numerous companies sell the Cas9 protein, which generally has higher cutting efficiency than the mRNA. To *in vitro* generate the sgRNA, cloning methods have been optimized allowing the synthesis of the sgRNA by using two partially overlapping oligonucleotides in a clone-free manner (Bassett et al., 2013). One oligonucleotide is specific to the genomic loci of interest whereas the other is a generic oligonucleotide that can be used for all constructs and contains the necessary secondary structure. These oligonucleotides form a double stranded template by annealing at a designed 20nt overlap and are extended via polymerase chain reaction (PCR). Then, the duplex DNA generated from this polymerization reaction can be used for the sgRNA synthesis via *in vitro* transcription (Varshney et al., 2016).

#### **1.4.2. Zebrafish heart**

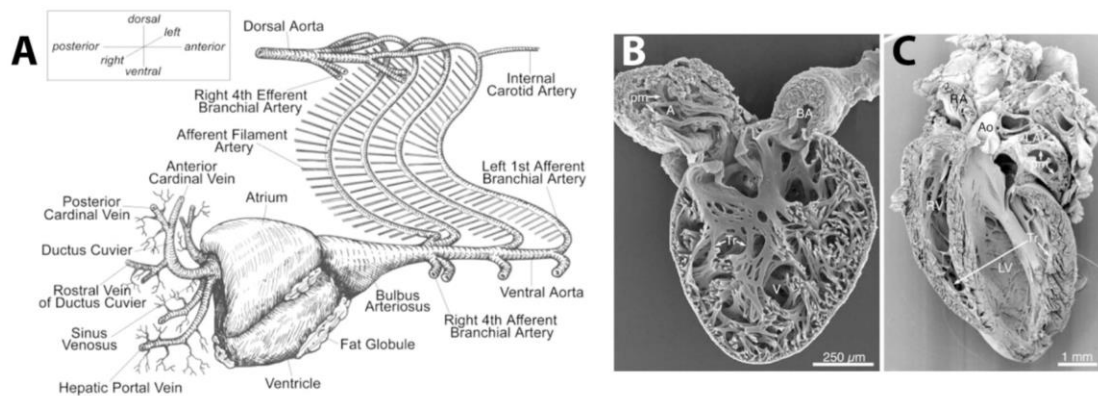
During vertebrate embryo development, heart is the first organ to form and function (Bakkers, 2011). However, early stages of zebrafish development are not yet completely dependent on a functional cardiovascular system. This is because early embryo can obtain oxygen from the medium by diffusion due to its small size (Hu et al., 2001). This peculiarity makes zebrafish embryo a good model to analyze mutants with compromised or no cardiac function, in contrast to mammals (Stainier et al., 1996, 1993). Still, regarding the general cardiovascular development, heart structure and composition, zebrafish are comparable to mammals (Chablais et al., 2011; Hu et al., 2001).

In comparison to the four-chambered human heart, the adult zebrafish heart is more simplistic and is composed of two chambers: one atrium and one ventricle (Figure I 9 and Figure I 10A). Moreover, zebrafish lacks pulmonary circulation resulting in a single-circulation system and simpler structures (Hu et al., 2001). Besides the two contractile chambers, the zebrafish heart is also composed of the sinus venosus and the outflow tract (or bulbus arteriosus) (Figure I 9). The blood enters at the atrium through the sinus venosus, which collects the blood from all the body, then is pumped to the

## 1. INTRODUCTION

ventricle and finally exits through the outflow tract, a simple bulbus arteriosus, which transfers the blood to the gills for oxygenation (Figure I 9) (Hu et al., 2001).

As in mammals, zebrafish heart is composed of three tissue layers, the epicardium, the myocardium and the endocardium. The myocardium is per se the cardiac muscle tissue, and is composed by contractile cardiomyocytes. This layer is surrounded by one-thick cell layer both inside and outside, named endocardium and the epicardium, respectively (Figure I 10B). Structurally, the myocardium can be divided in a peripheral wall of compact muscle, and an inner trabecular muscle (Hu et al., 2001). Lately, through lineage tracing experiments, it has been described that the compact layer can be actually divided into two different layers: the primordial and the cortical (Figure I 10B) (Gupta and Poss, 2012). During development, first is originated the primordial layer, from where some cardiomyocytes delaminate and generate the trabecular layer. It is the trabecular layer that later creates a breach through the primordial layer to finally originate the cortical layer (Gupta and Poss, 2012).



**Figure I 9 | Anatomy and morphology of the zebrafish heart.** (A) An illustration of a postero-anterior view of an adult zebrafish heart and the major vasculature in the cardiac region. (B and C) Comparative morphology of adult atrial and ventricular chambers in the zebrafish (B) and mouse (C). Despite considerable evolutionary distance and dramatically different life styles, the main features of chamber myocardial design (ventricles with trabeculae carneae, Tr; atria with pectinate muscles, pm) are conserved. The differences are in higher proportion of trabeculated ventricular myocardium and presence of a single atrial and ventricular chamber in the fish. Adapted from Hu et al., 2001 and Sedmera, 2011.

### **1.4.3. Zebrafish heart regeneration and injury models**

Ventricular amputation have been, for more than a decade, the exclusive method used to study zebrafish heart regeneration. Recently, other injury models that induce tissue death have been developed to study heart regeneration in zebrafish. Due to zebrafish reduced size, it has not been able to apply common injury methods to induce myocardial ischemia employed in larger animals such as coronary artery ligation.

#### **1.4.3.1. Amputation**

The first method to study zebrafish heart regeneration was developed in the early 2000's and helped to report the ability of the zebrafish to regenerate its heart (Poss et al., 2002; Raya et al., 2003). In this method, around 20-30% of the ventricle is surgically removed at its apex with iridectomy scissors and regeneration is evaluated as complete regrowth of the lost tissue (Figure I 10C) (Poss et al., 2002; Raya et al., 2003). After amputation, a blood clot rapidly appears sealing the wound and preventing the animal to bleed out. Within the next 2-3 days, the blood clot is turned into a fibrin clot and further on is invaded by new cardiomyocytes. Epicardium and endocardium activation, as well as cardiomyocyte proliferation and new vessel and nerve formation are known to be key processes needed for correct cardiac regeneration (Lien et al., 2012). The regeneration process finishes between 30-60 days where the newly formed myocardium is indistinguishable from the non-injured myocardium (Lien et al., 2012; Poss et al., 2002; Raya et al., 2003). Although gene profile analysis suggest that early stages of regeneration are similar to a wound healing process, there is a lack of scar tissue formation at the end (Lien et al., 2006).

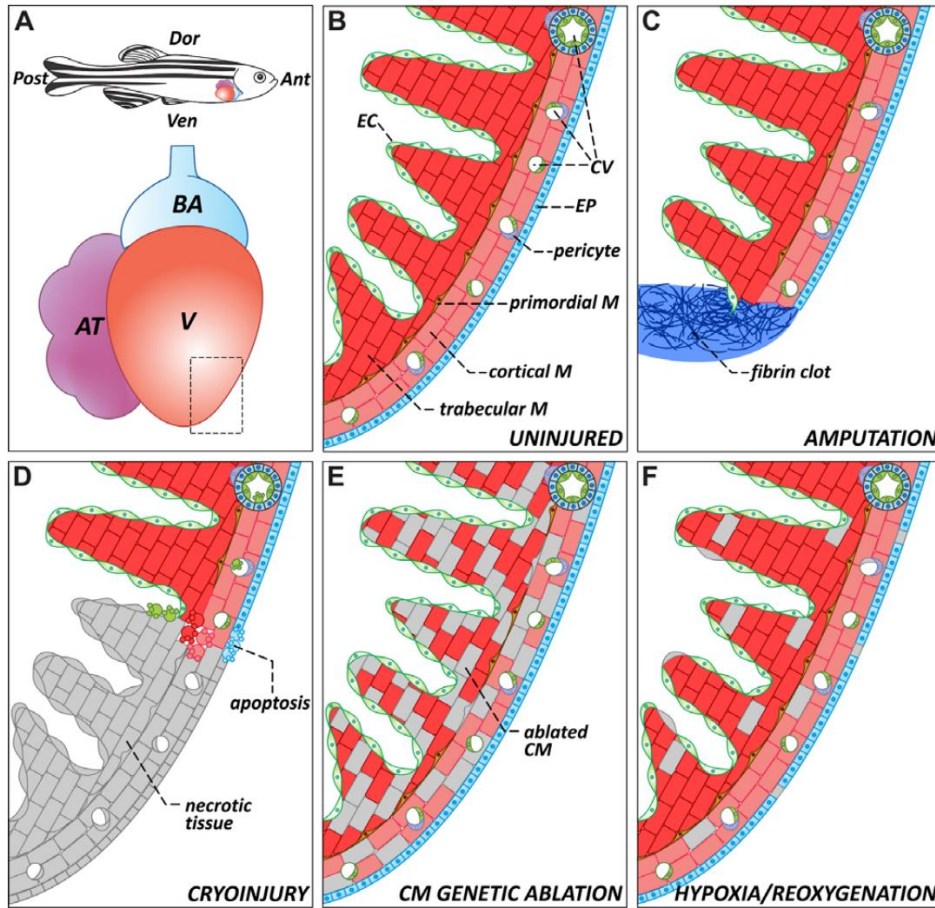
For more than a decade, the amputation model helped to study the zebrafish heart regeneration, and the majority of the findings have been achieved using this method. Yet, some alternative methods have been developed looking for an injury way without tissue loss but death, looking for a model more similar to myocardial infarction.

### 1.4.3.2. Cryoinjury

Some years ago, three groups in Europe established an alternative injury model, the cryoinjury (Chablais et al., 2011; González-Rosa et al., 2011; Schnabel et al., 2011). In this new paradigm, the cardiac tissue is damaged by applying dry ice or a probe precooled in liquid nitrogen to the ventricular surface. The fast freezing and thawing of cells results in tissue necrosis and further cellular apoptosis of approximately the 20-25% of the ventricle (Chablais et al., 2011; González-Rosa et al., 2011; Schnabel et al., 2011). In comparison to ventricular amputation, the cryoinjury model induces more apoptotic response affecting different cell types (Figure I 10D). Just after the injury, the damaged area is infiltrated with immune cells, leading an important immune response. This inflammatory response triggers an extensive disposition of fibrotic tissue greater than in the amputation model. Interestingly, this entire fibrotic scar is cleared and repopulated by cardiomyocytes allowing zebrafish heart fully regeneration (Gamba et al., 2017). However, all this process is slower than amputation taking 3-4 months to fully regenerate (González-Rosa et al., 2011; Lien et al., 2012). The process can take even more time when bigger injuries are done, as reported by Hein et al. where a thicker copper filament induced a greater injury and hearts regenerated after 180 days post-injury (dpi) (Hein et al., 2015). This fact suggests that injury severity influences the recovery window, probably due to the need to clear all the necrotic tissue and to resolute of the grater scar tissue (Lien et al., 2012). Importantly, this model have shown that fibrosis is not an inhibitory process for complete cardiac regeneration.

After regeneration, cryoinjured ventricles develop an enlargement of the ventricle, a thicker ventricular wall, and more rounded ventricular shape, as signs of ventricular remodeling, although heart function is completely restored (González-Rosa et al., 2011). Recently it has also been discovered that the primordial layer of the myocardium is unable to completely regenerate after cryoinjury (Pfefferli and Jaźwińska, 2017), findings not observed after ventricular amputation (Gupta and Poss, 2012).





**Figure 10 | The zebrafish heart and injury models.** (A) Schematic representation of the anatomical position of the heart in the adult zebrafish. The teleost heart is composed of a single atrium and a single ventricle. Bulbus arteriosus is an elastic, non-contractile chamber composed of smooth muscle. (B) Histological organization of the adult zebrafish ventricle. Cardiac muscle is covered externally by the epicardium and internally by the endocardium. The myocardium is divided into three distinctive populations: trabecular, primordial, and cortical. The cortical myocardium is highly irrigated by coronary vessels. Endothelial cells from the coronary vasculature are frequently surrounded by pericytes. For simplicity, the presence of fibroblasts in the uninjured heart has been omitted. (C) Apex amputation removes ~20% of the ventricle and leads to the formation of a fibrin clot. (D) Cryoinjury induces local tissue necrosis (~20% of the ventricle) and triggers apoptosis. (E) Cardiomyocyte genetic ablation causes diffuse loss of ~60% of cardiomyocytes in the heart, while preserving the remaining cell types. (F) Hypoxia/reoxygenation induces low levels of diffuse cell death in all cell types of the heart. Ant, anterior; AT, atrium; BA, bulbus arteriosus; CM, cardiomyocyte; CV, coronary vasculature; Dor, dorsal; EC, endocardium; EP, epicardium; M, myocardium; Post, posterior; V, ventricle; Ven, ventral. Adapted from González-Rosa et al., 2017.

### 1.4.3.3. Genetic ablation

Another strategy to induce cardiac injury is based on the expression of toxins or enzymes catalyzing the production of cytotoxic metabolites in an inducible manner. The first to design a transgenic system of genetic ablation were Curado et al.. They expressed the bacterial nitroreductase (NTR) specifically in cardiomyocytes (under the *mlc2a*

## 1. INTRODUCTION

promoter) (Curado et al., 2007). In the presence of metronidazole (Mtz), a non-toxic agent, the NTR generates a toxic metabolite that induces cell death. When expressed under cell specific promoters, as Curado et al. did, it can generate the ablation of a specific cell type without damaging any other cell type. It is a conditional system that allows a temporal control, since Mtz can be added upon interest in the fish water. When Mtz is removed, the toxin is no longer present and cardiomyocytes can recover again. Others used the same system to specifically ablate ventricular cardiomyocytes in the developing zebrafish (Zhang et al., 2013).

A second system of genetic ablation was created to express the diphtheria toxin chain A (DTA) under a cardiomyocyte promoter (Wang et al., 2011). Here, the conditional expression of DTA controlled under the CRE/loxP system can produce up to a ~60% of cardiomyocyte death (Figure I 10E). Although this may seem a huge loss, it is tolerated and regeneration is achieved in ~30 days with no scarring. Since only cardiomyocytes are affected, it reassembles more to an advanced cardiomyopathy rather than a myocardial infarction, but it is a great model to study factors that promote cardiomyocyte proliferation.

The genetic ablation mechanism has not only been used in cardiomyocytes but other cell types such as epicardial cells (under the *tcf21* promoter) (Cao et al., 2017; Wang et al., 2015), fibroblasts (under the *col1a2* promoter) (Sánchez-Iranzo et al., 2018), or T<sub>reg</sub> cells (under the *foxp3a* promoter) (Hui et al., 2017). All these systems used the NTR method.

### **1.4.3.4. Hypoxia/reoxygenation**

The last model implemented has been the hypoxia/reoxygenation, which tries to better model the human myocardial infarction (Parente et al., 2013). This paradigm is based on the maintenance of fish for a short time under hypoxia conditions, and returning them back to normal oxygen water. The principal limitation of this model is that it is not a heart specific and damages other organs. This injury generates cardiomyocyte apoptosis and proliferation; however, histologic analysis do not show

any gross injuries (Figure I 10F). Zebrafish after hypoxia/reoxygenation also exhibit transient reduction in cardiac function. Localized hypoxia, which would reassemble more to human myocardial infarction, has not been developed in zebrafish yet.

The comparison of the above-mentioned models is found in Table I 1. In addition to these models, different strategies have been developed in other to create milder injuries. These include scratching, piercing or stabbing the adult hearts (Gupta et al., 2013; Itou et al., 2014; Kikuchi et al., 2011b).

**Table I 1 | Comparison between different injury models for studying zebrafish heart regeneration.**

Adapted from González-Rosa et al., 2017.

	Injury method			
	Apex resection	Cryoinjury	Genetic ablation	Hypoxia/reox.
<b>Tissue affected (%)</b>	~20% (ventricle)	~25-30% (ventricle)	60% (atrium + ventricle)	?
<b>Tissue death (affected tissue)</b>	- (apoptosis limited to tissue around amputation plane)	+++ (all cell types)	+++ (only cardiomyocytes)	+
<b>Cardiac specific</b>	Yes	Yes	Yes	No
<b>Localized injury</b>	Yes	Yes	No	No
<b>Fibrosis</b>	- or low	+++	-	-
<b>Ventricular remodelling</b>	Low	High	-	-
<b>Hypoxia</b>	+ (local hypoxia)	?	?	+ (generalized hypoxia)
<b>Functional recovery</b>	+++ (electrical coupling, exercise tolerance)	Pumping efficiency ++ Segmental motility -	+++ (electrical coupling, exercise tolerance)	Pumping efficiency ++
<b>Regeneration time (days)</b>	30-60	80-130	30	NA
<b>Requires specific transgenes?</b>	No	No	Yes	No
<b>Can be applied in embryonic/larval stages?</b>	No	No	Yes	Yes

### 1.4.4. Cellular and molecular mechanisms of zebrafish heart regeneration

#### 1.4.4.1. Myocardial contribution

One of the most important objectives in the study of cardiac regeneration is the identification of the origin of the new tissue. When first described the capacity of zebrafish heart to regenerate (Poss et al., 2002; Raya et al., 2003), it was unknown if the newly formed cardiomyocytes originated from a pre-existing source of cardiac progenitor cells, from the transdifferentiation of other cell types, or from the proliferation of pre-existing cardiomyocytes. In this first studies, BrdU incorporation experiments suggested that proliferating cells could be cardiomyocytes (Poss et al., 2002; Raya et al., 2003). Later on Lepilina et al. suggested that the new myocardium arose from cardiac progenitor cells (Lepilina et al., 2006). The expression of cardiac progenitor markers such as *hand2*, *nkx2.5*, *tbx20* and *tbx5* further supported this hypothesis (Lepilina et al., 2006).

The origin of the new myocardium was further revised by two independent groups, which performed lineage tracing of cardiomyocytes during regeneration using the Cre/loxP system (Jopling et al., 2010; Kikuchi et al., 2010). They demonstrated that new cardiomyocytes were originated from pre-existing ones through cell proliferation. They observed that, after cardiac injury, proliferating cardiomyocytes in zebrafish suffer several morphological and transcriptional changes. Cardiomyocytes display partial sarcomere disassembly (Jopling et al., 2010; Kikuchi et al., 2010) and acquire a dedifferentiated state with reduced expression of sarcomeric proteins and reexpression of some embryonic myosins (Sallin et al., 2015; Wu et al., 2016). Cell proliferation assays using BrdU or EdU incorporation revealed that cardiomyocyte proliferation started at 7dpa and peaked at 14dpa (Poss et al., 2002; Raya et al., 2003). The majority of the proliferating cardiomyocytes were found at the injury site (65-75%), but there were also proliferating cardiomyocytes in other areas throughout the ventricle (10-30%) (Itou et al., 2012; Jopling et al., 2010; Sallin et al., 2015). In line with these findings, a

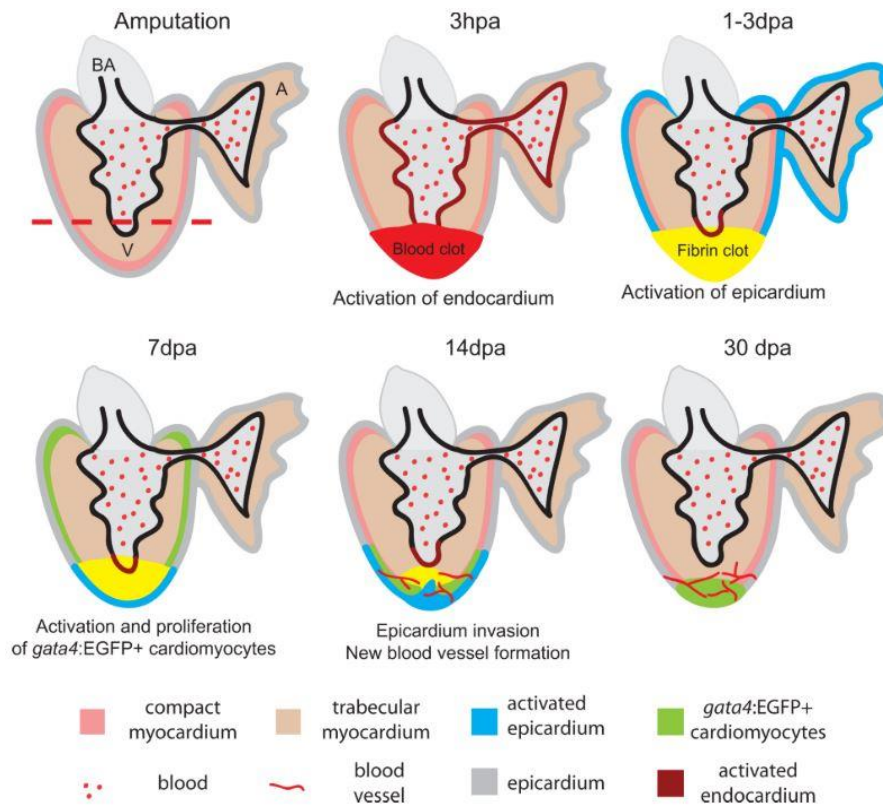
subepicardial population of *gata4* expressing cardiomyocytes were found to preferentially contribute to myocardial regeneration (Figure I 11) (Gupta et al., 2013).

Cardiomyocytes in the wound edge receive numerous signals from non-myocardial cells that induce their proliferation. Some of these discovered signals which cardiomyocytes are exposed to, are: Pdgf, RA, Igf, Shh, Tgf $\beta$  ligands, BMP, Nrg1, and Notch signaling (Chablais and Jazwinska, 2012; Choi et al., 2013; Gemberling et al., 2015; Huang et al., 2013; Kikuchi et al., 2011b; Kim et al., 2010; Münch et al., 2017; Wu et al., 2016). All these signals are secreted from the epicardium, epicardial derived cells (EPDCs), the endocardium, and circulating cells. An important factor secreted by circulating cells are inflammatory cytokines which are suggested to induce the activation of the NF- $\kappa$ B signaling in cardiomyocytes during regeneration. The blockade of this signaling pathway blocks cardiomyocyte proliferation and differentiation, and impairs epicardial regeneration (Karra et al., 2015). Another cardiomyocyte autonomous signal that induces cardiomyocyte proliferation during regeneration process is Brg1. Xiao et al. demonstrated that Brg1 increases DNA methylation in collaboration with Dnmt3ab, which prevents the expression of cyclin-dependent kinase inhibitors (Xiao et al., 2016). The contribution of additional epigenetic mechanisms to cardiac regeneration needs further study.

The pro-regenerative role of nerves have been recently described (Mahmoud et al., 2015). Nerves are present in the surface of the ventricle, and upon injury are known to regrow to the regenerated area. Mahmoud et al. described that the overexpression of *semaphorin3aa*, a neural chemorepellent, by cardiomyocytes inhibited innervation and subsequently reduced cardiomyocyte proliferation and impaired regeneration. They subsequently validated the results by a chemical inhibition of cholinergic but not adrenergic signaling, which also impaired cardiac regeneration. In addition, nerve production of Nrg1, but not acetylcholine, stimulate cardiomyocyte proliferation upon injury (Mahmoud et al., 2015). Another study identified that zebrafish Nrg1 is produced in perivascular cells rather than nerves, and is necessary and sufficient to induce cardiomyocyte proliferation (Gemberling et al., 2015). In general, many studies have

## 1. INTRODUCTION

been centered to decipher the signals produced during regeneration that induce cardiomyocyte proliferation.



**Figure I 11 | Summary of events during zebrafish heart regeneration.**

The process begins at amputation; time points of 3 hours post amputation (hpa) and 1–3, 7, 14 and 30 days post amputation (dpa) are illustrated. The amputation plane is marked by a red dashed line. Right after amputation, a blood clot (red) forms. Within hours, the endocardium (brown) is activated and shows morphological and gene expression changes. At 1–3dpa, the blood clot becomes a fibrin clot (yellow). The activated *raldh2* expression in endocardium becomes localized to the injury site (brown). At the same time, the epicardium (blue) is activated and expresses embryonic markers. At 7dpa, the epicardium encloses the apex and starts to invade the fibrin clot while a population of *gata4:EGFP* positive cardiomyocytes appears at the sub-epicardium and begins to proliferate. At 14dpa, the *gata4:EGFP* positive cardiomyocytes localize to the apex and newly formed blood vessels vascularize the newly formed myocardium. By 30dpa, the myocardium is almost fully regenerated. The new blood vessels vascularize the new myocardium. A, atrium; V, ventricle; BA, bulbus arteriosus. Adapted from Lien et al., 2012.

### 1.4.4.2. Epicardial contribution

During the regeneration process, epicardium is activated as early as 1-2dpa (Figure I 11) and expresses embryonic epicardial markers such as *raldh2*, encoding for retinoic acid (RA), and *tbx12*, a T-box transcription factor (Kikuchi et al., 2011b).

Epicardial proliferation studies revealed that epicardial cells proliferate from 3 to 7dpa, and that at 14dpa activated epicardial cells are localized at the injured apex (Lepilina et al., 2006).

There was a considerable interest to study the contribution of epicardium in zebrafish heart regeneration, due to numerous evidence from mouse studies suggesting that epicardium gave rise to a population of cardiomyocytes during cardiac development and after injury (Cai et al., 2008; Katz et al., 2012; Zhou et al., 2008). The first description of epicardial activation during zebrafish heart regeneration suggested that epicardial cells revascularize the injured area (Lepilina et al., 2006). However, fate-mapping experiments of cells expressing *tcf21*, which labels epicardial cells and a population of cardiac fibroblasts, demonstrated that epicardium gives rise to perivascular cells, but not to cardiomyocytes, endothelial cells, or smooth muscle cells (Kikuchi et al., 2011a). This finding was further supported by an alternative approach based on tissue transplantation. This study demonstrated that epicardial cells infiltrate into the damaged area and differentiate into myofibroblasts and perivascular cells, but not into cardiomyocytes or coronary endothelium (González-Rosa et al., 2012).

The formation of new blood vessels is another important event during zebrafish regeneration (Figure I 11). Animals lacking well-established vascular network, through *cxcr4a* knock-out, were unable to completely regenerate (Harrison et al., 2015). Pointing in the same direction, Marín-Juez et al. showed, using cryoinjury, that revascularization starts at 15hpi near the wound region. They showed that the inhibition of revascularization through the expression of a dominant negative form of *vegfaa* reduces cardiomyocyte proliferation and blocks regeneration (Marín-Juez et al., 2016).

#### **1.4.4.3. Endocardial contribution**

After amputation, endocardial cells are known to activate even faster than epicardial cells, as early as 1 hour post-amputation (hpa) (Figure I 11). Transmission electron microscopy helped to observe that endocardial cells near to the amputation plane, which have elongated nuclei and thin cell bodies attached to cardiomyocytes,

## 1. INTRODUCTION

round up and detach (Kikuchi et al., 2011b). After activation, endocardium proliferates and quickly regenerates to cover internally the wound. Münch et al. studied the recovery of endocardium following cryoinjury, and observed endocardial proliferation surrounding the wound between 3 and 5dpi, prior to the cardiomyocyte proliferation peak at 7dpi (Bednarek et al., 2015; Münch et al., 2017). Endocardium also expresses embryonic genes such as *raldh2* and recently it has been demonstrated that endocardial maturation is Notch-dependent, as mature endocardial cells in the injured area are reduced upon Notch inhibition (Münch et al., 2017).

Research done in epicardium and endocardium field indicate that both have important roles for cardiac regeneration in zebrafish. However, it is still unclear their molecular interaction with cardiomyocytes and more studies about how their organ-wide activation is triggered need to be done.

### **1.4.4.4. Immune cell contribution**

Independently of the method used to induce an injury to the zebrafish heart, an early inflammatory response is induced. Inflammatory cytokines and other molecules mediate the recruitment of phagocytes and neutrophils to the injury site, as soon as 3 hpi (Huang et al., 2013). Although we still miss a lot of understanding of the inflammation process, there are several evidences that point out that the early inflammatory response is essential for cardiac regeneration in zebrafish. Treatment with anti-inflammatory drugs and chemical depletion of phagocytes and neutrophils block regeneration through an impairment of revascularization and cardiomyocyte proliferation, promoting an accumulation of a fibrotic scar (de Preux Charles et al., 2016; Huang et al., 2013). In agreement with these results, leukocyte recruitment impairment due to a low activation of cytokines by inhibited matrix metalloproteinases (MMPs) also impairs regeneration (Xu et al., 2018). Not only seems important the recruitment of immune cells into the injury site, but also the time when they are recruited. Lai et al. treated regenerating zebrafish hearts with clodronate liposomes, an established method to deplete macrophages, in order to delay macrophage recruitment. They observed that this delay compromises revascularization, neutrophil clearance,



cardiomyocyte proliferation, and scar clearance (Lai et al., 2017). Furthermore, they also observed that the restoration of macrophage recruitment in medaka fish, which fail to regenerate the heart, can improve regenerative responses (Lai et al., 2017). Not only leukocytes have been demonstrated to be essential in the regeneration process, but also  $T_{reg}$  cells. Conditional ablation of  $T_{reg}$  cells block different organ regeneration in zebrafish, such as heart, spinal cord and retina (Hui et al., 2017).

As expressed in the previous three sections, numerous factors required for zebrafish heart regeneration have been identified. Still, it is essential to uncover other pathways that induce cardiomyocyte proliferation after injury in order to understand all the mechanisms governing zebrafish heart regeneration. Several transcriptomic and proteomic strategies have been used to characterize it (Lien et al., 2006; Ma et al., 2018; Sleep et al., 2010; Wang et al., 2013). Recently, Wu et al. realized a transcriptomic analysis of different regions of the cryoinjured heart with TomoSeq (Wu et al., 2016). They analyzed the transcripts expressed in the injured zone, in the border zone, and in the uninjured myocardium.

## **1.5. EXTRACELLULAR MATRIX IN ZEBRAFISH HEART REGENERATION**

Collagens, proteoglycans and glycoproteins form a complex structure, the ECM, which provides structural and mechanical support to tissues. In addition to its structural role, the ECM also instructs neighboring cells through biochemical and biomechanical signals, resulting in distinct biological responses (Hynes, 2014; Kim et al., 2011). Indeed, the composition and mechanical properties of the ECM play crucial roles modulating proliferation, migration, differentiation, and apoptosis (Le A. Trinh and Stainier, 2004; Lu et al., 2011). Studies using artificial ECM scaffolds have showed that physical properties of the ECM such as pore size, stiffness, fiber diameter, and chemical crosslinking also have effects on cell fate (Guilak et al., 2009; Yahalom-Ronen et al., 2015). For instance, substrate stiffness induced myoskeleton reorganization, thus determining the cell shape of rat and mice neonatal cardiomyocytes, whereas

## 1. INTRODUCTION

dedifferentiation of neonatal cardiomyocytes and enhanced proliferation occurred in compliant matrices (Yahalom-Ronen et al., 2015). ECM remodeling is an important factor to control processes such as development, wound healing and disease states like cancer (Bonnans et al., 2014; Dobaczewski et al., 2010; Jessen, 2015; Lu et al., 2012, 2011).

The role of the ECM during zebrafish heart regeneration has received little attention thus far. Gene expression analyses performed in regenerating hearts identified transcripts encoding ECM-related proteins among the most differentially expressed during this process (Lien et al., 2006; Mercer et al., 2013; Sleep et al., 2010). These included inhibitors of metalloproteinases, matrix metalloproteinases, and tenascin C (*tnc*), *tnc* transcripts being found overexpressed in the border zone between the healthy myocardium and the injury site (Chablais et al., 2011; Sallin et al., 2015). Another study showed that fibronectin (*fn*) synthesis by epicardial cells was essential for zebrafish heart regeneration, probably by providing cues for cardiomyocyte migration (Wang et al., 2013). A role of hyaluronic acid (HA) signaling during zebrafish heart regeneration has also been proposed, because components of this pathway were found expressed in response to injury, and blocking HA signaling impaired regeneration (Missinato et al., 2015). These three ECM components (*tnc*, *fn*, and HA) have been shown to form a pro-regenerative matrix in newt heart (Jaźwińska and Sallin, 2016; Mercer et al., 2013). Moreover, *collagen 1a2* and *collagen 12* have also been found in the regenerating ECM of zebrafish heart (Marro et al., 2016). Recently, Chen et al. examined the therapeutic potential of the regenerating zebrafish ECM by injecting purified ECM into infarcted mice (Chen et al., 2016), which induced cardiomyocyte proliferation and improved cardiac function. Others have centered their studies on the ECM-producing cells and defined them as key players in the regenerative process (Sánchez-Iranzo et al., 2018).

Another fascinating thing in zebrafish heart regeneration is how fibrosis promotes cardiac regeneration, while, in mice, fibrosis seems to be a detrimental element. Recently Gamba et al. characterized the collagenolytic activity induced after

zebrafish ventricle cryoinjury (Gamba et al., 2017). They detected an increase of collagenolytic activity in the injury area around 14-30dpi. This collagenolytic activity overlapped with collagen deposition areas, and coincided with the expression of several matrix metalloproteinases, such as *mmp2* and *mmp14a*. Thus, a comprehensive study of the zebrafish heart ECM composition, characteristics, and degradation may reveal other key points in the heart regeneration process.

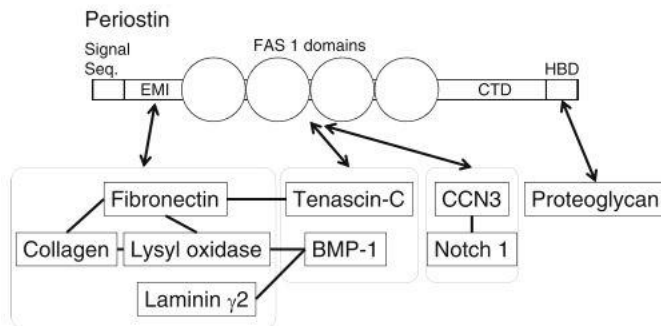
### 1.5.1. Periostin

Periostin is a 90 kDa matricellular protein originally named as osteoblast-specific factor 2 (Osf-2) (Horiuchi et al., 1999; Sugiura et al., 1995). Matricellular proteins are non-structural extracellular macromolecules which are rapidly turned over and have regulatory roles (Frangogiannis, 2012). Periostin is structurally composed of a secretory signal peptide, an amino-terminal cysteine-rich EMI domain, a tandem repeat of four fascilin-like-1 (FAS1) domains, and a carboxyl-terminal domain (CTD) (Horiuchi et al., 1999; Kudo, 2011). The sequence from the CTD varies as a result of alternative splicing (Figure 12) (Hoersch and Andrade-Navarro, 2010). Its EMI domain is responsible for binding to fibronectin (Kii et al., 2016), and the FAS1 domains bind to tenascin-C (Kii et al., 2009), CCN3 (Takayama et al., 2017) and integrins  $\alpha\beta3$  and  $\alpha\beta5$  (Gillan et al., 2002). Through its multiple domains, periostin have been suggested to act as a scaffold of assembly of numerous ECM proteins (type I collagen, fibronectin, tenascin-C, and laminin  $\gamma2$ ) and accessory proteins (BMP-1 and CCN3) allowing the generation of complex ECM meshworks. Thus, periostin structure allows the interaction between proteins by putting them in a close proximity. It has been demonstrated that periostin regulates cell adhesion, motility, cell differentiation and organization of ECM (Gillan et al., 2002; Horiuchi et al., 1999; Kii et al., 2009; Maruhashi et al., 2010).

In physiologic conditions, periostin has been described in mouse and human samples. It is located in collagen-rich regions such as periodontal ligament (Horiuchi et al., 1999; Rios et al., 2005; Suzuki et al., 2004), periosteum (Horiuchi et al., 1999; Rios et al., 2005), cardiac valves (R. a. Norris et al., 2009; R. A. Norris et al., 2009) and alveolar wall in the lung (Bozyk et al., 2012; Kondoh et al., 2016). In pathologic conditions,

## 1. INTRODUCTION

periostin have been identified as an important molecule in severe diseases gathered in Figure I 13. Some of the pathophysiological conditions in which periostin is found are infarcted myocardium (Oka et al., 2007; Shimazaki et al., 2008), fibrosis (Ishikawa et al., 2014; Naik et al., 2012; Uchida et al., 2012), tissues undergoing wound healing (Nishiyama et al., 2011; Norris et al., 2007; Ontsuka et al., 2012), and cancer-associated stroma (Conway et al., 2014; Nitsche et al., 2016; Qin et al., 2016; Sung et al., 2016; Tian et al., 2015; Underwood et al., 2015). Taking all these conditions together, there is a correlation between periostin and tissue regeneration (Conway et al., 2014). Recently, some reports relate periostin function with stem cell biology. Khurana et al. have reported that periostin regulates hematopoietic stem cells (HSC) maintenance via interaction with integrin- $\alpha$ v (Khurana et al., 2016). At the same time, Tanaka et al. showed that periostin secreted by stromal cells support hematopoietic progenitor cells and leukemia-initiating cells (Tanaka et al., 2016). The association of periostin with the matricellular protein CCN3 have further strengthen the role of periostin in stemness. There are studies demonstrating the role of CCN3 in regulating HSC and hematopoietic progenitor cells (Horiguchi et al., 2009; Ishihara et al., 2014).



**Figure I 12| Periostin interacts with multiple extracellular proteins.** The interactions of periostin with the extracellular/secretory proteins are depicted based on the multi-domain structure of periostin. CTD; carboxyl-terminal domain, HBD: heparin-binding domain. From Kudo, 2017.

Factors that are known to induce periostin expression are TGF- $\beta$ , and Th2 cytokines, IL-4 and IL-13, that can enhance periostin expression more effectively than TGF- $\beta$  (Sidhu et al., 2010; Takayama et al., 2006).

Periostin function has been further studied and it has been determined to be involved in many processes such as collagen crosslinking, fibronectin secretion, matrix metalloproteinase secretion, macrophage migration, and proliferation induction (Kii et

al., 2016; Kühn et al., 2007; Maruhashi et al., 2010; Oka et al., 2007; Tanabe et al., 2010; Yokota et al., 2017). Regarding collagen cross-linking, periostin promotes the proteolytic activation of lysyl-oxidase (LOX), an enzyme responsible for cross-link formation. Periostin does not exert this action directly, but through its binding to BMP-1, a protease that directly activates LOX (Maruhashi et al., 2010). Recently, it has been also demonstrated that periostin interacts with fibronectin in the endoplasmic reticulum (ER) to enhance its solubility and prevent its aggregation. Thus, periostin interacts with fibronectin in order to promote fibronectin secretion from the ER (Kii et al., 2016). Periostin does not only promote fibronectin secretion but also matrix metalloproteinase and Notch1 secretion (Tanabe et al., 2010). In terms of cell migration, periostin induces cardiac fibroblast migration through engagement with integrin  $\alpha\beta3$  (Oka et al., 2007; Shimazaki et al., 2008). It has also been shown to be produced in the lesion of a spinal cord injury promoting macrophage migration for scar formation (Yokota et al., 2017). The more controversial role of periostin is the induction of cardiomyocyte proliferation. Khun et al. proved that periostin induced proliferation of differentiated cardiomyocytes after myocardial injury in rats, improving ventricular remodeling and myocardial infarction (Kühn et al., 2007). However, others did not observe the same effects on cardiomyocyte proliferation and regeneration in the adult heart (Lorts et al., 2009; Taniyama et al., 2016).

It is proposed a new periostin action named “Periostin Switch”, which explains why periostin may have so many roles. C-terminal cleavage of periostin protein acts as a switch of differentiating between initial and late periostin functions (Kudo, 2017). In early stages, periostin will promote cell proliferation, migration, and collagen production; while after the C-terminal cleavage, collagen cross-linking would be induced.

#### **1.5.1.1. Periostin in myocardial infarction**

In the heart, periostin is expressed during embryogenesis at early stages; but, it is not detected in the normal adult heart, in exception of the valves (Kruzynska-Frejtag et al., 2001; Norris et al., 2007). As stated in some of the above examples, periostin has

## 1. INTRODUCTION

been described to be synthesized during myocardial infarction in humans and in rodent models of myocardial infarction (Oka et al., 2007; Shimazaki et al., 2008; Stanton et al., 2000). Quite are the studies done regarding periostin and myocardial infarction. Mice *postn*<sup>-/-</sup> were demonstrated to have reduced fibrosis and hypertrophy after myocardial infarction. Paradoxically, other studies showed the role of periostin in myocardial regeneration in adult and neonatal mice (Chen et al., 2017; Shimazaki et al., 2008). *postn*<sup>-/-</sup> adult mice had impaired cardiac healing with increased cardiac rupture due to reduced myocardial stiffness (Shimazaki et al., 2008). Moreover, myocardial regeneration process of *postn*<sup>-/-</sup> neonatal mice was suppressed with a reduction of the PI3K/GSK3 $\beta$ /cyclin D1 signaling pathway (Chen et al., 2017). Thus, the role of periostin in myocardial infarction still needs further investigation.

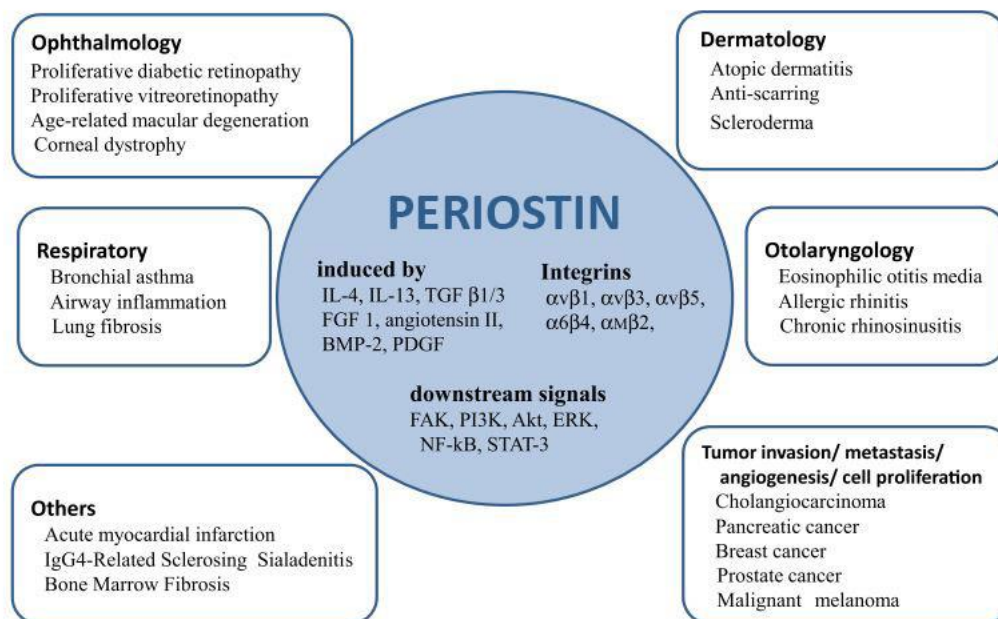
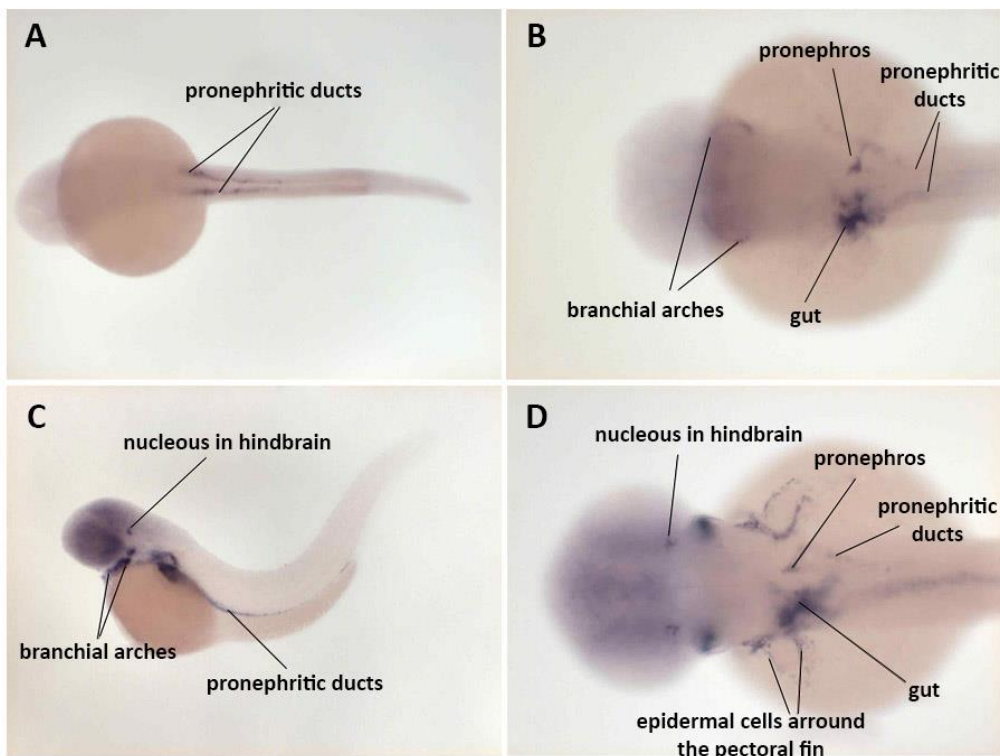


Figure I 13 | Periostin and associated diseases. From Kudo, 2017.

### 1.5.1.2. Homology between species

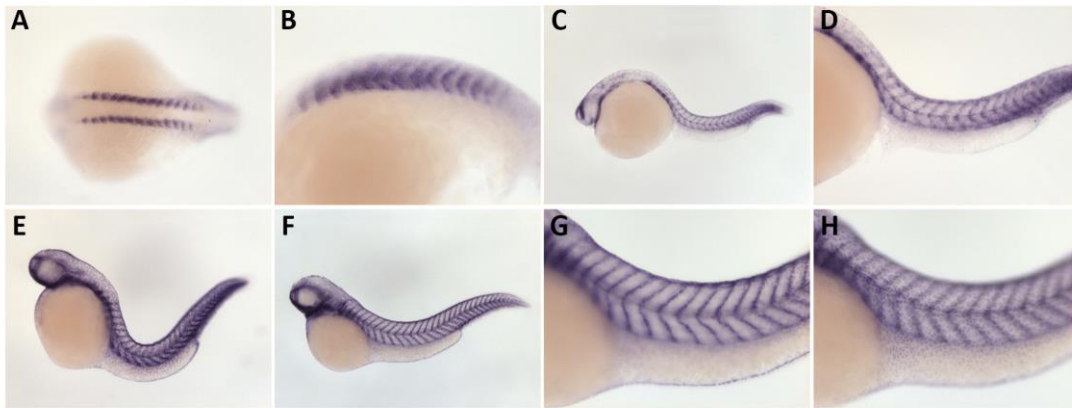
The mouse and human periostin genes maintain a homology of 90% in the amino acid sequence mature form (814aa). The mouse periostin gene is located in chromosome 3, while the human is in the chromosome 13, consisting both genes of 23 exons. In zebrafish though, the genomic homology lowers to 57% when comparing it to

mouse or human genes. As mentioned above, periostin is one of those genes that suffered the teleost genomic duplication, so in the zebrafish genome there are two periostin genes: periostin A, in chromosome 10, and periostin B, in chromosome 15. The former forms a 1016aa protein, and the latter with 26 exons suffers from alternative splicing giving rise to two isoforms, isoform 1 (756aa) and isoform 2 (782aa). The zebrafish periostin contains the four conserved FAS1 domains, and a newly found C-terminal repeat sequence (5 or 6 repeats of 13aa) characteristic of zebrafish periostin (Kudo et al., 2004). The embryonic expression of zebrafish paralogs was well described by Tessie et al. (Thisse et al., 2001; Thisse and Thisse, 2005) by whole mount *in situ* hybridization (Figure I 14 and Figure I 15). Periostin A is conferred to the nephritic system, gut, epidermis, one nucleus in hindbrain, and some pharyngeal arches (Figure I 14). Instead, Periostin B is expressed in the somites, epidermis, and myotomes (Figure I 15). Since they have completely different expression patterns, we believe that the function for each gene would be specific and diverged from the other paralog.



**Figure I 14 | Periostin A expression during development.** *postna* expression at different stages: (A) 20-25 somites – Prim5 (19-24h); (B) Prim 15 – Prim 25 (30-36h); and (C and D) Highpec – Longpec (42-48h).

## 1. INTRODUCTION



**Figure I 15 | Periostin B expression during development.** *postnb* expression at different stages: (A and B) 14-19 somites (16h); (C and D) 20-25 somites – Prim5 (19-24h); (E) Prim 15 – Prim 25 (30-36h); and (F-H) Highpec – Longpec (42-48h). (A and B) Expression in the somites and (C-H) expression in the epidermis and somites/myotomes.



## **2. OBJECTIVES**



The general objectives of the present thesis were to:

1. Determine which are the ECM proteins differentially expressed during zebrafish heart regeneration.
2. Determine the importance of *postnb* during zebrafish heart regeneration.

To pursue the mentioned objectives, the specific objectives were the following:

Objective 1:

- 1.1 Characterize the decellularization protocol used to enrich the sample with ECM proteins.
- 1.2 Perform a proteomic analysis of the matrisome of the zebrafish heart and its changes during heart regeneration.

Objective 2:

- 2.1 Characterize the expression of *postnb* during cardiac regeneration.
- 2.2 Generate a conditional shRNA expressing knock-down transgenic zebrafish line for *postnb*.
- 2.3 Generate a knock-out *postnb* line using CRISPR-Cas9 technology.
- 2.4 Determine if *postnb* is needed for zebrafish heart regeneration.
- 2.5 Study the processes in which *postnb* is needed for a correct cardiac regeneration.



# **3. MATERIALS AND METHODS**



### 3.1. ZEBRAFISH BREEDING AND HUSBANDRY

All the experiments performed in this work have been conducted according to the procedures approved by the Ethics Committee on Experimental Animals of the Barcelona Science Park and the Barcelona Biomedical Research Park.

Adult zebrafish between 3 and 18 months old were used to conduct all the experiments. They were maintained in a density of 3 fish/liter, according to the standard methodology (Westerfield, 2000). The zebrafish have been maintained in tanks in a 28.5°C closed system, and have been feed 2 times per day with fish food (SDS, Essex, UK), and 2 times per day with *Artemia salina*.

In this work, we have used wild type AB (ZIRC\_ZL1) and the following transgenic strains:

- Tg(bactin2:Cre-ERT2). Previously created in our laboratory.
- Tg(Periostin:Citrine). Kindly ceded by Nadia Mercader, CNIC, Madrid (Sánchez-Iranzo et al., 2018).
- dTg((bactin2:Cre-ER)(bactin2:lrl-Act-sh379-GFP)). Created in this thesis.
- dTg((bactin2:Cre-ER)(bactin2:lrl-Act-sh79-GFP)). Created in this thesis.
- dTg((bactin2:Cre-ER)(bactin2:lrl-Act-shAB-GFP)). Created in this thesis.
- PostnB<sup>-/-</sup>. Created in this thesis.

### 3.2. VENTRICULAR AMPUTATION SURGERY

In order to study cardiac regeneration, we used the ventricular amputation protocol (Raya et al., 2003). Following this protocol, zebrafish were anaesthetized with tricaine. The sedation grade was determined pinching the caudal fin with tweezers, starting the experiment as soon as the animals did not respond to the stimulus. Next, the fish were arranged in a sponge previously moistened with the ventral face of the animal upwards to make it accessible to manipulation. Once the heart area was located with the help of a binocular magnifier, the scales of the surface were teared by means of microdissection tweezers and a small aperture was ripped through the body wall and

### 3. MATERIALS AND METHODS

the pericardial sac, without damaging the heart. With the help of curved microdissection tweezers, the incision was opened and, with iridectomy scissors on the other hand, pressure on the abdomen of the fish was applied to force the ventricle to protrude. Once the ventricle was on the surface of the fish, the ventricle apex was clamped and the amputation of the ventricle's apex was finally performed with iridectomy scissors (~20% of the ventricular volume). In order to stop the initial bleeding, the wound was pressed with a tip made of absorbent paper.

Once the surgery was completed, the animals were returned in a tank with aquarium water and they were recovered from the anesthetic by pipetting water to the gills until a reestablishment of the mobility of the operculum was observed, and the animal began to swim normally. Later, the tanks were introduced to the aquarium system. As a control of the procedure, a sham intervention was performed. This consists in the opening of the pericardial sac without causing any ventricular injury and returning the fish back to its tank.

#### Solutions and material

**Tricaine** (anaesthetising solution): 4.2ml of 0.4% tricaine (A5040, Sigma) in 100ml of aquarium water (final concentration of 0.02%).

**Iridectomy scissors:** Moria Pascheff-Wolff Spring Scissors (ref. 15371-92).

**Microdissection tweezers:** Dumount #5 – fine forceps (ref. 11254-20).

**Curved microdissection tweezers:** Dumount #5/45 forceps (ref. 11251-35).

### 3.3. EdU LABELLING

For pulse-chase experiments with EdU, zebrafish that had previously undergone ventricular amputation surgery were anaesthetized with tricaine and were injected intraperitoneal with 20µl EdU with the help of a Hamilton syringe. The injection of EdU was repeated daily between the days 7 and 14 after the amputation.



Solutions and reagents

**Tricaine** (anaesthetizing solution): 4.2ml of 0.4% tricaine (A5040, Sigma) in 100ml of aquarium water (final concentration of 0.02%).

**EdU solution:** 2.5mg/ml of EdU (900584, Sigma) in PBS.

### 3.4. CARDIAC TISSUE COLLECTION

Regenerating hearts at different time points (1, 3, 7, 14 or 30dpa) were collected for further analysis. Fishes were slaughtered by submerging them 10min in an overdose of tricaine, and 20 $\mu$ l heparin were intraperitoneally injected with a 27G needle to prevent blood coagulation.

In order to collect the hearts, the fish were positioned on a wet sponge with the ventral face of the animal upward to make it accessible to manipulation. Once the heart area was located with the help of a binocular magnifier, the scales of the surface were teared by means of microdissection tweezers and an aperture was ripped through the body wall and the pericardial sac, without damaging the heart. Once the heart was visible, the atrium was carefully separated from the sinus venosus and the heart was extracted by taking the outflow tract with the help of microdissection tweezers and pulling all the heart out of the cardiac cavity. Once extracted, the hearts were cleansed in a solution of PBS with heparin to minimize blood clotting.

Solutions and material

**Tricaine** (euthanizing solution): 20ml of 0.4% tricaine (A5040, Sigma) in 100ml of aquarium water (final concentration of 0.08%).

**Heparin solution:** 1,000U/ml heparin (H3149, Sigma) in PBS.

**Cleaning solution:** 100U/ml heparin (H3149, Sigma) in PBS.

**Microdissection tweezers:** Dumount #5 – fine forceps (ref. 11254-20).

#### 3.5. SAMPLE PROCESSING

Once extracted, hearts were fixed over-night with PFA at 4°C, washed 3 times with PBS, balanced with 30% sucrose over-night, and frozen in OCT (Tissue-Tek) to cryosect. For immunohistochemistry and stainings hearts were cut at 10µm and for in situ hybridization at 16µm with a Leica CM3050S cryostat. For *in situ* zymography hearts were not fixed with PFA but fast frozen, dipping in cold isopentane, the sample embedded in OCT. Hearts were then cryosected at 25µm. The sections were positioned in series over 5-10 Superfrost Plus slides (Fisher Scientific), so in each slide there was a whole-hearted representation. The sections were dried over-night at RT and subsequently stored at -20°C until used.

##### Solutions and reagents

**PFA:** 4% PFA (Electron Microscopy Sciences) in MQ-H<sub>2</sub>O.

**30% Sucrose:** 30% sucrose (S1888, Sigma) in PBS.

#### 3.6. IMMUNOHISTOCHEMISTRY

For immunofluorescence detection of proteins in tissues, sections were thawed and let dry one night before, and an antigen retrieval treatment was performed with a sodium citrate buffer (pH8.5) or pH9 Target retrieval solution for 40min at 80°C in a decloaking chamber (Biocare Medical). Sections were washed 3x5min 1xTBS, and the non-specific junctions blocked with blocking solution. Subsequently, the sections were incubated over-night at 4°C with the desired primary antibodies dissolved in TBS++ solution. After performing 3x5min TBS++ washes, samples were incubated for 2h at 37°C with the desired secondary antibodies dissolved in TBS++ solution. Finally, samples were washed 3x5min with TBS; self-fluorescence of the tissue was decreased by treating the samples with Sudan Black 4min at RT; samples were again washed 3x5min with 1xTBS; and counter stained with 1:10,000 DAPI 10min at RT. Lastly, the stains were preserved with mounting medium at 4°C.

Table MM 1 summarizes the primary antibodies used in this work.

**Table MM 1 | List of primary antibodies.**

Antibody	Species	Isotype	Clonality	Dilution	Reference
Myosin heavy chain (MF20)	Mouse	IgG2b	Polyclonal	1:1	MF20 supernatant, DSHB
$\alpha$ -sarcomeric actin (ASA)	Mouse	IgM	Polyclonal	1:400	A2172, Sigma
Periostin	Rabbit	IgG	Polyclonal	1:150	NBP1-59151, Novus Biol.
PeriostinB	Rabbit	IgG	Polyclonal	1:500	A. Kudo's lab (Itou et al., 2014)
Vimentin	Mouse	IgM	Polyclonal	1:20	40E-C, DSHB
FITC/Oregon-AlexaFluor 488	Goat	IgG	Polyclonal	1:100	A11096, Invitrogen

Table MM 2 summarizes the secondary antibodies used in this work.

**Table MM 2 | List of secondary antibodies.**

Antibody	Species	Conjugated	Dilution	Reference
Mouse IgG	Donkey	AlexaFluor 488	1:200	715-545-151, Jackson
Mouse IgG	Donkey	Cy3	1:200	715-165-151, Jackson
Mouse IgG	Donkey	AlexFluor 647	1:200	715-605-151, Jackson
Mouse IgM Fcmu spec	Donkey	Cy3	1:200	715-165-140, Jackson
Mouse IgM Fcmu spec	Donkey	Cy2	1:200	715-225-140, Jackson
Rabbit IgG	Donkey	AlexaFluor 488	1:200	711-545-152, Jackson
Rabbit IgG	Donkey	Cy3	1:200	711-165-152, Jackson

### Solutions and reagents

**Sodium citrate buffer:** sodium trihydrate 10mM (C8532, Sigma) in MQ-H<sub>2</sub>O. Adjust pH at 8.5.

**pH9 Target retrieval solution:** dilute 1/10 the 10x pH9 target retrieval solution (S2367, Dako) in MQ-H<sub>2</sub>O.

**TBS 10x:** 1M Tris HCl (T3253, Sigma), 160mM Trizma base (T6791, Sigma) and 1.5M NaCl (S7653, Sigma) in dH<sub>2</sub>O. Adjust pH at 7.4-7.5. To prepare 1x TBS make a 1/10 dilution of 10x TBS in dH<sub>2</sub>O.

**Blocking solution:** 1x TBS with 0.5% Triton X-100 (X100, Sigma) and 3% Donkey serum (S30-100ml, Chemicon).

**TBS++ solution:** 1x TBS with 0.1% Triton X-100 (X100, Sigma) and 3% Donkey serum (S30-100ml, Chemicon).

**Sudan Black:** 1% Sudan Black (252069, Panreac) in 70% ethanol.

### 3. MATERIALS AND METHODS

**DAPI:** Rehydrate with 2ml of filtered dH<sub>2</sub>O the DAPI compound (D21490, Invitrogen) to have a solution of 5mg/ml. As working solution use a 1:10,000 dilution in TBS 1x.

**Mounting medium:** 56mM Glycine (G7126, Sigma), 5mM NaOH (S8045, Sigma), 87mM NaCl (S7653, Sigma), 4.6mM Sodium azide (S2002, Sigma), 0.23M Propyl gallate (P3130, Sigma) and 70% Glycerol (G9012, Sigma) in dH<sub>2</sub>O. Dissolve the reagents with heat, maximum 40°C.

#### 3.6.1. EdU signal development

EdU signal development was done using the Click-It EdU Alexa Fluor 488 or 555 Imaging kit (C10337 or C10338, ThermoFisher). An immunohistochemistry protocol was followed with some modifications. After the antigen retrieval, samples were blocked with blocking solution for 1h, washed 3x5min with 1xTBS, and incubated with the Click-It reaction cocktail for 30min at RT. Then, samples were washed again 3x5min with TBS, and blocked a second time with blocking solution for 1h. At this point, the immunohistochemistry was continued as usual after the blocking step.

##### Solutions and reagents

**Blocking solution:** 1x TBS with 0.5% Triton X-100 (X100, Sigma) and 3% Donkey serum (S30-100ml, Chemicon).

**Click-It reaction cocktail:** for 1ml preparation. All the reagents are from the kit. 860µl 1x Click-iT<sup>®</sup> reaction buffer (1/10 dilution in dH<sub>2</sub>O of the component D), 40µl of CuSO<sub>4</sub> (Component E), 2.5µl Alexa Fluor<sup>®</sup> azide (component B, AF488 or AF555 upon interest) and 100µl of reaction buffer additive (1/10 dilution in dH<sub>2</sub>O of the component F).

#### 3.6.2. TUNEL staining

The TUNEL signal development was done using the In situ Cell Death Detection Kit POD (11684817910, Roche). An immunohistochemistry protocol was followed with

some modifications. For TUNEL detection, no antigen retrieval was performed. Slides were rinsed three 3x5min with 1xTBS, and treated 30min at RT with the solution 1. After rinsing again the slides 3x5min with 1x TBS, samples were treated 5min with the solution 2 and subsequently 15min in a proteinase K (PK) solution at RT. To stop the PK permeabilization, samples were rinsed twice with the solution 3 for 10min each. Then, a 10min equilibration in TdT buffer was done, and the development of the TUNEL signal was performed for 2h at 37°C with the In situ Cell Death Detection Kit POD (11684817910, Roche) following manufacturer instructions. To finish the TUNEL development, samples were rinsed twice with solution 4, and 2x10min with 1xTBS. Then, slides were blocked for 1h and, in the primary antibody incubation, an antibody anti-FITC/Oregon-AlexaFluor 488 conjugated (Invitrogen) was added to increase the TUNEL signal. Immunohistochemistry protocol was resumed after the blocking step.

#### Solutions and reagents

**Solution 1:** 0.2% Triton X-100 (X100, Sigma) and 0.05% Tween-20 (P1379, Sigma) in TBS 1x.

**Solution 2:** 10mM Tris-HCl (T3253, Sigma) and 5mM EDTA (EDS, Sigma) in dH<sub>2</sub>O. Adjust pH at 8.

**Protease K solution:** 20µg/ml Proteinase K (Quiagen), 10mM Tris-HCl (T3253, Sigma) and 5mM EDTA (EDS, Sigma).

**Solution 3:** 5mM EDTA (EDS, Sigma) in dH<sub>2</sub>O.

**TdT buffer:** 10mM Tris-HCl in dH<sub>2</sub>O adjust pH at 7.2 and add Sodium cacodylate (12310, Electron Microscopy Sciences) and Cobalt(II) chloride anhydrous (8025400010, Millipore) at 30mM and 0.02mM respectively.

**In situ cell death detection kit reaction solution:** for 50µl add 45µl nucleotide-FITC, 2.5µl enzyme and 2.5µl TdT buffer. Prepare 100µl for a whole slide and help with a pipette tip to extend the solution though the slide.

**Solution 4:** 3mM EDTA (EDS, Sigma), 150mM NaCl (S7653, Sigma) and 15mM Sodium citrate (W302600, Sigma).

**Blocking solution:** 1x TBS with 0.5% Triton X-100 (X100, Sigma) and 3% Donkey serum (S30-100ml, Chemicon).

#### 3.7. HEMATOXILIN AND EOSIN STAINING

For Hematoxilin and Eosin staining, sections were thawed and let dry one night before, and OCT was washed with a 5min immersion of dH<sub>2</sub>O. The sections were dyed for 5min with Harris Hematoxilin (253949.1612, Panreac), washed with running tap water for 5min, and the cytoplasms were destained by dipping the sections in a hydrochloric alcohol solution. After another washing with running tap water for 5min, the cytoplasms were stained with alcoholic eosin for 30sec. Once dyed, the sections were dehydrated with ethanol series (70%, 90%, 96% and 100%), dipped in Xylene (251769.2711, Panreac), and finally mounted with DPX (8312-4, Thermo Scientific). All dyes were pre-filtered before use.

##### Solutions and reagents

**Hydrochloric alcohol solution:** 1% hydrochloric acid solution in 70% ethanol.

**Alcohol eosin:** for 500ml, dissolve 5g Eosin yellowish (251299.1606, Panreac) in 75% ethanol. To prepare the working solution make a 1:4 dilution with 80% ethanol.

**Ethanol:** all ethanol solutions are prepared as a dilution with dH<sub>2</sub>O of absolute ethanol (251086.1214, Panreac).

#### 3.8. MASSON'S TRICHROME STAINING

For Masson's Trichrome staining, sections were were thawed and let dry one night before, and incubated over-night at RT in Bouin (254102.1611, Panreac). Then, the sections were washed with running dH<sub>2</sub>O for 10min, dyed 3min with Weigert Hematoxilin, washed subsequently with running tap water for 5min, and running dH<sub>2</sub>O for 3min. Then, the sections were immersed in a Xilidine Ponceau - Acid Fuchine solution for 2.5min, and incubated 5min with phosphotungic acid / phosphomolibdic acid solution. Sections were then washed 5min in running dH<sub>2</sub>O and dyed 3min with aniline blue solution. Finally, sections were incubated 2min in 1% acetic acid and washed 3min with running dH<sub>2</sub>O. Prior mounting the sections with DPX (8312-4, Termo Scientific) they

were dehydrated with 96% ethanol, 100% ethanol and Xylene (251769.2711, Panreac). All dyes were pre-filtered for use.

#### Solutions and reagents

**Weigert's Hematoxylin:** mix at equal volumes solution A (253453.1210, Panreac) and solution B (253454.1210, Panreac) of weigert Hematoxylin.

**Xilidine Ponceau - Acid Fuchine solution:** to prepare 300ml dissolve 2.7g of Biebrich scarlet (253986.1605 , Panreac), 0.3g Acid fuchsine (251331.1605, Panreac), 3ml Acetic acid glacial (1.00063.1000, Merck) in 300ml of dH<sub>2</sub>O.

**Phosphotungic acid / phosphomolibdic acid solution:** to prepare 400ml dissolve 10g of phosphotungic acid (79690, Sigma) and 10g of phosphomolibdic acid (79560, Sigma) in 400ml of dH<sub>2</sub>O.

**Aniline blue solution:** to prepare 300ml dissolve 7.2g of aniline blue (253708.1606 , Panreac) and 6ml Acetic acid glacial (1.00063.1000, Merck) in 300ml of dH<sub>2</sub>O.

**1% acetic acid solution:** to prepare 500ml mix 5ml of Acetic acid glacial (1.00063.1000, Merck) with 495ml of dH<sub>2</sub>O.

**Ethanol:** all ethanol solutions are prepared as a dilution with dH<sub>2</sub>O of absolut ethanol (251086.1214, Panreac).

### **3.9. PROBE SYNTHESIS FOR IN SITU HYBRIDIZATION**

Primers were designed in order to amplify a ~500bp region specific of the gene of interest and the PCR\* product was cloned into the pCR4-TOPO TA vector (450030, Life Technologies). The product was transformed in DH5α cells and colonies were sequenced to check the directionality of the PCR fragment. Then vectors were digested either with NotI (R0189S, New England BioLabs) or PstI (R0140S, New England BioLabs), depending on the direction of the PCR fragment. The probe was synthesized with the DIG RNA-labelling Mix (11277073910, Roche) and the T7 or T3 RNA polymerases (Roche), when digested with PstI or NotI, respectively. RNA probes were finally purified using the RNA clean and concentrator-5 (R1015, Zymo research).

### 3. MATERIALS AND METHODS

Table MM 3 shows primers used to amplify the region that was used as mold to synthesize the probes.

**Table MM 3 | Primers to amplify a *postna* and *postnb* region to generate the RNA probes**

Gene	Primer sequence (5'-3')
PostnA	Fw: 5'- TTGATGCTGGCGGAGAAATC -3'
	Rv: 5'- CTAAACTGGATCTCAGGGTC- 3'
PostnB	Fw: 5'- AGCCTACCATCACCAAAGTG -3'
	Rv: 5'- CACATAAGAGCACTTACACGTC -3'

#### Note

\*The PCR was performed with Phusion High-Fidelity DNA polymerase (F530S, ThermoFisher).

### 3.10. *IN SITU* HYBRIDIZATION IN CRYOSECTIONS

Zebrafish hearts were collected as above stated, and fixed over-night with 4% PFA. Then they were dehydrated and rehydrated with methanol series (25%, 50%, 75% and 100% methanol), washed with 1x PBS (P5493, Sigma) 3 times, balanced with 30% sucrose over-night, and frozen in OCT (Tissue-Tek) to cryosect. Hearts were cut at 16µm with a Leica CM3050S cryostat.

In situ hybridizations were performed with digoxigenin-labelled RNA probes synthesized as explained in the above section. Hybridization was performed over-night at 68°C for *postna* and *postnb* probes in Hybridization buffer (1:200 probe dilution). Slides were washed 4x30min in wash solution and then washed 3x30min in MABT solution. Blocking was performed for 4h in blocking solution and then the solution was changed for new blocking solution containing anti-DIG antibody (1:5,000; 11093274910, Roche). Antibody incubation was done at 4°C over-night. Slides were washed 5x30min with MABT, and 2x10min with AP staining buffer. Signal was developed in Poly(vinyl alcohol) solution containing NBT/BCIP (11681451001, Roche) over-night at 37°C. When the signal appeared, slides were washed twice with PBT, dehydrated with ethanol series



(75%, 96% and 100%) and Xylene (251769.2711, Panreac), and mounted in DPX (8312-4, Thermo Scientific).

### Solutions and reagents

**\*\*Make sure that all the solutions are nuclease free\*\***

**PFA:** 4% PFA (Electron Microscopy Sciences) in MQ-H<sub>2</sub>O.

**30% Sucrose:** 30% sucrose (S1888, Sigma) in PBS.

**Methanol:** all methanol solutions are prepared as a dilution with dH<sub>2</sub>O of methanol (1.06018.2500, Merck).

**10x salts solution:** 2M NaCl (S7653, Sigma), 100mM Tris HCl (T3253, Sigma), 10mM Tris Base (T6791, Sigma), 50 mM NaH<sub>2</sub>PO<sub>4</sub> (S8282, Sigma), 50mM Na<sub>2</sub>HPO<sub>4</sub> (S7907, Sigma) and 50mM EDTA (03690, Sigma). Dissolve in Sigma H<sub>2</sub>O (W4502, Sigma) and adjust pH at 7.4.

**Hybridization buffer:** 1x Salts (1/10 dilution of 10x salts solution), 50% deionized formamide (S4117, EMD Millipore), 10% dextran sulfate (D8906, Sigma), 1mg/ml yeast RNA (R6750, Sigma), 1x Denhardt's (D2532, Sigma).

**Wash solution:** 1x SCC (S6639, Sigma), 50% formamide (F7503 Sigma), 0.1% Tween-20 (P1379, Sigma).

**5x Maleic acid solution:** 0.5M maleic acid (8.00380, Sigma), 0.75M NaCl (S7653, Sigma). Dissolve in MQ-H<sub>2</sub>O and adjust pH at 7.5.

**MABT solution:** 0.1% Tween-20 (P1379, Sigma) and 1x Maleic acid solution (dilute 1:5 the 5x maleic acid solution). Dilute in MQ-H<sub>2</sub>O.

**Blocking reagent stock solution:** 10% Boehringer Blocking Reagent (11096176001, Roche) in 1x maleic acid solution. Heat to dissolve, autoclave, aliquot and store at -20°C.

**Blocking solution:** 20% Sheep serum (S3772, Sigma) and 2% Blocking reagent (from 10% blocking reagent stock solution) in MABT.

**AP (alkaline phosphatase) staining buffer:** 100mM NaCl (S7653, Sigma), 50mM MgCl<sub>2</sub> (M2393, Sigma), 100mM Tris-HCl pH9 (T3253, Sigma) and 0.1% Tween-20 (P1379, Sigma). Prepare a stock solution for each component in MQ-H<sub>2</sub>O.

### 3. MATERIALS AND METHODS

**Poly(vinyl alcohol) solution:** dilute 4g of Poly(vinyl alcohol) (341584, Sigma) in 40ml of AP staining buffer.

**PBT:** 0.1% Tween-20 (P1379, Sigma) in PBS.

#### 3.11. GENOMIC DNA EXTRACTION FROM EMBRYOS OR FINCLIPS

Genomic DNA was extracted by adding 100µl of 50mM NaOH to one embryo or a finclip. Samples were incubated at -20°C for 15min and then 5min at 95°C. To neutralize the NaOH, 10µl of Tris-HCl pH 7.5 was added. The resulting solution was used as input genomic DNA for genotyping PCRs.

In order to perform a finclip, the fish were anesthetized with tricaine and a portion of the caudal fin was cut with a blade. The fins were then processed as the embryos.

##### Solutions and reagents

**50mM NaOH:** NaOH (S8045, Sigma) was dissolved as a 50mM solution in MQ-H<sub>2</sub>O.

**Tris-HCl pH 7.5:** Tris-HCl (T3253, Sigma) was dissolved as a 1M solution in MQ-H<sub>2</sub>O. pH was adjusted with NaOH to 7.5.

**Tricaine** (anaesthetising solution): 4.2ml of 0.4% tricaine (A5040, Sigma) in 100ml of aquarium water (final concentration of 0.02%).

#### 3.12. RNA EXTRACTION

RNA was extracted from pools of 3-5 ventricles or 1-10 embryos following the Trizol/ chlorophorm protocol. Samples were homogenized with 1ml of TRI Reagent (TR-118, Molecular Research Center Inc.) and with a 25G needle. 200µl of chloroform (C2432, Sigma) were added, samples were vortexed intensely and let stand for 15min. After 15min of centrifugation at 12,000g at 4°C, the aqueous transparent phase was collected, mixed with the same volume of isopropanol (190764, Sigma) and let stand for 15min at RT. After 10min of centrifugation at 12,000g at 4°C, the pellet was washed with 1ml of 75% ethanol and centrifuged again. The pellet was let dry, making sure that all

the ethanol was evaporated and resuspended with 10-15 $\mu$ l of nuclease-free H<sub>2</sub>O (3098, Sigma). RNA was incubated at 55°C for 10min and stored at -80°C until further use.

### 3.13. cDNA SYNTHESIS

cDNA was synthesized ideally from 1 $\mu$ g RNA with Transcriptor First Strand cDNA Synthesis Kit (04379012001, Roche) using random hexamers, and following manufacturer's instructions.

### 3.14. qRT-PCR PRIMER DESIGN AND EFFICIENCY TEST

Primers for qPCR were designed with the help of the IDT PrimerQuest Tool (<https://eu.idtdna.com/PrimerQuest/Home/Index>). The characteristics of the chosen primers were the following: (1) ~50% GC content, (2) similar T<sub>m</sub> between forward and reverse primers, and (3) overlapping of at least one primer in an exon junction.

In order to calculate the efficiency of a new set of primers, we took a cDNA sample from a pool of embryos at 48hpf and did known concentrations. We generated a pattern line with the following cDNA dilutions: 5, 1, 0.5, 0.1, 0.05, 0.01 and 0.005ng/ $\mu$ l. A pattern line was plotted using the  $\Delta$ Ct values multiplied for 100 for each known concentrations. Known concentrations were plotted at the X-axis and the  $\Delta$ Ct values at the y-axis. The slope of the pattern line determined the efficiency of the primer pair and calculated with the qPCR Efficiency Calculator from ThermoFisher (<https://www.thermofisher.com/es/es/home/brands/thermo-scientific/molecular-biology/molecular-biology-learning-center/molecular-biology-resource-library/thermo-scientific-web-tools/qpcr-efficiency-calculator.html>).

Efficiencies between 90-110% were considered acceptable.

### 3.15. qRT-PCR

qRT-PCRs were done with SybrGreen (4364344, LifeTechnologies) and specific primers in a 7900HT Fast Real-Time PCR system (Applied Biosystems). Each PCR reaction

### 3. MATERIALS AND METHODS

contained 5ng of cDNA and the primer concentration was at 100nM. The end volume of each PCR reaction was 10 $\mu$ l. Triplicates were done for each sample.

The qRT-PCR primers used in this thesis can be found at Appendix I.

#### 3.15.1. qPCR data processing

The triplicate Ct values for each sample were averaged and normalized subtracting the Ct average of the housekeeping gene of the given sample. Then  $\Delta$ Ct was calculated as  $2^{-\text{normalized Ct}}$ . The results were multiplied for 100 and plotted.

### 3.16. GENERATION OF A POSTNB CONDITIONAL KD ZEBRAFISH TRANSGENIC LINE WITH TOL2 SYSTEM

The shRNA<sup>postn</sup> expressing zebrafish line was generated following the basic principles published in 2012 (De Rienzo et al., 2012).

#### 3.16.1. Generation of the construct

Hairpins against *postnb* and *postna+b* were designed using the Whitehead Institute for Biomedical Research hosts a siRNA Selection Program (<http://jura.wi.mit.edu/bioc/siRNAext/>) and following all the instructions given in Addgene webpage.

Table MM 4 indicates the *postnb* sequences targeted were:

**Table MM 4 | *postnb* sequences targeted**

sh79	AATAGTTGCACACAGCCGTAT
sh379	AAGGTGCAGGATCATACACCT
shAB	AACTGTGCCAGGATCATTAC

The transgenic fish were generated with the Tol2 system. The first part of the construct contained the bactin2 promoter fused to a floxed RFP sequence and a STOP codon at the end. The second part of the construct contained the first exon, the first

intron and 22 nucleotides of the second exon of the zebrafish actin gene (*actb2*, gene ID: 57935), fused in-frame to the GFP sequence. In the middle of the intron, we cloned the shRNA in the context of the zebrafish miR30e (gene ID: 100033613). This second part of the construct was generated following Dong M et.al protocol (Dong et al., 2009).

The detailed cloning protocol is explained below\*\*. The precursor sequence of zebrafish mir30e (409bp) was cloned from the genomic DNA of WT-AB adult fish into the pSpark®TA vector (C0020, Canvax). The 68-bp mir30e stem-loop region was replaced with a linker sequence containing two BbsI sites using two-step PCR. The shRNA sequences were synthesized as DNA oligonucleotides (IDT), annealed and inserted at the BbsI sites by digestion of the mir30e with BbsI (R3539, New England BioLabs). The genomic sequence of zebrafish *actb2* containing an intact exon 1 and intron 1, and the first 22bp of exon 2 was cloned into pSpark®TA vector. Then, the mir-shRNA was inserted into an endogenous BglII site within the *actb2* intron 1 by BglII digestion (R0144, New England BioLabs). The GFP was cloned into a pcDNA3 vector. The *actb2*-mir-shRNA was then in-frame infused to the open reading frame of the GFP into a pcDNA3 plasmid through EcoRI and BamHI (R0101 and R0136, New England BioLabs). The resultant *actb2*-mir-shRNA-GFP was then inserted into the p3E-PolyA (302) Tol2 vector through att specific recombination with the BP clonase (11789020, ThermoFisher), generating the p3E element (Kwan et al., 2007). The p5E element was the p5E-bactin2 (299) construct from the Tol2kit, and the pME element was previously generated in the lab placing loxP sites around a RFP sequence followed by 4 polyA signals. The loxP sites are oriented to excise the floxed fragment. Based on the multisite Gateway approach the 3 entry vectors were recombined, with the LR clonase (12538120, ThermoFisher), inside the pDestTol2pA2 (394) destination vector. All primer sequences used are available in Table MM 5.

#### Note

\*\*The PCRs from this section were performed with Phusion High-Fidelity DNA polymerase (F530S, ThermoFisher).

### 3. MATERIALS AND METHODS

**Table MM 5 | Primers used to generate the *postnb* KD conditional line**

#	Sequence name	Sequence with restriction site underlined
1	miR30e_F miR30e_R	ATAGAATTCACAGCCATGCCATAGTTTTAGG ATCCTCGAGAGTTCATCATATGACCAAGTGAC
2	miR30e-linker_F miR30e-linker_R	ATGTCTTCGTCTAGAAGAAGACAA AGCCAAGTCTGTTACTCTC (Bbs I) TTGTCTTCTTAGACGAAGACAT AGCCCGTACTGCCAGCTG (Bbs I)
3	mir-shRNA-PostnB-79-F mir-shRNA-PostnB-79-R	<u>GGCTAGCAA</u> ATAGTTGCTTACACAGCCGTATCTGGTGCACATGATGGA GATACGGCTGTGTGCAACTATTC <u>GGCTGA</u> ATAGTTGCACACAGCCGTATCTCCATCATGTGCACCAGATAC GGCTGTGTAAGCAACTATTTGCT
4	mir-shRNA-PostnB-379-F mir-shRNA-PostnB-379-R	<u>GGCTAGCAA</u> AGGTGCAGTTGATCATAACCTCTGGTGCACATGATGGA GAGGTGTATGATCCTGCACCTTC <u>GGCTGA</u> AGGTGCAGGATCATAACCTCTCCATCATGTGCACCAGAGGT GTATGATCAACTGCACCTTTGCT
5	mir-shRNA-PostnAB-F mir-shRNA-PostnAB-R	<u>GGCTAGCAA</u> ACTGTGCCTTAGGATCATTACCTGGTGCACATGATGGA GGTGAATGATCCTGGCACAGTTC <u>GGCTGA</u> ACTGTGCCAGGATCATTACCTCCATCATGTGCACCAGGTGA ATGATCCTAAGGCACAGTTTGCT
6	$\beta$ -actin_F $\beta$ -actin_R	ATAGGATCCATGGATGAGGAAATCGCTGCCCTG TCAGAATTCGTCATGCCAACCATCACTC
7	GFP_F_EcoRI GFP_R_XhoI	TATGAATTCTC ATGGTGAAGCAAGGGCGAG ATACTCGAG GCTTACAATTTACGCCTTAAG
8	$\beta$ -actin_F_attB2 GFP_R_pA_attB3R	GGGGACAGCTTTCTGTACAAAGTGG ATGGATGAGGAAATCGCTGCCCTG GGGGACAACCTTTGTATAATAAAGTTG GCTTACAATTTACGCCTTAAG

1	To clone the zebrafish miR30e precursor from genomic DNA.
2	To replace mir30e stem-loop region with the shRNA sequences.
3	Primers containing the sh79 sequence and the miR30e loop sequence in the middle. Underlined fragments are overhang for the BbsI sticky ended subcloning with the miR30e backbone construct.
4	Primers containing the sh379 sequence and the miR30e loop sequence in the middle. Underlined fragments are overhang for the BbsI sticky ended subcloning with the miR30e backbone construct.
5	Primers containing the shAB sequence and the miR30e loop sequence in the middle. Underlined fragments are overhang for the BbsI sticky ended subcloning with the miR30e backbone construct.
6	To clone the zebrafish <i>actb2</i> fragment from genomic DNA.
7	To clone the GFP protein inside the pcDNA3 vector.
8	Primer pair with the att specific sites to clone the Actin-miR30e_shRNA-GFP construct inside the p3E-polyA (#302) Tol2kit vector.

### 3.16.2. $\mu$ Needles and injection plates for zebrafish embryo injection

Glass capillaries (Model G-1, Narishige) were pulled with a micropipette puller (Model P-97, Sutter Instrument). With a ramp test of 395, the puller program chosen was: Heat 415; pull 85; velocity 130; time 150; and pressure 500. Store the needles stuck on a plasticine line in a Petri dish.

Injection plates were prepared with 1% agarose (A9939, Sigma) dissolved in embryo medium (heat to dissolve in a microwave). 40ml of the agarose solution were poured into a Petri Dish and a microinjection mould was placed to generate six lanes.

#### Solutions and material

**Microinjection mould:** Six ramps, one 90 degree and one 45 degree bevelled side.

**Embryo medium:** it is prepared as 60x concentrate and diluted at 1x upon need. For 1L of the 60x medium add 17.2g NaCl (S7653, Sigma), 4.9g MgSO<sub>4</sub>·7H<sub>2</sub>O (M1880, Sigma), 2.9g CaCl<sub>2</sub>·2H<sub>2</sub>O (C3306, Sigma) and 0.76g KCl (P5405, Sigma) in 1L of dH<sub>2</sub>O. Adjust pH to 7.2 with NaOH (221465, Sigma).

### 3.16.3. *In vitro* transcription of Cre-nls mRNA

pCS2-NLS-CRE plasmid was linearized with NotI for 1h at 37°C. DNA was precipitated over-night with ethanol and resuspended in nuclease-free H<sub>2</sub>O. mRNA was synthesized with the mMESSAGING mMACHINE SP6 transcriptor kit (AM1340, ThermoFisher) following manufacturer's instructions. Finally, mRNA was precipitated with lithium chloride and resuspended in nuclease-free H<sub>2</sub>O. 50ng/ $\mu$ l aliquots were done.

#### **3.16.4. Embryonic injection of Tol2-construct and transposase mRNA**

The previous day of the injection, incrosses of Tg(bactin2:CRE-ERT2) were set. The same day, the injection mix with the Tol2 vector (pDest) and the transposase was prepared and 3 $\mu$ l were loaded into the  $\mu$ -needle using a microloader pipette. The  $\mu$ -needle was then placed into the micromanipulator that was connected to the FemtoJet<sup>®</sup> (Eppendorf). This equipment helped to inject the desired volume to each embryo. One-cell stage embryos were placed in the lines of the agarose plates and injected in the yolk with 10nl of the injection mix.

At 48hpf embryos were screened, and those expressing RFP fluorescence were selected and grown.

##### Solutions and material

**Injection mix:** 1 $\mu$ l of transposase mRNA (50ng/ $\mu$ l), 1 $\mu$ l of pDest (50ng/ $\mu$ l), 1 $\mu$ l of phenol red (P0290, Sigma) and 7 $\mu$ l of nuclease-free H<sub>2</sub>O (3098, Sigma).

#### **3.16.5. Founder, F1 and F2 screening**

When injected fishes (F0) reached adulthood (~3 months of age), fishes were outcrossed with Tg( $\beta$ Actin:CRE-ERT2), and those which generated an offspring with some RFP positive embryos were selected as founders. The positive embryos were grown to generate the F1 generation. Each founder was used to generate an individual line. When F1 reached adulthood, it was again outcrossed with Tg( $\beta$ Actin:CRE-ERT2) to generate the F2 generation. In each generation, embryos were screened for RFP fluorescence and only the positive ones were grown. Figure MM 1 explains the workflow of the transgenic line generation.

Functional analysis with tamoxifen treatment and CRE-nls injection were done in order to select the line which recombined and worked the best.



### 3.17. EMBRYONIC TAMOXIFEN TREATMENT

In order to accomplish construct recombination, 24hpf embryos were treated overnight with 5 $\mu$ M tamoxifen (85256, Sigma). Recombination success was observed through GFP expression.

#### Solutions

**5 $\mu$ M Tamoxifen:** a 10mM stock solution was prepared in absolute ethanol. A 1/2,000 dilution was directly performed in embryo medium.

### 3.18. EMBRYONIC CRE-NLS INJECTION

In the previous day, crosses of Tg( $\beta$ Actin:CRE-ERT2) and the shRNA line were set. One-cell stage embryos were injected in the yolk with 10nl of injection mix.

At 48hpf embryos were screened for GFP fluorescence at 24hpf and 48hpf. Regeneration experiments were done in the GFP+ fishes when adult (Figure MM 1).

#### Solutions

**Injection mix:** 1 $\mu$ l of CRE-nls mRNA (50ng/ $\mu$ l), 1 $\mu$ l of phenol red (P0290, Sigma) and 8 $\mu$ l of nuclease-free H<sub>2</sub>O (3098, Sigma).

### 3.19. ADULT TAMOXIFEN TREATMENT

The treatment that at our hands accomplished a better change in our shRNA lines was 20 $\mu$ l intraperitoneal injection of 1mM 4OH-Tamoxifen (H7904, Sigma) during 5 consecutive days and 24h of 4 $\mu$ M 4OH-Tamoxifen in-water treatment. In this thesis, it has not been accomplished a full recombination in adult hearts from shRNA lines.

#### Solutions

**4OH-Tamoxifen:** a 10mM solution was prepared dissolved in ethanol. To prepare the working solutions, the stock solution was dissolved in PBS 1x.

### 3. MATERIALS AND METHODS

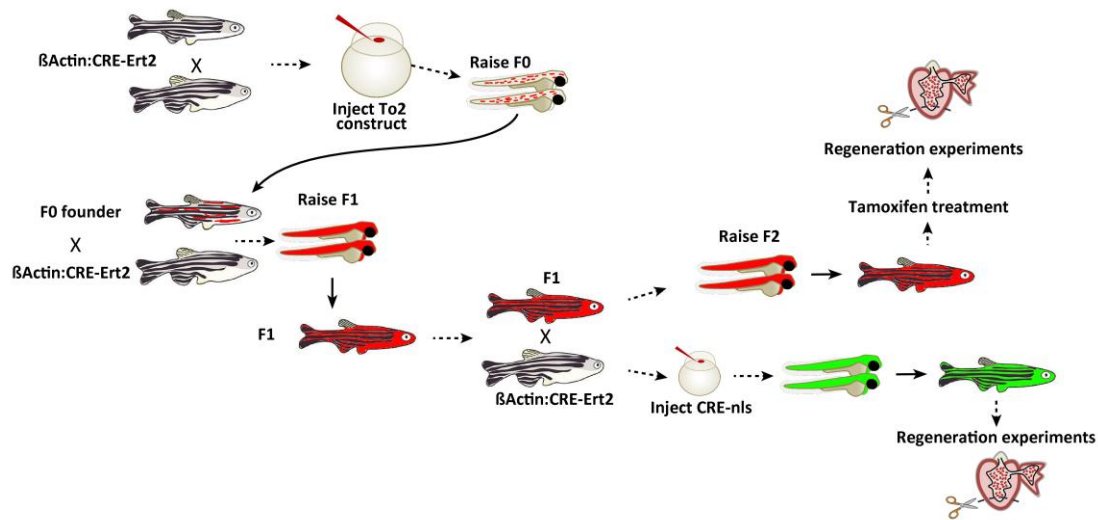


Figure MM 1 | Workflow to generate the  $shRNA^{postnb}$  knock-down line.

## 3.20. CRISPR-CAS9 *POSTNB* BIALLELIC KO ZEBRAFISH TRANSGENIC LINE

### 3.20.1. sgRNA design and synthesis

The sgRNA targeted sequences were designed with the CRISPR.TEFOR platform ([www.crispr.tefor.net](http://www.crispr.tefor.net)). A total of 4 sgRNAs were designed against *postnb* and another 4 against *postna*. sgRNAs were synthesized following the Gagnon et. al method (Gagnon et al., 2014).

In order to *in vitro* transcribe the sgRNA, gene-specific oligonucleotides containing the T7 (5'-TAATACGACTCACTATA-3') promoter sequence, the 20bp target site without the PAM, and a complementary region were annealed to a constant oligonucleotide encoding the reverse-complement of the tracrRNA tail. The ssDNA overhangs were filled in with T4 DNA polymerase (M0203S, NEB), and the resulting sgRNA templates were purified using the Quiaquick PCR purification kit (28106, Qiagen). sgRNAs were transcribed using the MEGAScript T7 Kit (AM 1334, Ambion). All sgRNAs were then DNase treated (AM2238, ThermoFisher) and purified with the RNA Clean &

Concentrator (R1015, Zymo). RNA concentration was quantified using Nanodrop spectrophotometer. All primer sequences used are available in Table MM 6.

**Table MM 6 | Primers for sgRNA *in vitro* synthesis**

	Targeted sequence	Primer
sg_594_PostnB	AGGTGAAGAATCTGCCTGGT	TAATACGACTCACTATAGGTGAAGAATCTGCC TGGTCAAGTTTTAGAGCTAGAAATAGCAAG
sg_665_PostnB	AGGGTATTCGTGCAAAGAAA	TAATACGACTCACTATAGGGTATTCGTGCAAAA GAAACAAGTTTTAGAGCTAGAAATAGCAAG
sg_21_PostnB	GTGCAAAAAGTAGCTGCAAAG	GAAATTAATACGACTCACTATAGTGCAAAAAGT AGCTGCAAAGTTTTAGAGCTAGAAATAGCA AG
sg_66_PostnB	CATAAGCTGAAGAATCTGCC	GAATTAATACGACTCACTATAGCATAAGCTGA AGAATCTGCCGTTTTAGAGCTAGAAATAGCAA G
Scaffold primer	AAAAGCACCGACTCGGTGCCACTTTTTCAAGTTGATAACGGACTAGCCTATTTTAAC TTGCTATTCTAGCTCTAAAAC	

### 3.20.2. Cas9 and sgRNA injection

WT-AB embryos at one-cell stage were microinjected into the cell as specified in the 3.16.4 section (Embryonic injection of Tol2-construct and transposase mRNA) of this thesis. 300pg of Cas9 protein (A36497, ThermoFisher) and 25pg of one sgRNA were injected at the cell of one-cell stage embryos.

Fluorescence PCR analysis was done at 24hpf in order to assess sgRNAs efficiency. Embryos from the same injection from those sgRNAs that cut the genomic DNA were grown.

#### Solutions

**Injection mix:** 1.5µl of Cas9 protein (1/10 dilution of A36497, ThermoFisher), 25pg of sgRNA, 1µl of phenol red (P0290, Sigma) and add nuclease-free H<sub>2</sub>O (3098, Sigma) up to an end volume of 5µl.

### 3. MATERIALS AND METHODS

#### 3.20.3. Fluorescence PCR

Fluorescence PCR was performed as Varshney GK et al. (Varshney et al., 2016), and analyzed using an ABI 3730xl genetic analyzer (Life Technologies). LIZ 500 (4322682, Applied biosystems) was used as size standard. The polymerase used in these PCRs is GoTaq DNA polymerase (M3008, Promega). Primers used to follow this strategy can be found at Table MM 7.

**Table MM 7 | Primers to amplify a *postnb* genomic region for fluorescence PCR and T7 assay**

Primer name	Primer sequence (5'-3')	Comment
M13-FAM	GTAAAACGACGGCCAGT	FAM labelled for fluorescence PCR
M13_sgPostnB_F	TGTTAAAACGACGGCCAGT ACTGAAATCGCTGCCTGTGT	For fluorescence PCR with a M13 sequence at the 5' end.
Pigtail_sgPostnB_R	GTGTCTT AGCTACACGTGCAAATAAGAAT	For fluorescence PCR. With a pigtail sequence at the 5' end.

#### 3.20.4. Founder, F1 and F2 screening

At 1 month-of-age injected fishes were finclipped and genotyped for *postnb* insertions and deletions. This screening was done by means of PCR product screening and Fluorescence PCR (Varshney et al., 2016). In those fishes that the fluorescence PCR detected no WT allele, a PCR\* of the region of interest (primers at Table MM 7) was performed and cloned into a TOPO-TA pCR2.1 vector (450641, ThermoFisher). 10 colonies were sequenced for each fish. The fishes were grouped according the number of different indels detected and the number of sequences that changed the reading frame. Those with low detected mosaicism and low sequences that followed the reading frame were selected to be in-crossed when reached adulthood (3 month-of-age), to generate a bulk KO F1 line. F1 fishes were genotyped for biallelic KO at 1 month-of-age by performing a PCR of the region of interest (primers for fluorescence PCR at Table MM 7) and cloning it into a TOPO-TA pCR2.1 vector. Experiments were performed on this F1 compound KO. Figure MM 2 explains the workflow of the *postnb*<sup>-/-</sup> line generation.

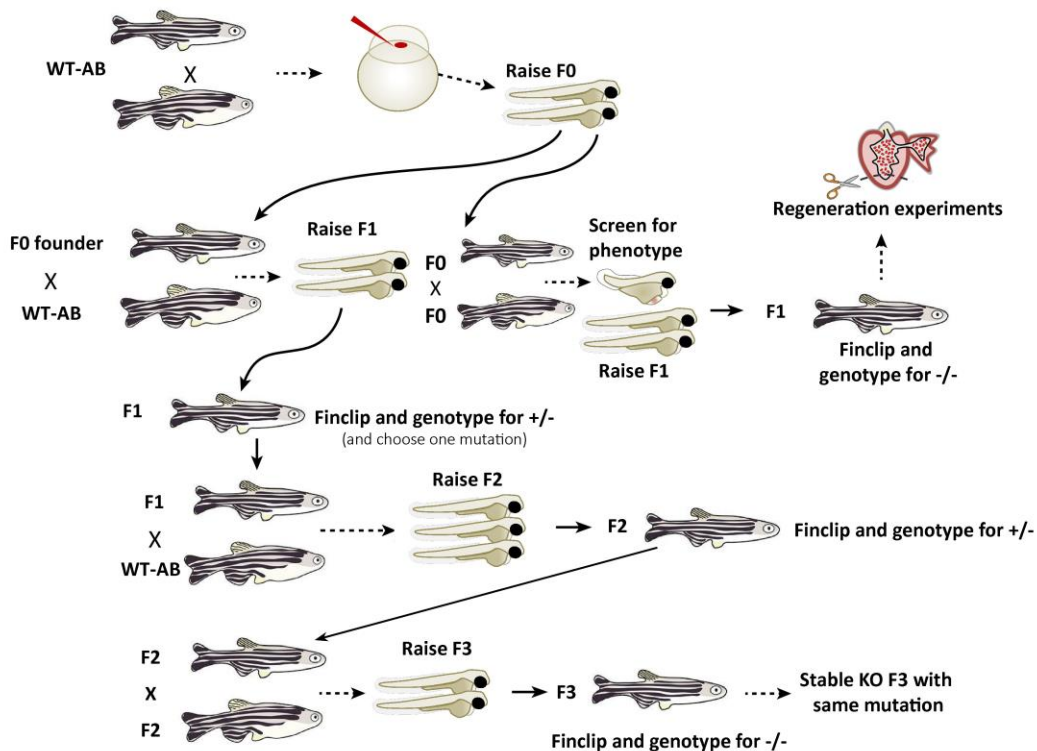
#### Note

\*PCRs of this section have been done with GoTaq DNA polymerase (M3008, Promega).

### 3.20.5. KO stable line generation

F0 selected fishes were out-crossed with WT-AB fishes. F1 was genotyped cloning the *postnb* region of interest into a TOPO-TA pCR2.1 vector (primers at Table MM 7). Different indels were detected, and one with 8bp insertion and 3bp deletion (+8,-3) which also changed the reading frame was chosen to generate the stable line.

The desired F1 was out-crossed with WT-AB to maintain a stable line in heterozygosity. To generate KO fishes with the same mutation in both alleles, F2 generation was in-crossed.



**Figure MM 2 | Workflow to generate the CRISPR/Cas9 knock-out transgenic line.** An incross of F0 fishes was done to faster obtain compound *postnb*<sup>-/-</sup> zebrafish. To establish the stable *postnb*<sup>-/-</sup> line, F0 was outcrossed with WT-AB fishes to obtain heterozygous fishes. One F1 heterozygous fish with a desired mutation was selected and outcrossed with WT to obtain more progeny. To generate *postnb*<sup>-/-</sup> fishes this F2 was genotyped and heterozygous fishes were incrossed. 1/4 of the F3 fishes will KO (-/-).

#### 3.21. *IN SITU* ZYMOGRAPHY

Hearts were processed as specified in the 3.5 section (Sample processing) of this thesis. Gelatinolytic activity was assessed by incubating 25µm cryosections with DQ-gelatin (EnzChek; Molecular Probes) at 28 °C for 1h in the dark. The DQ-gelatin was removed with PBS and autofluorescence was reduced with 0.1% Sudan Black solution. Finally, sections were fixed, and MMPs inactivated with 4% PFA. 10min washed with PBS rinsed the PFA and at the end sections were preserved in mounting medium. Images were taken using an SP5 confocal microscope.

The intensity was measured in 3 images of each stack with Fiji program. Intensities were normalized by ROI size.

##### Solutions and reagents

**DQ-gelatin:** dissolve one vial (1mg) in 1ml of H<sub>2</sub>O. If necessary, heat to 50°C to better dissolve. For long-term storage at 4°C, add 2mM sodium azide, NaN<sub>3</sub>, and protect from light. The working concentration is a 1/10 dilution in reaction buffer.

**Sudan Black:** 1% Sudan Black (252069, Panreac) in 70% ethanol.

**Mounting medium:** 56mM Glycine (G7126, Sigma), 5mM NaOH (S8045, Sigma), 87mM NaCl (S7653, Sigma), 4.6mM Sodium azide (S2002, Sigma), 0.23M Propyl gallate (P3130, Sigma) and 70% Glycerol (G9012, Sigma) in dH<sub>2</sub>O. Dissolve the reagents with heat, maximum 40°C.

#### 3.22. VENTRICLE DECELLULARIZATION

Animals were slaughtered and hearts were extracted. Only the ventricles were decellularized by immersion in a 0.5% SDS solution for 4h. Then ventricles were washed with dH<sub>2</sub>O for 30min. Then immersed into a 1% Triton-X solution for 30min and finally washed three times with dH<sub>2</sub>O for 10min each wash. All solutions were previously

filtered with a 0.2µm filter, and all incubations steps were done in a horizontal shaking plate at 30°C and 28 rpm.

#### Solutions and reagents

**0.5% SDS:** SDS (S4390, Sigma) was dissolved in MQ-H<sub>2</sub>O.

**1% Triton-X:** Triton-X 100 (X100, Sigma) was dissolved in MQ-H<sub>2</sub>O.

### **3.23. ECM PROCESSING AND STAINING**

The decellularized ventricles were embedded in OCT, snap frozen with isopentane (154911, Sigma) and fixed after sectioning incubating them 10min in 4% PFA. 10µm thick ECM slices were counterstained with DAPI (1:10,000) for 4min, and stained with Hematoxylin and Eosin, and Masson's Thrichrome stainings.

#### Solutions and reagents

**PFA:** 4% PFA (Electron Microscopy Sciences) in MQ-H<sub>2</sub>O.

**DAPI:** Rehydrate with 2ml of filtered dH<sub>2</sub>O the DAPI compound (D21490, Invitrogen) to have a solution of 5mg/ml. As working solution use a 1:10,000 dilution in TBS 1x.

### **3.24. GENOMIC DNA EXTRACTION FROM ZEBRAFISH VENTRICLES**

Genomic DNA was extracted from non-decellularized and decellularized zebrafish ventricles. Samples were homogeneized by adding 200µl of PBS, 20µl Proteinase K (Qiagen) and 4ul of RNaseA (Qiagen) and vortexed. Tissue lysis was done adding 200µl of AL Lysis buffer (Qiagen). DNA was purified by chloroform (C2432, Sigma) and precipitated using isopropanol (190764, Sigma). Finally, the pellets were dried and 20µl of TE buffer (Quiagen) was added. DNA concentration was measured with a spectrophotometer (NanoDrop® ND-100, Thermo Fisher Scientific).

#### 3.25. PROTEIN EXTRACTION AND QUANTIFICATION

Protein was extracted from pools of 3-5 ventricles or 15 embryo at 4dpf. Prior protein extraction embryos were deyolked. Hearts were homogenized with the help of a 27G syringe and deyolked embryos with a blue pestle in RIPA buffer. Homogenized tissues were incubated 2h at 4°C in RIPA buffer. Then samples were centrifuged at 10,000rpm for 10min at 4°C. Supernatant was kept, and protein was quantified with Bradford method.

For Bradford quantification, 8 standards were prepared with Bovine Albumin Serum (BSA; A7638, Sigma). Samples and standards were measured as triplicates. Each reaction consisted with 10µl of the protein and 200µl of Bradford solution. The color was let to develop for 10min and read at 595nm with a plate reader.

##### Solutions and reagents

**RIPA buffer:** 150mM NaCl (S7653, Sigma), 1% Triton X-100 (X100, Sigma), 0.5% sodium deoxycholate (D6750, Sigma), 0.1% SDS (S4390, Sigma), 50mM Tris-HCl pH 8.0 (T3253, Sigma). Freshly add protease, PIC (11836153001, Roche), and phosphatase inhibitors, PMSF (10837091001, Sigma).

**Bradford solution:** do a 1:5 dilution in MQ-H<sub>2</sub>O of the Bradford reagent (500-0006, BioRad).

**5x loading buffer:** 10% SDS (S4390, Sigma), 10mM beta-mercapto-ethanol (M7522, Sigma), 20% Glycerol (03117502001, Roche), 0.2M Tris-Hcl pH 6.8 (T3253, Sigma) and 0.05% Bromophenolblue (B8026, Sigma).

##### 3.25.1. Deyolking embryos in batches

Embryos (N=15) were transferred to a 1.5ml tube filled with 1ml deyolking buffer and pipetted with a 200µl tip so that the yolk sac was disrupted. Embryos were shaken for 5min at 1,100rpm to dissolve the yolk (Thermomixer, Eppendorf). Cells were pelleted at 300g for 30sec and the supernatant discarded. Two wash steps were performed by



adding 1 ml of wash buffer, shaking 2min at 1,100rpm and pelleting the cells as before. Then protein was extracted as stated in the protein extraction and quantification section.

#### Solutions and reagents

**Deyolking buffer:** 55mM NaCl (S7653, Sigma), 1.8mM KCl (P5405, Sigma), 1.25mM NaHCO<sub>3</sub> (S8875, Sigma).

**Washing buffer:** 110mM NaCl (S7653, Sigma), 3.5mM KCl (P5405, Sigma), 2.7mM CaCl<sub>2</sub> (C3306, Sigma), 10mM Tris/Cl pH8.5 (T3253, Sigma).

### **3.26. WESTERN BLOT**

Normalized total protein was subjected to a 7.5-10% acrylamide SDS-PAGE, and western blotting was performed according to standard procedure. First, running gel was polymerized inside the Mini-PROTEAN system (BioRad), 1.5mm separator was used. Some isopropanol was added on top to straight the surface of the running gel. Then, isopropanol was cleaned and the stacking gel was poured to polymerized and the well-combs added at the end. Known concentrations of proteins were then loaded in the gel wells, as well as a protein standard (Novex sharp pre-stained protein standards. LC5800, Invitrogen). Electrophoresis was run for approximately 1h at 160-180V. Protein was transferred in a methanol activated PVDF membrane (IPVH00010, Millipore) for 2h at 200mA (alternatively over-night at 30mA). Transferred membranes were blocked for 1-3h with blocking solution, and incubated with primary antibodies in blocking solution over-night at 4°C. Next day, membranes were washed 3x10min with TBST and incubated for 2h at RT with the secondary antibodies in blocking solution. After washing the membrane 3x10min with TBST, signal was developed with ECL prime western blotting system (RPN2232, GE Healthcare) and imaged with a Chemidoc Touch (BioRad).

The primary antibodies used for western blotting were: rabbit anti-postnb at 1:2,000 (developed by Akira Kudo (Ito et al., 2014)) and mouse anti-βactin at 1:5,000 (A1978, Sigma).

### 3. MATERIALS AND METHODS

The secondary antibodies used for western blotting were: 1:5,000 anti rabbit-HRP (NA934, GE Healthcare) and 1:5,000 anti-mouse-HRP (NA931, GE Healthcare).

#### Solutions and reagents

**Stacking acrylamide gel (3.9%):** for 10ml mix the following reagents in the stated order, 6ml MQ-H<sub>2</sub>O, 2.5ml 1M Tris-HCl pH 6.8 (T3253, Sigma), 50µl 20% SDS (S4390, Sigma), 1.3ml 30% acrylamide (161-0156, BioRad), 100µl 10% ammonium persulfate (A3678, Sigma) and 10µl TEMED (T9281, Sigma).

**Running acrylamide gel (10%):** for 30ml mix the following reagents in the stated order, 12.2ml MQ-H<sub>2</sub>O, 7.5ml 1.5M Tris-HCl pH 8.8 (T3253, Sigma), 150µl 20% SDS (S4390, Sigma), 9.8ml 30% acrylamide (161-0156, BioRad), 250µl 10% ammonium persulfate (A3678, Sigma) and 25µl TEMED (T9281, Sigma).

**Running buffer:** 25mM Tris base (T6791, Sigma), 192mM Glycine (G7126, Sigma) and 0.1% SDS (S4390, Sigma).

**Transfer buffer:** 25mM Tris base (T6791, Sigma), 192mM Glycine (G7126, Sigma) and 20% methanol (32213, Sigma).

**10x TBS buffer:** 1M Tris-HCl (T3253, Sigma), 160mM Trizma base (T6791, Sigma) and 1.5M NaCl (S7653, Sigma) in dH<sub>2</sub>O. Adjust pH at 7.4-7.5. To prepare 1x TBS make a 1/10 dilution of 10x TBS in dH<sub>2</sub>O.

**TBST buffer:** dilute 100ml of 10x TBS buffer in 1L of MQ-H<sub>2</sub>O. Add 1ml of Tween-20 (P1379, Sigma) to have a final concentration of 0.1%.

**Blocking solution:** add 5g of skim milk powder (70166, Sigma) to 100ml of TBST to have a final concentration of 5%.

### 3.27. LIQUID CHROMATOGRAPHY-MASS SPECTROMETRIC ANALYSES

In this thesis, two different proteomic analyses were performed: one to assess the decellularization protocol, and another one to assess the regeneration process. For the first one, native zebrafish ventricles, half-decellularized ventricles (after SDS treatment), and fully decellularized ventricles were analyzed. For the second one,

decellularized zebrafish ventricles at 7days post-amputation (dpa), 14dpa and 30dpa, were analyzed compared to sham operated fishes.

For LC-MS/MS spectrometric analysis of the decellularization protocol, we used three pools of 3 native zebrafish ventricles per pool, three pools of 10 ventricles after SDS treatment per pool, and three pools of 20 decellularized ventricles per pool. A two-way ANOVA was used for comparing ECM proteins over the decellularization states.

For LC-MS/MS spectrometric analysis during regeneration, 6 ventricles per sample were pooled for 7dpa, 14dpa and 30dpa. In control (sham) samples 8 ventricles were pooled. Each sample was analyzed in duplicate. One-way ANOVA was used to determine the statistical significant differences. Raw p-values have been controlled by adjusting the Benjamini-Hochberg False Discovery Rate (FDR).

Proteins of each sample were solubilized by mixing with 50 $\mu$ L of 1% SDS, 100mM Tris-HCl pH 7.6, 100mM DTT, 10min sonication and boiling for 3min. Protein extracts were clarified by centrifugation at 16,000xg for 5min, and quantified using the RcdC kit (BioRad).

In the first proteomic analysis, 12 $\mu$ g of protein of each sample were digested with LysC and trypsin using a Filter-Aided Sample Preparation (FASP) protocol and further analyzed by mass spectrometry. The LC separation was conducted on an Easy-nLC 1000 (Thermo) using 0.1% formic acid as Solvent A and acetonitrile with 0.1% formic acid as B. Each run was carried out at 250 nL/min with a gradient of 95% of solvent A to 65% A in 180min. Blank samples with solvent A injections were run in between each sample. Sample was concentrated in an Acclaim PepMap 100 trap column (Thermo), and fractionated in a Nikkyo Technos Co., 75  $\mu$ m ID, 3 A pore size, 12.5 cm in length with built in emitter column, coupled to a Nanospray Flex (Thermo) ESI source. Shotgun LC-MS/MS analysis was performed online with an electrospray voltage of 1.9 kV using a Q Exactive HF mass spectrometer (Thermo) with HCD fragmentation using top 15 precursor with charge 2 to 5 for data-dependent acquisition (DDA). MS1 spectra were

### 3. MATERIALS AND METHODS

acquired in the mass range 390–1700 m/z at a resolution of 60,000 at m/z 400 with a target value of  $3 \times 10^6$  ions and maximum fill time of 20ms. MS2 spectra were collected with a target ion value of  $2 \times 10^5$  and maximum 100ms fill time using a normalized collision energy of 27. Dynamic precursor exclusion was set at 15s. The raw files were processed with the MaxQuant software (version 1.6.2.6a) using the built-in Andromeda Search Engine. The Danio rerio TrEMBL database downloaded from [www.uniprot.org](http://www.uniprot.org) (Oct, 8th 2018) (62,078 entries) was used to search for peptides. MS/MS spectra were searched with a first search precursor mass tolerance of 20ppm. Then, the peptide masses were corrected and a second search was performed at 4.5ppm of mass tolerance. The fragment tolerance was set to 0.5Da, the enzyme was trypsin and a maximum of 2 missed cleavages were allowed. The cysteine carbamidomethylation was set as fixed modification, and methionine oxidation as well as protein N-terminal acetylation as variable modifications. To improve the identifications the “match between runs” was enabled among the replicates of every experimental condition.

In the second proteomic analysis, the protein amount recovered was around 5µg. The buffer was changed to 2M Urea 50mM Ammonium Bicarbonate using a 5kD Amicon Ultrafiltration device and the samples were digested with trypsin. Each sample was analyzed by LC-MS/MS in duplicate. 500ng of each sample was analyzed on a Maxis Impact high-resolution Q-TOF spectrometer (Bruker, Bremen), coupled to a nano-HPLC system (Proxeon, Denmark). The samples, evaporated and dissolved in 5% acetonitrile, 0.1% formic acid in water, were first concentrated on a 100mm ID, 2cm Proxeon nanotrapping column and then loaded onto a 75mm ID, 25cm Acclaim PepMap nanoseparation column (Dionex). Chromatography was run using a 0.1% formic acid - acetonitrile gradient (5-35% in 120min; flow rate 300nL/min). The column was coupled to the mass spectrometer inlet through a Captive Spray (Bruker) ionization source. MS acquisition was set to cycles of MS (2Hz), followed by Intensity Dependent MS/MS (2-20Hz) of the 20 most intense precursor ions with an intensity threshold for fragmentation of 2,500 counts, and using a dynamic exclusion time of 0.32min. All spectra were acquired on the range 100-2200Da. LC-MS/MS data was analyzed using the Data Analysis 4.0 software (Bruker). Proteins were identified using Mascot (ver. 2.5;

Matrix Science, London UK) to search against the *Danio rerio* proteins in the SwissProt 20160108 database (43,095 sequences). MS/MS spectra were searched with a precursor mass tolerance of 10ppm, fragment tolerance of 0.05Da, trypsin specificity with a maximum of 2 missed cleavages, cysteine carbamidomethylation set as fixed modification and methionine oxidation as variable modification.

Both mass spectrometry proteomics datasets, for the decellularization protocol proteome and for the regeneration proteome, have been deposited to the ProteomeXchange Consortium (<http://proteomecentral.proteomexchange.org>) via the PRIDE partner repository (Vizcaíno et al., 2012) with the dataset identifiers <PXD011627> and <PXD010092>, respectively.

### 3.27.1. Proteomic data Availability

Raw LC-MS/MS data are deposited in PRIDE archive. URL: <http://www.ebi.ac.uk/pride>

#### Decellularization protocol proteome

Project accession: PXD011627

Username: reviewer98071@ebi.ac.uk

Password: iicOLdGJ

#### Regeneration process proteome

Project accession: PXD010092

Username: reviewer79153@ebi.ac.uk

Password: Qmxk3Bi

## 3.28. CRITERIA FOR PROTEIN IDENTIFICATION

For the decellularization protocol proteomic analysis, MaxQuant software (version 1.6.2.6a) was used to validate the peptides and proteins identifications. The final list of peptides was obtained after applying a 5% False Discovery Rate (FDR). For proteins, only the proteins with at least 1 assigned peptide after applying a 5% FDR were considered. The non-unique peptides were assigned to the corresponding protein group according to the Razor peptides rule implemented in the software (principle of parsimony). Finally, the identified peptides and proteins were filtered to remove the peptides/proteins tagged as “Reverse” (significantly identified in the reverse database) and “potential contaminant” (items identified as contaminants in the

### 3. MATERIALS AND METHODS

“contaminants.fasta” file) as well as the proteins “Only identified by site” (proteins identified only with modified peptides). The lists can be found in the supplementary material uploaded to the PRIDE repository, with project accession code <PXD011627>.

For the regeneration process proteomic analysis, Scaffold (version Scaffold\_4.0.5, Proteome Software Inc., Portland, OR) was used to validate MS/MS based peptide and protein identifications. Peptide identifications were accepted if they could be established at greater than 99% probability by the Peptide Prophet algorithm (Keller et al., 2002). Protein identifications were accepted if they could be established at greater than 98% probability to achieve an FDR less than 1% and contained at least 1 identified peptide. Protein probabilities were assigned by the Protein Prophet algorithm (Nesvizhskii et al., 2003). Protein isoforms and members of a protein family would be identified separately only if peptides that enable differentiation of isoforms had been identified based on generated MS/MS data. Otherwise, Scaffold would group all isoforms under the same gene name. Different proteins that contained similar peptides and which were not distinguishable based on MS/MS data alone were grouped to satisfy the principles of parsimony. The lists of identified peptides and proteins can be found in Supplementary Table 7 and Supplementary Table 8, respectively (Appendix II).

#### **3.29. LABEL-FREE PROTEIN QUANTIFICATION**

For the decellularization protocol proteomic analysis, the proteins were quantified with the help of the label-free algorithm (LFQ) implemented in the MaxQuant software using the unique and razor peptides. The minimum number of peptides to be available in all the pair-wise comparisons was set to 2 and the “stabilize large LFQ ratios” option enabled.

For the proteomic analysis of heart regeneration, relative label-free protein quantification analysis was performed on the different samples analyzed using spectral counting. The “Quantitative Value - Total Normalized Spectra” function of Scaffold software was used for quantitative comparison. This function provides the total number of spectra that matched to a protein identified in each sample, after normalizing the

values for each sample by a factor calculated so that the total number of normalized spectral counts is identical for all samples, thus correcting for differences in sample load. Only those proteins for which the total sum of spectral counts for the eight runs was greater than 5 were considered for quantitative comparison.

### **3.30. ANALYSIS AND VALIDATION OF PROTEOMIC DATA ON REGENERATION**

In order to annotate proteins associated with Extracellular Matrix we downloaded the GO annotations of zebrafish, human, and mouse organisms from the repository of Gene Ontology Consortium (Ashburner et al., 2000; The Gene Ontology Consortium, 2017). The resulting list of proteins falling into the GO Term GO:0031012 (i.e. Extracellular Matrix) was supervised and curated by hand.

To determine an enrichment in ECM proteins in decellularized samples, the proteomics data obtained was compared to zebrafish proteomic data already published (Abramsson et al., 2010; Ma et al., 2018) with Panther (pantherdb.org). GO enrichment analysis were done with Enrichr tool (version August 24<sup>th</sup>, 2017).

To stabilize the variance, Variance Stabilization Normalization (VSN) was applied to spectral counts (Huber et al., 2002). A hierarchical clustering analysis via 1,000 bootstrap resampling replications was performed, using the R (version 3.2.3) statistical language package pvclust (Suzuki and Shimodaira, 2006), to construct a dendrogram with correlation distance and average method. Normalized data values were z-scaled by rows in order to build the heatmap.

Validation of the proteomic data was performed by qRT-PCR analyzing 3 biological replicates comprised of 5 ventricles each for each time point (7dpa, 14dpa, 30dpa and sham). RNA extraction and cDNA synthesis were done as specified in the RNA extraction and cDNA synthesis sections of this thesis.

#### **3.31. ATOMIC FORCE MICROSCOPY (AFM) FOR THE MEASUREMENT OF THE EXTRACELLULAR MATRIX STIFFNESS**

Zebrafish hearts were extracted, included in OCT and frozen at -80°C. Then slices of 25µm were cut with a cryostat (HM 560, CryoStar Thermo Scientific) and placed on top of Superfrost Plus Slides (Thermo Fisher) and stored at -20°C. Before measurements, slices were washed with 1xPBS and decellularized in order to remove all cellular components and preserve the ECM. A detergent-based protocol was used to decellularize the slices. Briefly, slices were immersed in 0.1% sodium-dodecyl disulfate (SDS) during 5min, followed by 10min of 1% Triton X-100 and finally washed during 20min with 0.9% NaCl solution. The slices were kept in constant moderate agitation.

Immediately after decellularization process, the samples were measured by AFM. The perimeter of glass slides was outlined with a water repellent marker (Super PAP PEN, Invitrogen), keeping 1ml of 1x PBS over the slices. Then, slides were placed on the sample holder of a custom-built AFM coupled to an inverted optical microscope (TE 2000, Nikon). The Young's modulus ( $E$ ) of the ECM was measured using V-shaped Au-coated silicon nitride cantilever (nominal spring constant of  $k = 0.06\text{N/m}$ ) with a spherical polystyrene bead of 2.25µm radius glued at its end (Novascan Technologies, Ames, IA), which was previously calibrated by thermal tune method. 3-D piezoactuators coupled to strain gauge sensors (Physik Instrumente, Karlsruhe, Germany), allowed to place the cantilever on the region of interest with nanometric resolution and to measure the vertical displacement of the tip ( $z$ ). The deflection of the cantilever ( $d$ ) was measured with a quadrant photodiode (S4349, Hamamatsu, Japan) using the optical lever method. The slope of a deflection-displacement curve ( $d$ - $z$ ) obtained on a bare region of the rigid substrate was used to calibrate the relationship between cantilever deflection and photodiode signal. Therefore, the force exerted by the cantilever was computed as  $F=k\cdot d$ . The indentation of the sample ( $\delta$ ) was computed as  $\delta = (z - z_0) - (d - d_0)$ , where  $z_0$  and  $d_0$  are the positions of the contact point. To extract  $E$ ,  $F$ - $\delta$  curves were analyzed by the spherical Hertz contact model (Jorba et al., 2017).



Myocardial stiffness was analyzed at 7, 14 and 30 dpa (n=5 per time point) and also in animals with no injury (control, n=5). For each sample time point, two slices were measured. In every slice, measurements were performed in two zones: uninjured and regenerating heart. In each zone, two locations separated by ~500µm were measured. At each of the two locations, 5 measurements were made separated by ~10µm. E of each measurement point was the average of five force curves, obtained with ramp amplitude of 5µm and frequency of 1Hz, resulting in tip velocity of 5µm/s.

#### Reagents and Solutions

**0.5% SDS solution:** for 50ml preparation, add 250µl of SDS (S4390, Sigma) to 49.75ml of MQ-H<sub>2</sub>O.

**1% Triton X-100 solution:** for 50ml preparation, add 500µl of Triton X-100 (X-100, Sigma) to 49.5ml of MQ-H<sub>2</sub>O.

**0.9% NaCl solution:** for 50ml preparation add, 450mg of NaCl (S7653, Sigma) to 50ml of MQ-H<sub>2</sub>O.

### **3.32. STATISTICAL ANALYSIS**

GraphPad software was used to carry out all the statistics. All results are expressed as mean ± standard error of mean (SEM). Each specific statistical test is specified in each figure legend.



## **4. RESULTS**



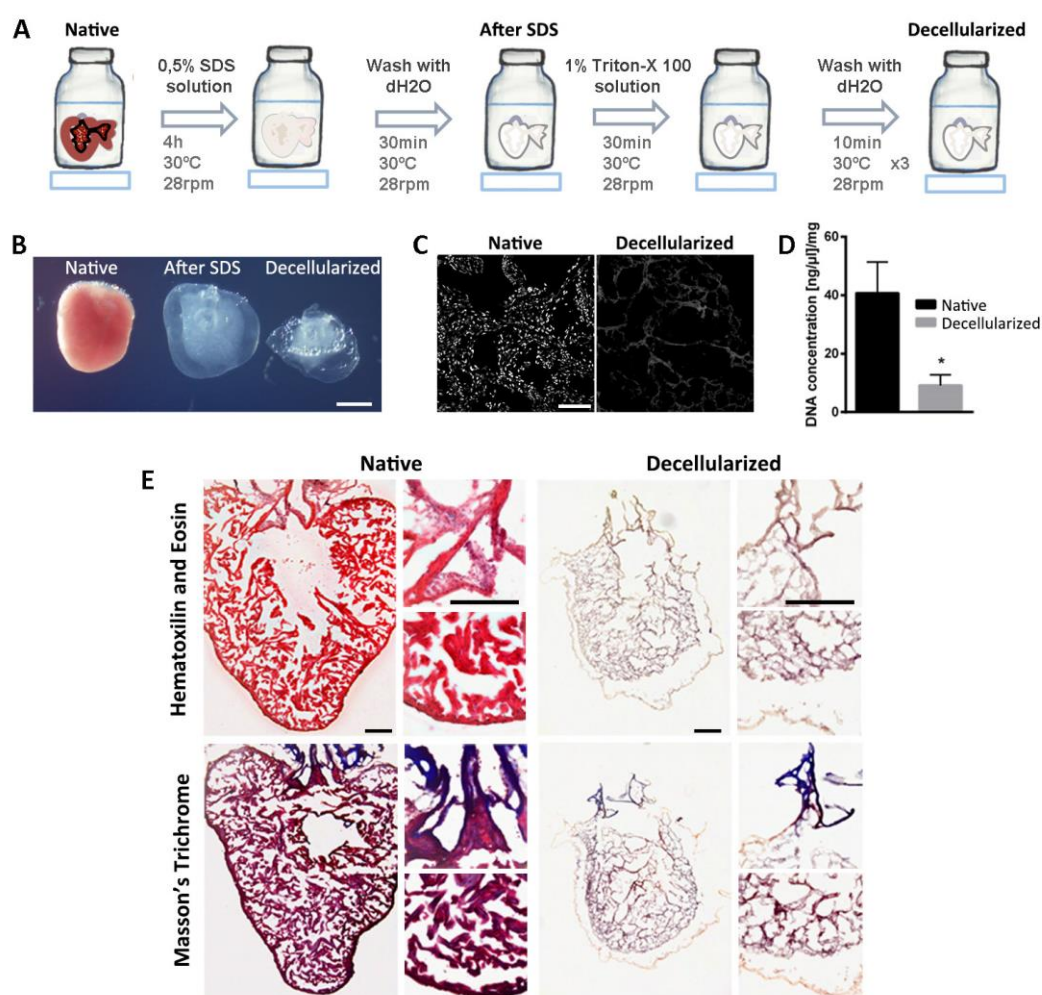
## **CHAPTER 1: STUDY OF THE ECM PROTEIN DYNAMIC CHANGES IN ZEBRAFISH HEART REGENERATION**

### **4.1.1. Development and characterization of a decellularization protocol for zebrafish ventricles**

To study the ECM protein composition of zebrafish ventricles, we developed a decellularization protocol consisting on detergent treatment with 0.5% sodium dodecyl sulfate (SDS), followed by 1% Triton-X 100 to remove SDS prior to processing for analysis (Figure R 1A). This treatment produced translucent decellularized scaffolds that structurally resembled the zebrafish ventricle (Figure R 1B). Following decellularization, DAPI staining and other histological stainings were used to assess the extent of cell removal and the integrity of the ECM. No DAPI staining was seen after treatment (Figure R 1C), and spectrophotometric analysis showed an ~80% reduction in DNA content after decellularization of zebrafish hearts (Figure R 1D). Moreover, Hematoxylin and Eosin, and Masson trichrome stainings revealed no conspicuous damage to the ECM, while further confirming the absence of nuclei in decellularized samples (Figure R 1E). To analyze whether the decellularization process altered the relative abundance of ECM proteins, we characterized the proteome of zebrafish hearts before (native), after SDS treatment, and at the end of decellularization by liquid chromatography – tandem mass spectrometry (LC-MS/MS). A total of 447 unique proteins were detected in native hearts, of which only 15 (3.4%) corresponded to extracellular proteins as annotated by Gene Ontology and manual curation (see Experimental Procedures for details). The numbers of extracellular proteins detected after SDS treatment and at the end of the decellularization protocol increased to 35 and 36, respectively, while those of intracellular proteins decreased from 432 in native hearts to 352 after SDS treatment,

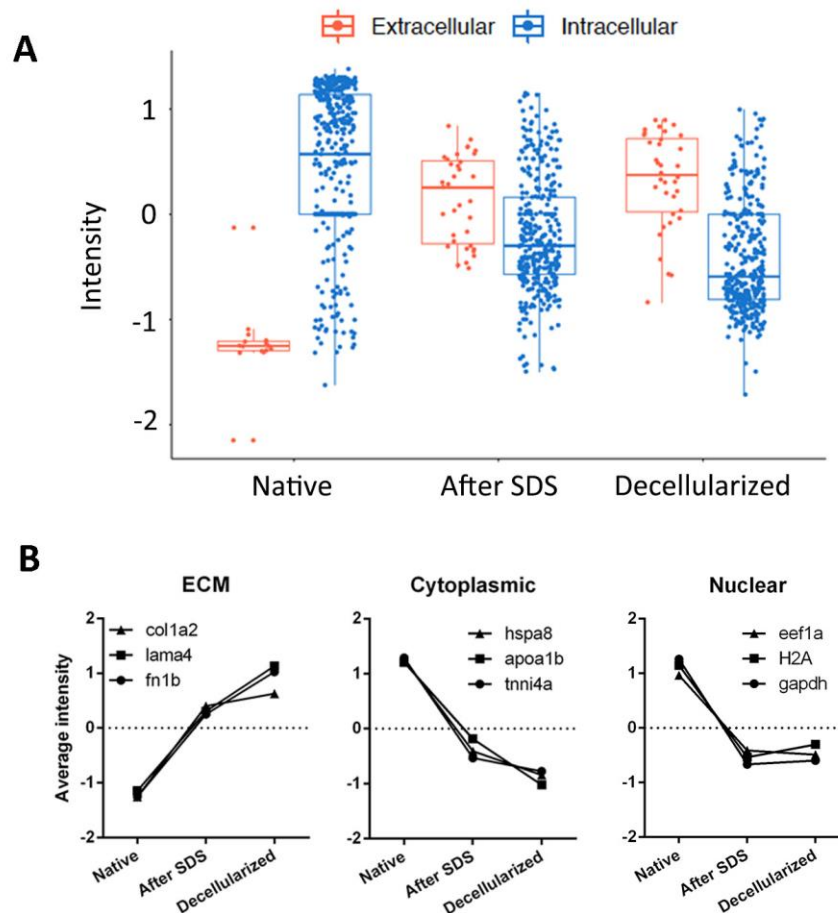
#### 4. RESULTS

and 341 in fully decellularized hearts (Supplementary Table 2 in Appendix II). As expected, decellularization not only decreased the number of intracellular proteins detected, but also their abundance as quantified by peptide peak intensity, whereas the opposite trend was observed for extracellular proteins (Figure R 2A). Importantly, all extracellular proteins identified in native hearts were also detected in samples after SDS treatment, and after complete decellularization, demonstrating that the protocol used for decellularizing zebrafish hearts did not introduce bias in our analyses due to preferential removal of specific ECM components.



**Figure R 1 | Decellularization protocol for zebrafish hearts.** (A) Representation of the protocol used to decellularize zebrafish ventricles. (B) Images of the ventricles at different points of the decellularization protocol. From left to right, native ventricle, after 0.5% SDS, and at the end of the decellularization protocol (scale bar 500μm). (C-E) The efficiency of the decellularization process was characterized by DAPI staining (scale bar 50μm) (C), spectrophotometric quantification of DNA (N=3) (D), and Masson's trichrome (E, upper images) and Hematoxylin and Eosin (E, lower images) staining (scale bar 100μm). Statistical significance of DNA content was analyzed with unpaired Student's *t* test. \*, *p*<0.05.

The end result of the decellularization protocol was, therefore, an enrichment of ECM proteins at the expense of cytoplasmic and nuclear proteins (Figure R 2B). The results of these analyses validate the applicability of our zebrafish heart decellularization protocol to enrich for ECM proteins, while not altering the relative abundance of ECM protein components.



**Figure R 2 | Preservation and enrichment of ECM proteins after decellularization. (A)** Box plot representing an overall distribution of the average intensities of each protein in each sample group. ECM proteins and intracellular proteins have been independently plotted to better visualize the effect of decellularization in each class of proteins. **(B)** The profile of specific ECM, cytoplasmic and nuclear proteins is plotted to indicate the loss of intracellular proteins while the maintenance and enrichment of ECM proteins.

#### 4.1.2. Profile of ECM proteins in adult zebrafish hearts

Proteomics analysis of the decellularized sham zebrafish hearts by LC-MS/MS allowed us to identify a total of 63 proteins with  $\geq 3$  spectral counts, of which 24 were ECM proteins (Table R 1). Collagens, fibronectin 1b and fibrinogens were the most

## 4. RESULTS

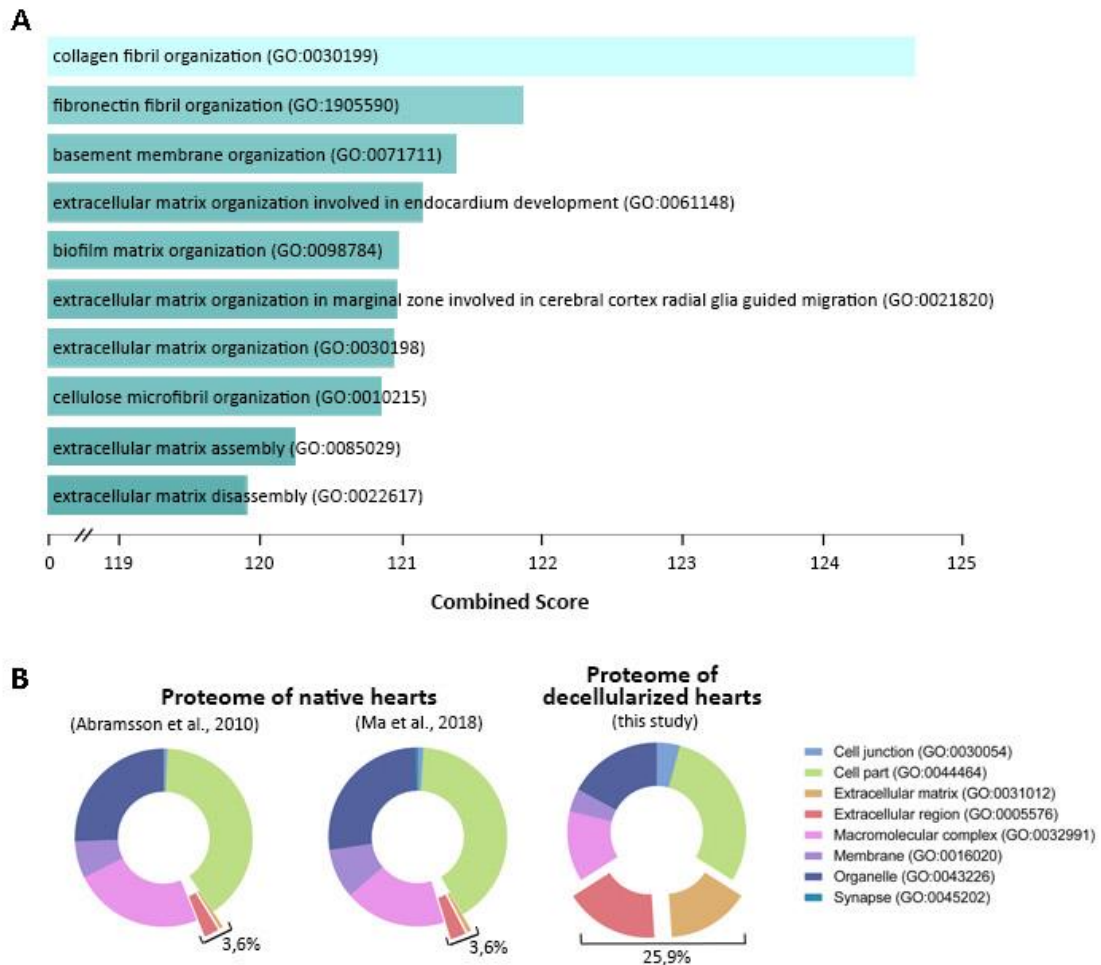
abundant proteins in the decellularized zebrafish ventricle proteome. Binding, structural molecule activity, receptor activity, and catalytic activity were the most represented molecular function Gene-Ontology (GO) terms (GO:0005488, GO:0005198, GO:0004872, and GO:0003824, respectively) for these identified ECM proteins. A search for GO enriched terms using Enrichr analysis revealed that the 10 most enriched biological processes in our control proteome (GO:0030199, GO:1905590, GO:0071711, GO:0030198, GO:0098784, GO:0010215, GO:0061148, GO:1901148, GO:0021820 and GO:0022617) were all ECM related (Figure R 3A).

We next compared the GO cellular component terms represented in our ECM-enriched zebrafish ventricle proteome with those of whole cardiac zebrafish proteomes previously reported by Abramsson et al. (Abramsson et al., 2010) and Ma et al. (Ma et al., 2018) Analysis by Panther revealed an enrichment of ECM and extracellular region terms in our decellularized samples compared to whole heart proteomes (Figure R 3B). These results further confirmed that ventricle decellularization allows a better detection of changes in ECM protein composition.

### **4.1.3. Changes in ECM protein composition during zebrafish heart regeneration**

To determine whether ECM protein composition changes during zebrafish heart regeneration, we also analyzed with LC-MS/MS decellularized ventricle samples of zebrafish hearts at 7, 14, and 30dpa. From the 274 proteins detected among all samples (Supplementary Table 3 in Appendix II), 96 were represented by an overall across sample averages of >5 spectral counts (Supplementary Table 4 and Supplementary Table 5 in Appendix II). From these 96 proteins, 29 corresponded to extracellular proteins and 67 to intracellular proteins. Of note, 23 out of the 50 most abundant proteins found in these analyses were ECM proteins (Supplementary Table 4 and Supplementary Table 5 in Appendix II). Heatmap representation of protein profiles showed large differences between control and 7dpa samples. However, profile changes among other regeneration time points were less evident (Figure R 4A). Overall, hierarchical clustering



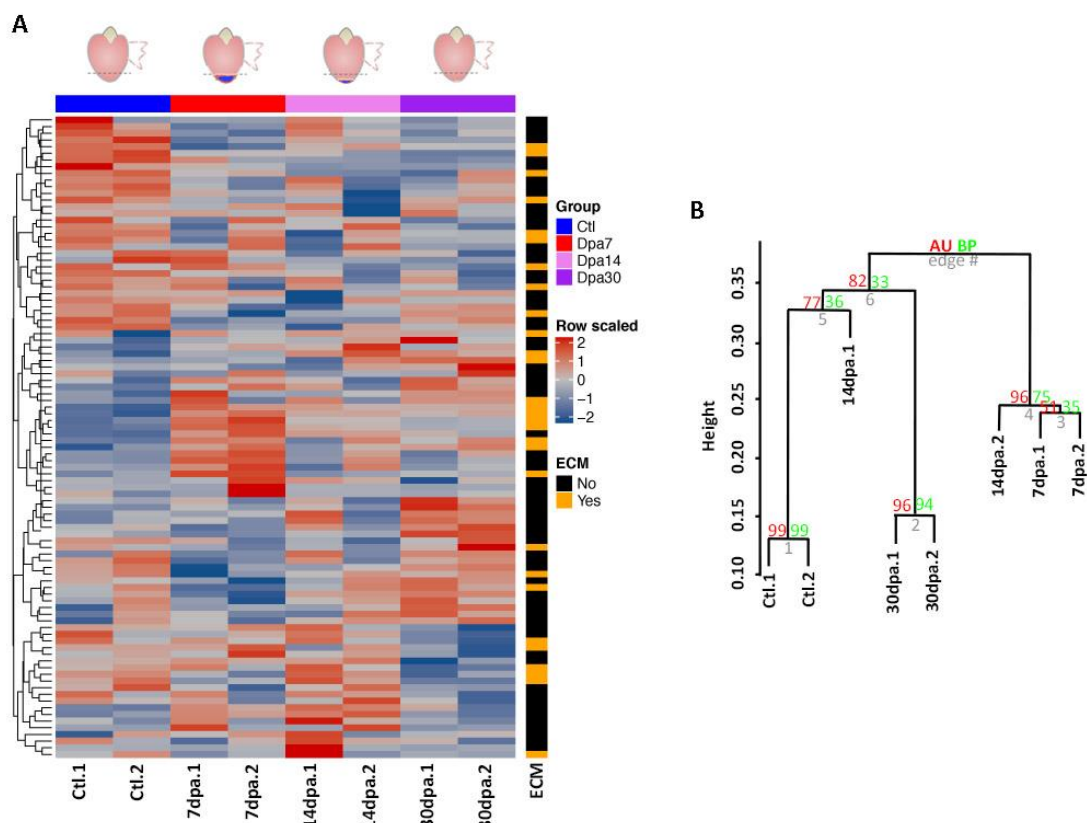


**Figure R 3 | Decellularization increases ECM protein detection.** (A) Representation of the 10 most enriched Biological Process GO terms in our proteome of control hearts. Combined score is taken from Enrich program, which takes the log of the p-value from the Fisher exact test and multiplies it by the z-score of the deviation from the expected rank. (B) Representation of the Cell Component Gene Ontology (GO) of the published zebrafish heart proteome of Abramsson et al. (Abramsson et al., 2010), the published sham heart proteome of Ma et al. (Ma et al., 2018) and our proteomic analysis of decellularized zebrafish ventricles. Panther assigned GO terms to 138, 1902, and 60 proteins from the proteomes described in Abramsson et al. (Abramsson et al., 2010), Ma et al. (Ma et al., 2018), and the one described here, respectively.

analysis grouped sample replicates together for all time points with good Approximately Unbiased p-values (AU) indexes, except for those of the 14dpa condition. Control and 30dpa samples clustered together, and away from 7dpa samples, while the 14dpa samples clustered apart from each other (Figure R 4B). ANOVA analysis revealed that 17 out of the overall 96 proteins detected showed statistically significant changes during regeneration, of which 9 were ECM proteins (Supplementary Table 6 in Appendix II). Among the ECM proteins whose levels changed significantly during regeneration,

#### 4. RESULTS

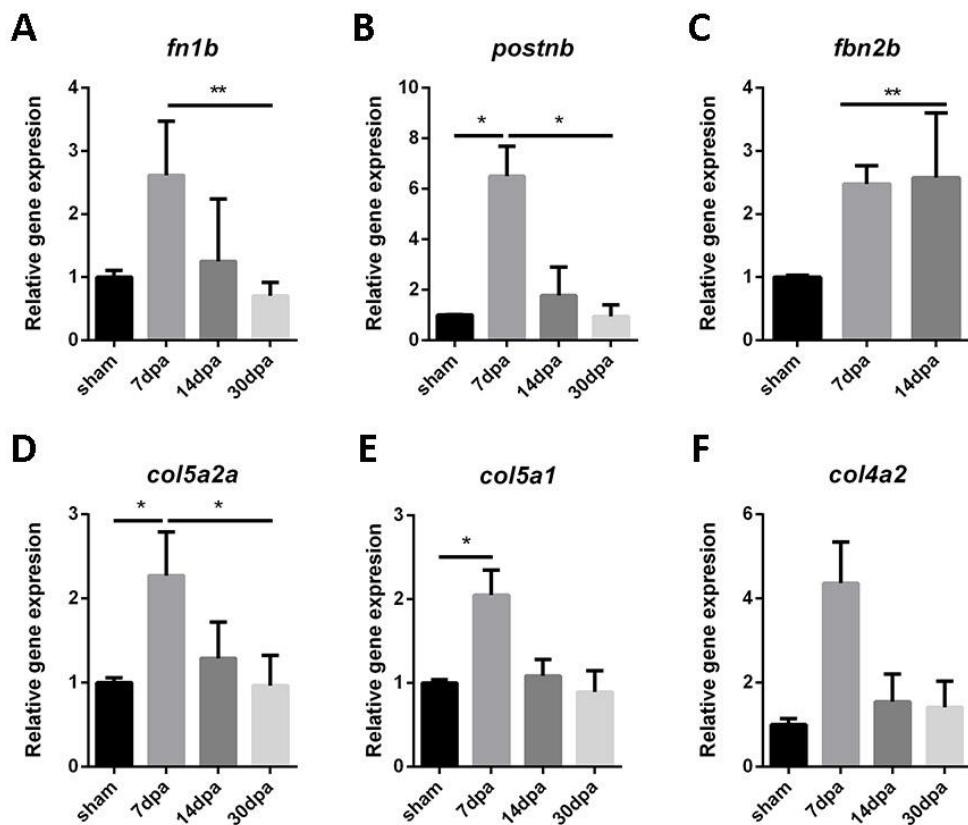
fibrinogen a, b, and g, as well as fibronectin 1b and periostin b, showed a peak at 7dpa. In contrast, the levels of collagens and fibrillin 2b showed a statistically significant decrease during regeneration, which was more evident at 7dpa.



**Figure R 4 | Changes in ECM protein composition during heart regeneration.** (A) Heat-map for the 96 proteins detected across samples in zebrafish control decellularized hearts (Ctl) and at different time points of regeneration. The time points analyzed were 7 days post-amputation (dpa), 14 dpa, and 30 dpa. Red indicates increased protein expression and blue indicates reduced protein expression. The ECM column indicates the ECM proteins in orange. Data are row scaled. (B) Hierarchical clustering with bootstrap analysis of all the samples. AU, Approximately Unbiased p-value; BP, Bootstrap Probability value.

To ascertain if changes in protein abundance were the result of differential gene expression, we measured by quantitative reverse transcription polymerase chain reaction (qRT-PCR) the expression level of 6 genes encoding ECM proteins that change in abundance during regeneration. We found positive correlation between mRNA and protein levels in the case of fibronectin/*fn1b* and periostin b/*postnb*, in which increased transcription levels were also found peaking at 7 dpa (Figure R 5C-D). However, expression levels of *col4a2*, *col5a1*, *col5a2a*, and *fn2b* were all found to be upregulated at 7dpa (Figure R 5E-H), in contrast with the decreased protein levels found in

regenerating heart ECM (Supplementary Table 6 in Appendix II). This suggests that changes in *fn1b* and *postnb* protein levels during regeneration are regulated transcriptionally, whereas the regulation of *col4a2*, *col5a1*, *col5a2a*, and *fnb2b* would be post-transcriptional.



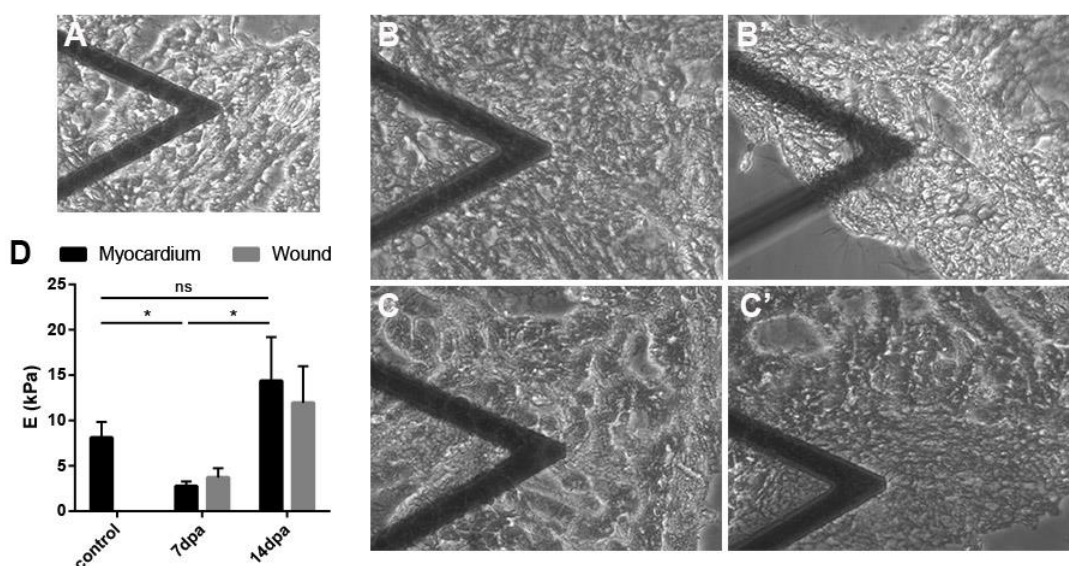
**Figure R 5 | mRNA expression changes of ECM proteins significantly changed during zebrafish heart regeneration.** (A-F) Gene expression assessment by real time qPCR of the ECM proteins significantly changing in the proteomic analysis during the regeneration process. *fn1b*, fibronectin 1b; *postnb*, periostin b; *col5a1*, collagen type 5  $\alpha$ 1 chain; *col4a2*, collagen type 4  $\alpha$ 2 chain; *col5a2a*, collagen type 5  $\alpha$ 2a chain; *fnb2b*, fibrillin 2b. Significance was analyzed with Kruskal-Wallis followed by a Dunn's multiple comparisons test. \*, p<0.05; \*\*, p<0.01.

#### 4.1.4. Changes in ECM biomechanical properties during zebrafish heart regeneration

Changes in ECM protein composition can result in modifications in the biomechanical properties of the matrix. Atomic Force Microscopy (AFM) allowed us to measure and compare the stiffness of the ECM during heart regeneration (Figure R 6).

#### 4. RESULTS

For this purpose, 25 $\mu$ m thick slices of control or regenerating zebrafish hearts were decellularized and the ECM regions of interest identified by phase contrast microscopy (Figure R 6A-C). The Young's modulus of control zebrafish ventricle ECM was calculated at  $8.1 \pm 1.7$  kPa. We then compared these values with those of regenerating hearts at 7 and 14dpa (Figure R 6D). We chose these time points because our proteomic analysis had revealed the major ECM changes at 7dpa (Figure R 4A and B, and Supplementary Table 4 and Supplementary Table 5 in Appendix II). AFM measures of the non-injured myocardium and the regenerating area revealed an overall significant decrease of the ventricular ECM stiffness at 7dpa (myocardium  $2.8 \pm 0.5$  kPa and wound  $3.7 \pm 1.0$  kPa).



**Figure R 6 | Stiffness of the extracellular matrix of regenerating hearts.** (A-C) Bright field images of decellularized zebrafish hearts being analyzed by AFM at the myocardium away from the injury area. (B'-C') Bright field images of decellularized zebrafish hearts being analyzed by AFM at the regenerating area. (A) Control decellularized heart, (B,B') 7dpa decellularized hearts, (C,C') 14dpa decellularized heart. The triangular shape in A-C and B'-C' is the AFM cantilever. (D) Young's modulus of the heart ECM of non-injured, 7dpa, and 14dpa hearts (N=5 each). dpa, Days post-amputation. Statistically significance was assessed with Man-Whitney test. \*,  $p < 0.05$

The stiffness of decellularized ventricles returned back to control values by 14dpa (myocardium  $14.4 \pm 4.8$  kPa and wound  $11.9 \pm 4.0$  kPa) (Figure R 6D). No significant differences were detected between the non-injured myocardium and the regenerating area in any time points analyzed, suggesting that the ECM changes observed take place at the organ level.

**Table R 1 | Proteome of decellularized zebrafish ventricles.** List of proteins identified in the proteomic analysis that were represented over 3 spectral counts. Spectral counts were normalized by the total spectral counts in the proteomic analysis. MW, molecular weight. GO, gene ontology.

	Gene symbol	NAME	Accession number	% Seq. Coverage	Unique peptides	MW	ECM proteins	Spec. Counts Average normalized	GO Molecular function
1	myh7l	Ventricular myosin heavy chain-like	F1QSE1	49.3	108	223 kDa		306	Enzyme regulator activity, catalytic activity, structural molecule activity
2	my7	Myosin-7	A0A0G2L365	18	3	225 kDa		86	Enzyme regulator activity, catalytic activity, structural molecule activity
3	col6a3	Collagen Type VI, $\alpha$ 3 chain	F1Q4X1	17.1	41	309 kDa	*	68	Receptor activity, transporter activity
4	col1a2	Collagen Type I, $\alpha$ 2 chain	Q6IQX2	18.4	20	127 kDa	*	64	Receptor activity, transporter activity, structural molecule activity
5	hspg2	Heparan sulfate proteoglycan 2 (Perlecan)	F1RCP6	17.7	50	391 kDa	*	56	Receptor activity
6	desma	Desmin a	F1R8W4	48.8	24	54 kDa		55	Structural molecule activity
7	fn1b	Fibronectin 1b	A2CEW3	51.7	94	276 kDa	*	50	Binding
8	ahnak	AHNAK nucleoprotein	F1QZ50	8.8	40	685 kDa		48	Binding
9	fga	Fibrinogen, $\alpha$ polypeptide	B8A5L6	49.1	48	75 kDa	*	41	Binding
10	actc1a	Actin, alpha, cardiac muscle 1a	Q6IQR3	61.3	23	42 kDa		39	Structural molecule activity
11	tpm4a	Tropomyosin 4a	Q7T3F0	27.8	5	33 kDa		38	Catalytic activity, structural molecule activity
12	col1a1b	Collagen Type I, $\alpha$ 1b chain	F1QDL1	13.2	20	137 kDa	*	37	Structural molecule activity, receptor activity, transporter activity
13	cmlc1	Cardiac myosin light chain-1	BOR0F7	60.7	11	22 kDa		35	Structural molecule activity
14	fgg	Fibrinogen, $\gamma$ polypeptide	Q7ZVG7	78.7	43	49 kDa	*	35	Binding
15	spna2	Spectrin alpha 2	F1R446	24.6	44	285 kDa		34	Binding, structural molecule activity
16	fgb	Fibrinogen, $\beta$ polypeptide	Q6NVE1	76.1	50	54 kDa	*	25	Binding
17	col1a1a	Collagen Type I, $\alpha$ 1a chain	F1QJC9	14.6	17	137 kDa	*	24	Receptor activity, transporter activity, structural molecule activity
18	col6a1	Collagen Type VI, $\alpha$ 1 chain	F1Q6P3	22.8	21	107 kDa	*	22	Receptor activity, transporter activity, Structural molecule activity
19	fbn2b	Fibrillin 2b	E7FG71	13.1	19	212 kDa	*	21	Binding, structural molecule activity
20	actb2	$\beta$ -Actin 2	A8WG05	32	13	42 kDa		21	Structural molecule activity

	<b>Gene symbol</b>	<b>NAME</b>	<b>Accession number</b>	<b>% Seq. Coverage</b>	<b>Unique peptides</b>	<b>MW</b>	<b>ECM proteins</b>	<b>Spec. Counts Average normalized</b>	<b>GO Molecular function</b>
<b>21</b>	emilin1b	Emilin 1b	F1Q9G3	28.3	25	117 kDa	*	20	Binding
<b>22</b>	myhb	Myosin, heavy chain b	F1QVX3	7	1	223 kDa		20	Enzyme regulator activity, binding, catalytic activity, structural molecule activity
<b>23</b>	ttna	Titin a	F1R7N8	1.6	29	3090 kDa		20	Catalytic activity, structural molecule activity, binding, enzyme regulator activity
<b>24</b>	atp5b	ATP synthase subunit beta	A8WGC6	46.2	17	55 kDa		20	Catalytic activity, transporter activity, binding
<b>25</b>	atp5a1	ATP synthase subunit alpha	Q08BA1	32.8	15	60 kDa		18	Receptor activity, transporter activity, binding, catalytic activity
<b>26</b>	sptb	Spectrin, beta, erythrocytic	F1QQE5	14.9	25	273 kDa		16	Binding, structural molecule activity
<b>27</b>	postna	Periostin A	F1QM50	20.9	2	97 kDa	*	16	Binding
<b>28</b>	mybpc3	Myosin binding protein C, cardiac	F1Q615	15.2	17	144 kDa		15	Binding, structural molecule activity
<b>29</b>	col6a2	Collagen Type VI, $\alpha$ 2 chain	E7FCV8	24.2	21	107 kDa	*	15	Receptor activity, transporter activity, structural molecule activity
<b>30</b>	sptbn1	Spectrin, beta, non-erythrocytic 1	A0A0G2L1F5	12.1	24	263 kDa		15	Binding, structural molecule activity
<b>31</b>	actn2b	Actinin, alpha 2b	E9QFR8	22.7	17	103 kDa		15	Binding
<b>32</b>	krt8	Keratin, type II cytoskeletal 8	K2C8	19.6	12	58 kDa		15	Structural molecule activity
<b>33</b>	myl7	Myosin light chain 2	Q801M3	58.1	6	19 kDa		13	Structural molecule activity
<b>34</b>	itih2	Inter-alpha-trypsin inhibitor heavy chain 2	Q5RH29	16.5	13	106 kDa		12	Enzyme regulator activity, Binding
<b>35</b>	col4a1	Collagen Type IV, $\alpha$ 1 chain	F1Q8S5	3.5	4	154 kDa	*	11	Receptor activity, transporter activity, structural molecule activity
<b>36</b>	col4a2	Collagen Type IV, $\alpha$ 2 chain	F1QZI8	4.9	6	165 kDa	*	10	Receptor activity, transporter activity, Structural molecule activity
<b>37</b>	col5a1	Collagen Type V, $\alpha$ 1 chain	F6NPA4	3.8	6	199 kDa	*	10	Structural molecule activity, binding
<b>38</b>	ttnb	Titin b	B0S6Y0	0.8	4	627 kDa		9	Catalytic activity, binding
<b>39</b>	col5a2a	Collagen Type V, $\alpha$ 2a chain	F1QT86	4.7	5	147 kDa	*	9	Structural molecule activity
<b>40</b>	lamc1	Laminin subunit $\gamma$ -1	Q1LVF0	8.1	10	176 kDa	*	9	Receptor activity
<b>41</b>	emilin1a	Emilin 1a	F1QC17	12.9	10	113 kDa	*	8	Binding
<b>42</b>	col6a6	Collagen Type VI, $\alpha$ 6 chain	F1Q924	10.4	20	278 kDa	*	7	Receptor activity, transporter activity

	<b>Gene symbol</b>	<b>NAME</b>	<b>Accession number</b>	<b>% Seq. Coverage</b>	<b>Unique peptides</b>	<b>MW</b>	<b>ECM proteins</b>	<b>Spec. Counts Average normalized</b>	<b>GO Molecular function</b>
<b>43</b>	atp2a2a	Calcium-transporting atpase	A9C3Q4	12.5	10	115 kDa		6	Transporter activity, catalytic activity
<b>44</b>	mb	Myoglobin	Q6VN46	51.7	6	16 kDa		6	Transporter activity, binding
<b>45</b>	palm1b	Paralemmin 1b	B0V0Y4	18.9	4	27 kDa		6	Protein binding, D3 dopamine receptor binding
<b>46</b>	atp1a1a.1	Atpase, Na+/K+ transporting, alpha 1a polypeptide, tandem duplicate 1	Q9DGL6	8.7	6	113 kDa		6	Transporter activity, catalytic activity
<b>47</b>	mfap5	Microfibrillar associated protein 5	E9QCC4	16.7	3	15 kDa	*	5	Structural molecule activity
<b>48</b>	slc25a5	Solute carrier family 25 alpha	Q8JHI0	13.1	4	33 kDa		5	Transporter activity
<b>49</b>	aldoaa	Fructose-bisphosphate aldolase	Q803Q7	25	7	40 kDa		4	Catalytic activity
<b>50</b>	fina	Filamin A, alpha	E9QI62	3.6	6	273 kDa		4	Binding
<b>51</b>	mfap2	Microfibrillar-associated protein 2	F1QSF1	6.3	1	18 kDa	*	4	-
<b>52</b>	slc8a1a	Solute carrier family 8	F1R4F4	9.8	6	107 kDa		4	Transporter activity
<b>53</b>	slmapa	Sarcolemma associated protein a	F6NHV5	8.3	6	94 kDa		4	Binding
<b>54</b>	tln1	Talin 1	A0A0R4IDZ8	6.3	8	271 kDa		4	Binding
<b>55</b>	tpma	Tropomyosin 1 (alpha)	F6NVA3	27.8	6	33 kDa		4	Binding
<b>56</b>	palm2	Paralemmin 2	E7F8N8	7.8	6	92 kDa		4	-
<b>57</b>	pleca	Plectin a	A5WV02	1.5	6	523 kDa		4	Binding, structural molecule activity
<b>58</b>	postnb	Periostin B	Q75U66	37.1	19	86 kDa	*	4	Binding
<b>59</b>	sorbs1	Sorbin and SH3 domain containing 1	A0A0R4IP30	11.2	7	86 kDa		4	Binding
<b>60</b>	wfdc2	Wfdc2	E7F3G3	26.8	5	18 kDa		4	Binding, catalytic activity
<b>61</b>	aco2	Aconitate hydratase, mitochondrial	F8W4M7	10.9	6	86 kDa		3	Binding, catalytic activity
<b>62</b>	ldhba	L-lactate dehydrogenase B-A chain	Q9PVK4	11.4	3	36 kDa		3	Catalytic activity
<b>63</b>	myom1b	Myomesin 1b	A0A0R4IGQ8	4.9	7	181 kDa		3	Binding, structural molecule activity

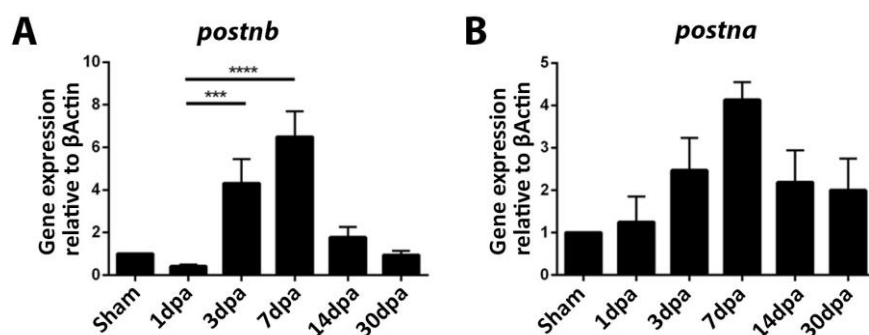




## CHAPTER 2: ROLE OF POSTNB DURING ZEBRAFISH HEART REGENERATION

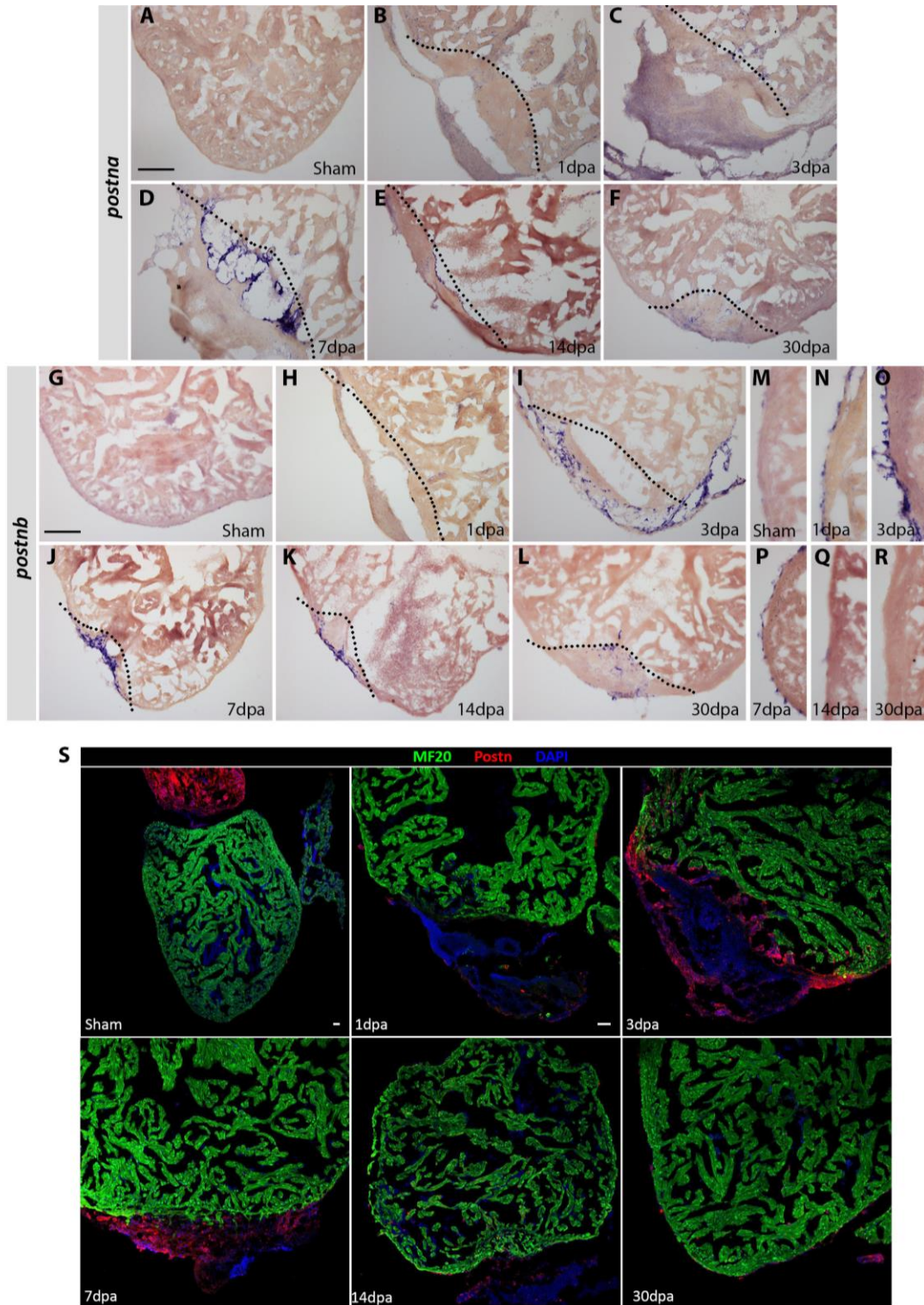
### 4.1.5. Characterization of *postnb* in zebrafish cardiac injury

One of the proteins observed in the proteome to be dynamically expressed during cardiac regeneration was periostin B (*postnb*). Thus, first we wanted to confirm and characterize its expression during zebrafish heart regeneration. By qRT-PCR, we corroborated that *postnb* levels increase after adult ventricular resection, raising above baseline at 3dpa and peaking at ~7-fold above sham levels by 7dpa. Sham *postnb* expression levels were already acquired by 14dpa (Figure R 7A). We also checked the expression pattern of the other periostin paralog, *postna*, having a ~4-fold increase above baseline at 7dpa, but not being differentially expressed in any other time point assessed (Figure R 7B). To examine the expression patterns of the individual *postn* paralogs during zebrafish heart regeneration, we did *in situ* hybridization with DIG-labelled RNA probes specific for either *postna* or *postnb*. Both *postna* and *postnb* were



**Figure R 7 | Periostin is dynamically expressed during cardiac regeneration.** Ventricular expression of *postnb* (A) and *postna* (B) during zebrafish heart regeneration by qRT-PCR. Expression relative to  $\beta$ -actin. Kluskal Wallys analysis with Dunn's multiple comparison test was used to assess for statistical significance. \*\*\*,  $p < 0.001$ ; \*\*\*\*,  $p < 0.0001$ .

#### 4. RESULTS



**Figure R 8 | Periostin is expressed in the injury site.** (A-F) *In situ* hybridization for *postna* in uninjured (A) and regenerating hearts at 1dpa (B), 3dpa (C), 7dpa (D), 14dpa (E), and 30dpa (F). (G-R) *In situ* hybridization for *postnb* in uninjured (I,M) and regenerating hearts at 1dpa (H,N), 3dpa (I,O), 7dpa (J,P), 14dpa (K,Q), and 30dpa (L,R). (M-R) Epicardial expression of *postnb* in uninjured (M) and regenerating hearts (N-R). In each section, violet indicates positive signal. (S) Periostin expression by immunohistochemistry in uninjured (sham) and regenerating hearts 1dpa, 3dpa, 7dpa, 14dpa, and 30dpa. dpa, days post-amputation; *postn*, periostin. Scale bars 100µm.

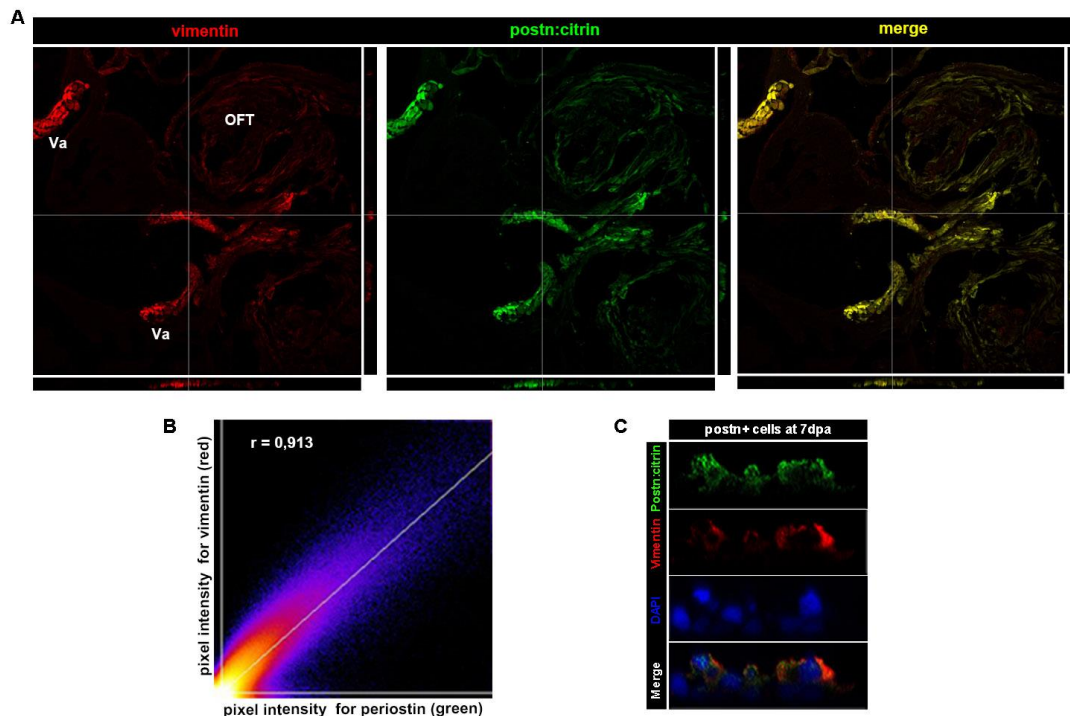
undetectable in the uninjured ventricle (Figure R 8A and G) but some minor staining in the epicardium. The expression of both paralogs was also localized in the out-flow tract and valves in uninjured hearts. *postna* was shyly localized in the injured ventricular apex by 3dpa (Figure R 8C) and higher expressed in the inner part of the injury and endocardium by 7dpa (Figure R 8D). By 14dpa, some endocardial localization was still detected (Figure R 8E), and by 30dpa, a time when the myocardial wall has been typically replaced, we detected little or no *postna* (Figure R 8F). Contrary, *postnb* paralog was expressed along the epicardium of injured ventricles (Figure R 8M-R), and was strongly induced at 3dpa and 7dpa in the injured ventricular apex (Figure R 8J and I). By 14dpa, the expression was maintained at the injury but clearly reduced (Figure R 8K), and by 30dpa little expression was detected (Figure R 8L). These results revealed dynamic distribution of both *postn* paralogs, possibly in different cell type(s) within the injured apex. The *postnb* paralog displayed an injury profile that suggested a role specific to ventricular regeneration.

It is known that the cell type that express periostin is a group of activated fibroblasts called myofibroblasts (Sánchez-Iranzo et al., 2018). Thus, we further checked whether the observed periostin expressing cells were fibroblasts. By immunohistochemistry against vimentin, a fibroblast specific marker, we observed that citrin positive cells from the Periostin:citrin line were also vimentin positive (Figure R 9A and B). When calculated the Pearson correlation coefficient with ImageJ program, a highly confident correlation between both signals was obtained ( $r=0.913$ ) (Figure R 9B). We checked also the periostin signal during regeneration, and cells expressing periostin were also vimentin positive (Figure R 9C). Contrary, when checking periostin colocalization with a cardiomyocyte marker no colocalization was observed (Figure R 8S). Thus, we corroborated that the periostin expressing cells were not cardiomyocytes but fibroblasts.

To confirm the induction at protein level, we assessed the ventricles injured by apical resection at different time points, using an antibody that recognizes zebrafish *postn*. We identified a strong localization of the protein in injury site at 3dpa and 7dpa

## 4. RESULTS

(Figure R 8S), indicating that the presence of the protein is conferred to the more external part of the wound.

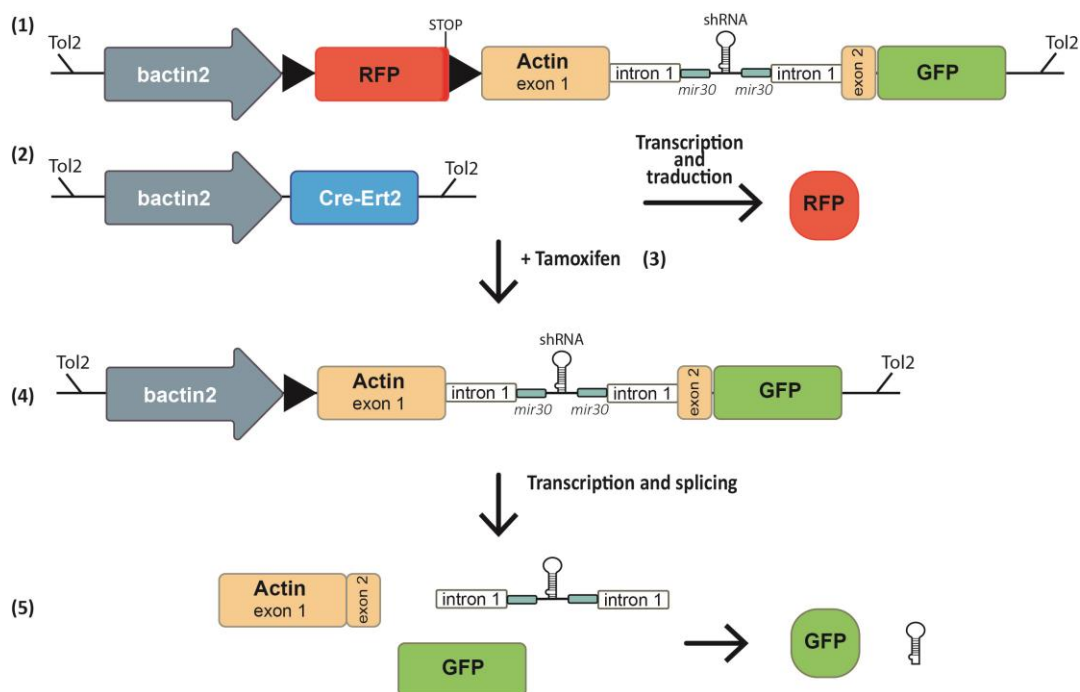


**Figure R 9 | Periostin colocalization with vimentin.** (A) Citrin signal from periostin:citrin zebrafish colocalizes with vimentin signal in the out-flow tract and valves of zebrafish heart. (B) Colocalization analysis with Imagej between periostin (green) and vimentin (red) signals.  $r$ , pearson correlation value. (C) Cells at the wound site of 7dpa regenerating hearts expressing periostin and vimentin. OFT, out-flow tract; Va, valve.

### 4.1.6. Generation of a conditional shRNA expressing knock-down zebrafish line for *postnb* to study cardiac regeneration

Periostin has been implicated in numerous biological processes related to collagen cross-linking, wound healing, cell migration, cell proliferation and development (Nishiyama et al., 2011; Norris et al., 2007; Rios et al., 2005; Shimazaki et al., 2008; Yokota et al., 2017). In order to know if *postnb* is also needed for zebrafish heart regeneration, we generated a shRNA-mediated LOF transgenic zebrafish strain expressing a shRNA under the ubiquitous promoter  $\beta$ -actin, which knocked-down *postnb* all over the organism (dTg((bactin2:loxP-RFP-STOP-loxP-bactin2-miR30-shRNA-GFP)(bactin2:CRE-Ert2)), from now on Tg(bactin2:IRFPI-shRNA-GFP)) (Figure R 10). We

designed this transgenic strain following Dong et. al and De Rienzo et. al strategy, where the shRNA is within the context of the *mir30e* and placed inside the intron of the *bactin2* gene to help its processing and increase its efficiency (De Rienzo et al., 2012; Dong et al., 2009). The map of the construct can be found at Supplementary Figure 2 in appendix III. We decided to generate a knock-down transgenic line instead of a knock-out, since literature regarding *postn*<sup>-/-</sup> mice revealed valve developmental defects and perinatal death (Rios et al., 2005). Therefore, we wanted to deplete *postnb* only in adult zebrafish during regeneration.

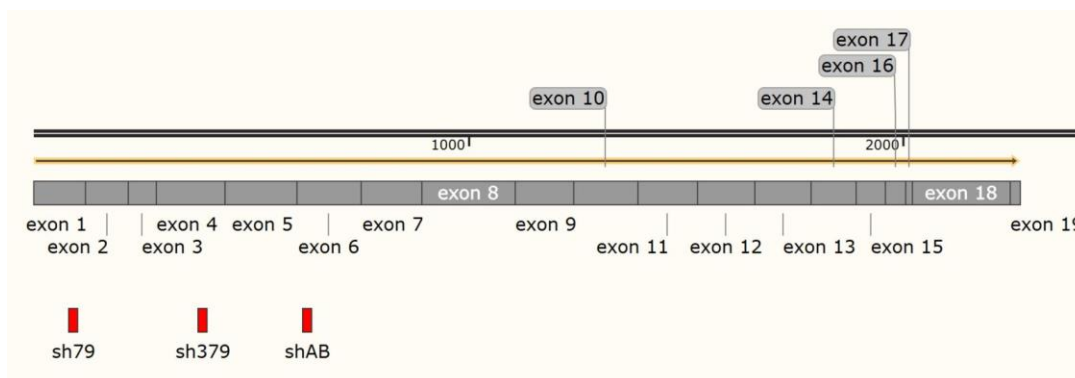


**Figure R 10 | Constructs of the conditional shRNA expressing knock-down transgenic zebrafish line for *postnb*.** (1) and (2) are the independently integrated constructs of the double-transgenic (dTg) zebrafish line. (1) The ubiquitous promoter *bactin2* controls the expression of the downstream construct, which contains a floxed RFP with an STOP codon at the end followed by 4 polyA tails. Then the first exon, the first intron and 22bp of the second exon of the *bactin2* gene were cloned. Inside the intron the shRNA was placed in the context of the *mir30e*. At the end, the GFP protein was in frame fused. (2) The second construct of the dTg line allows the expression of an inducible Cre recombinase fused to an estrogen receptor. Thus, fishes with these two constructs express RFP but not GFP in basal conditions. (3) When fishes are treated with 4OH-tamoxifen (an estrogen analogous) the construct recombines within the loxP sites (black triangles) and the RFP with the STOP codon is excised (4). After transcription and splicing (5) the shRNA and the GFP can be correctly processed in order to be recognized by the Argo/RISC complex and correctly translated, respectively. loxP sites, black triangles. Promoter has an arrow shape and proteins a round shape.

Three different shRNAs were designed targeting different regions of the *postnb* mRNA. The sh79 was designed against exon 1, the sh379 against exon 4 and the shAB

#### 4. RESULTS

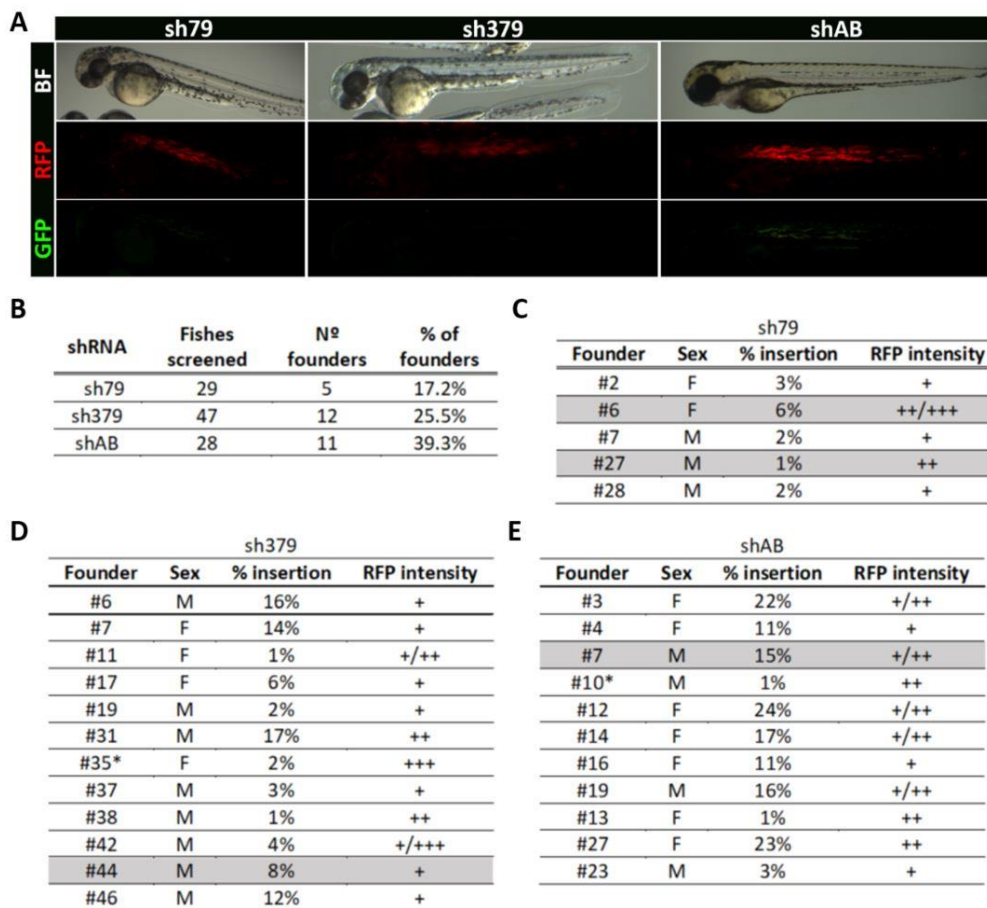
against exon 6. The last one targeting a small region conserved in both *postna* and *postnb* (Figure I 11). After generating one construct for each shRNA, they were individually injected at one cell stage of Tg(bactin2:CRE-Ert2) embryos in order to create three individual transgenic lines (Figure R 12A). When the injected fishes reached adulthood (~3 months), they were crossed with Tg(bactin2:CRE-Ert2) fishes in order to look for positive offspring, and therefore identify founder fishes. The percentage of founder fishes detected varied among the shRNAs from 17% to 39% (Figure R 12B). The identified founders had also variability among the percentage of insertion (percentage of positive offspring) and fluorescence intensity. The percentage of insertion varied between 1 and 24%, and the intensities could be sorted into low (+), middle (++), and high (+++) (Figure R 12C-E). All the founders detected were individually assessed for correct construct functionality in order to generate a stable transgenic line from the selected ones.



**Figure R 11| Localization of the designed shRNAs.** Mapping of the shRNAs over *postnb* transcript 1.

Correct CRE recombination was assessed by 4OH-tamoxifen and nuclear CRE (CRE-nls) injection (Figure R 13A and B). Both systems displayed a good recombination rate in many lines from different shRNAs, increasing the GFP signal all over the embryo indirectly being a sensor for shRNA expression. After detecting a good recombination and verifying that all the construct was inserted in the genome by the GFP fluorescence detection, efficiency of the shRNAs to decrease the *postnb* mRNA was evaluated by qRT-PCR (Figure R 13C). Four different lines from different shRNAs were selected, since they displayed good construct recombination and reduction of *postnb* RNA (Figure R 13). The reduction of *postnb* after embryonic 4OH-tamoxifen treatment for the founders n<sup>o</sup>6 and

n<sup>o</sup>27 from sh79, n<sup>o</sup>44 from sh379 and n<sup>o</sup>7 from shAB was 26.86%, 47.16%, 54%, and 60.83%, respectively (Figure R 13C). When CRE-nls was injected the *postnb* reduction was 25.22%, 22.37%, 18%, and 60.41%, respectively. Not any effect on *postna* RNA was observed in any of the shRNAs. Hence, the shAB line from the founder n<sup>o</sup> 7 was the one obtaining a greater decrease of *postnb* RNA and the one from which the definitive shRNA line was originated.

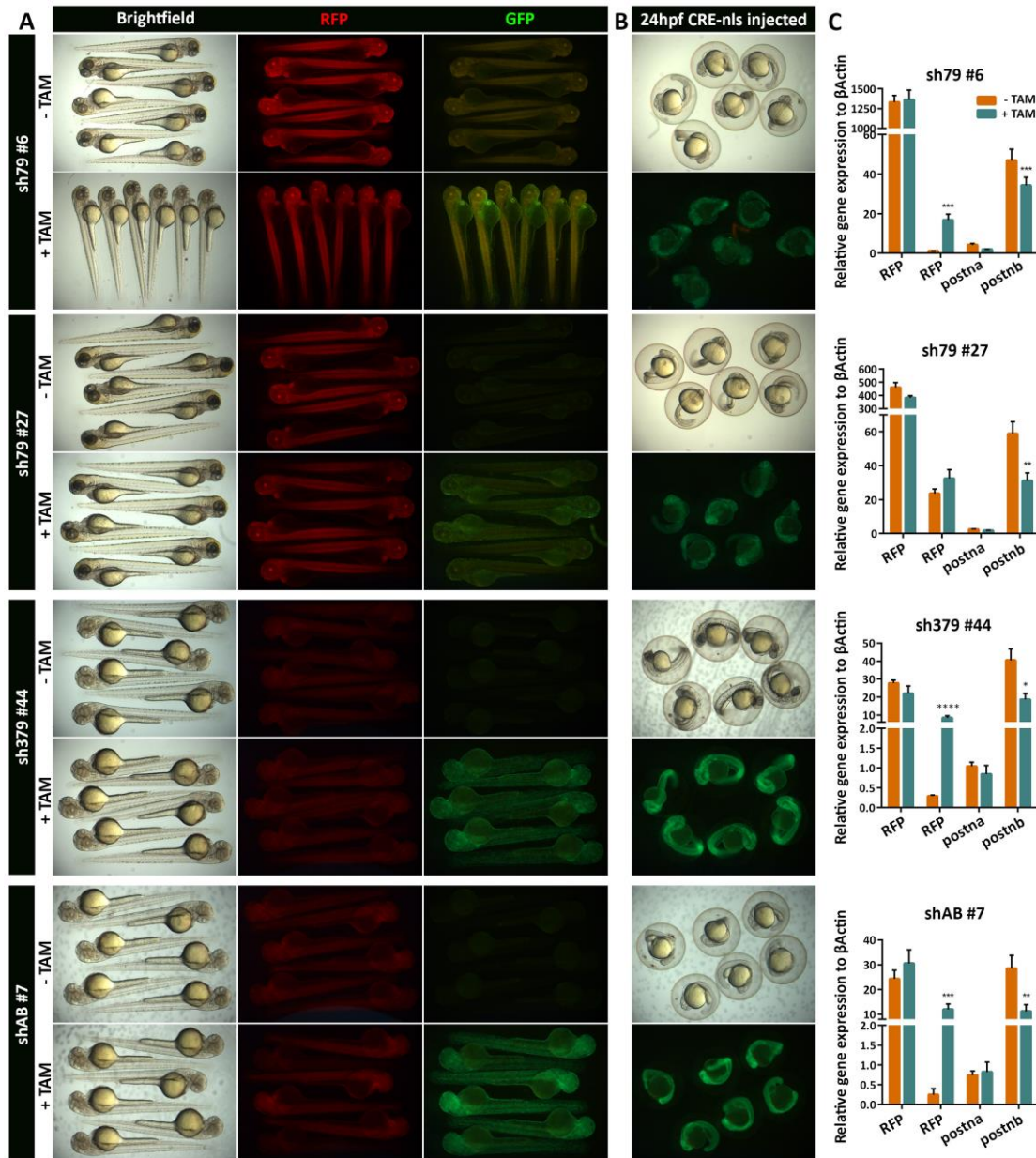


**Figure R 12 | shRNA construct injection and founders.** (A) Representative injected fishes from each shRNA. Bright Field, RFP and GFP channels are shown. (B) Number of founders encountered for each shRNA injected. (C-E) Characteristics of all the founders detected from sh79 (C), sh379 (D), and shAB (E). Fishes highlighted in grey were the selected ones after functionality assessment. \*, died before functional assessment. M, Male; F, Female; +, low; ++, middle; +++, high.

To sum up, the final Tg(bactin2:IRFPI-shRNA-GFP) line contained the shAB and achieved a ~10-fold increase of GFP levels at 48hpf upon 4OH-tamoxifen treatment. Moreover, levels of *postnb* were decreased by 60% on average, while *postna* levels did not change (Figure R 13C). This decrease may reflect mosaic expression of the shRNA,

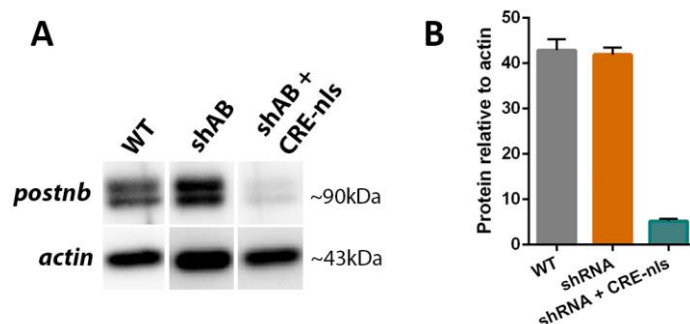
#### 4. RESULTS

conferred by the 4OH-tamoxifen treatment efficiency, or targeting efficiency of the shRNA.



**Figure R 13 | Functionality assessment of the best shRNA lines.** (A) F2 embryos at 48hpf from the best founders from different shRNAs with (+ TAM) and without (- TAM) 4OH-tamoxifen treatment. GFP expression indicates construct recombination. (B) GFP expression at 24hpf after Cre-nls injection at 1 cell-stage. (C) RNA expression of RFP, GFP, *postna* and *postnb* by qRT-PCR of 48hpf embryos (+ TAM) and without (- TAM) 4OH-tamoxifen treatment. Kluskal Wallys analysis with Dunn's multiple comparison test was used to assess for statistical significance. \*,  $p < 0.05$ ; \*\*,  $p < 0.01$ ; \*\*\*,  $p < 0.001$ ; \*\*\*\*,  $p < 0.0001$ .

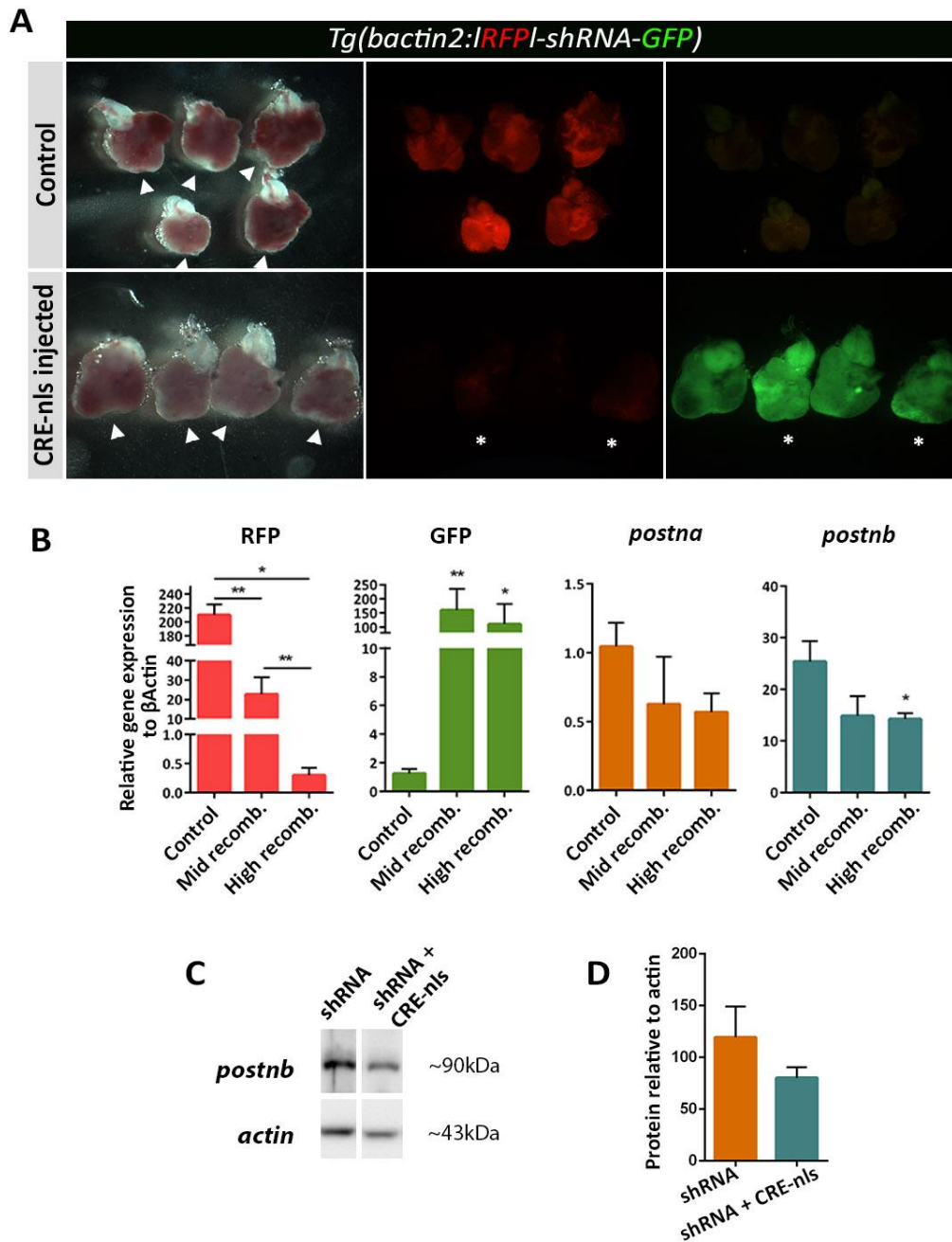




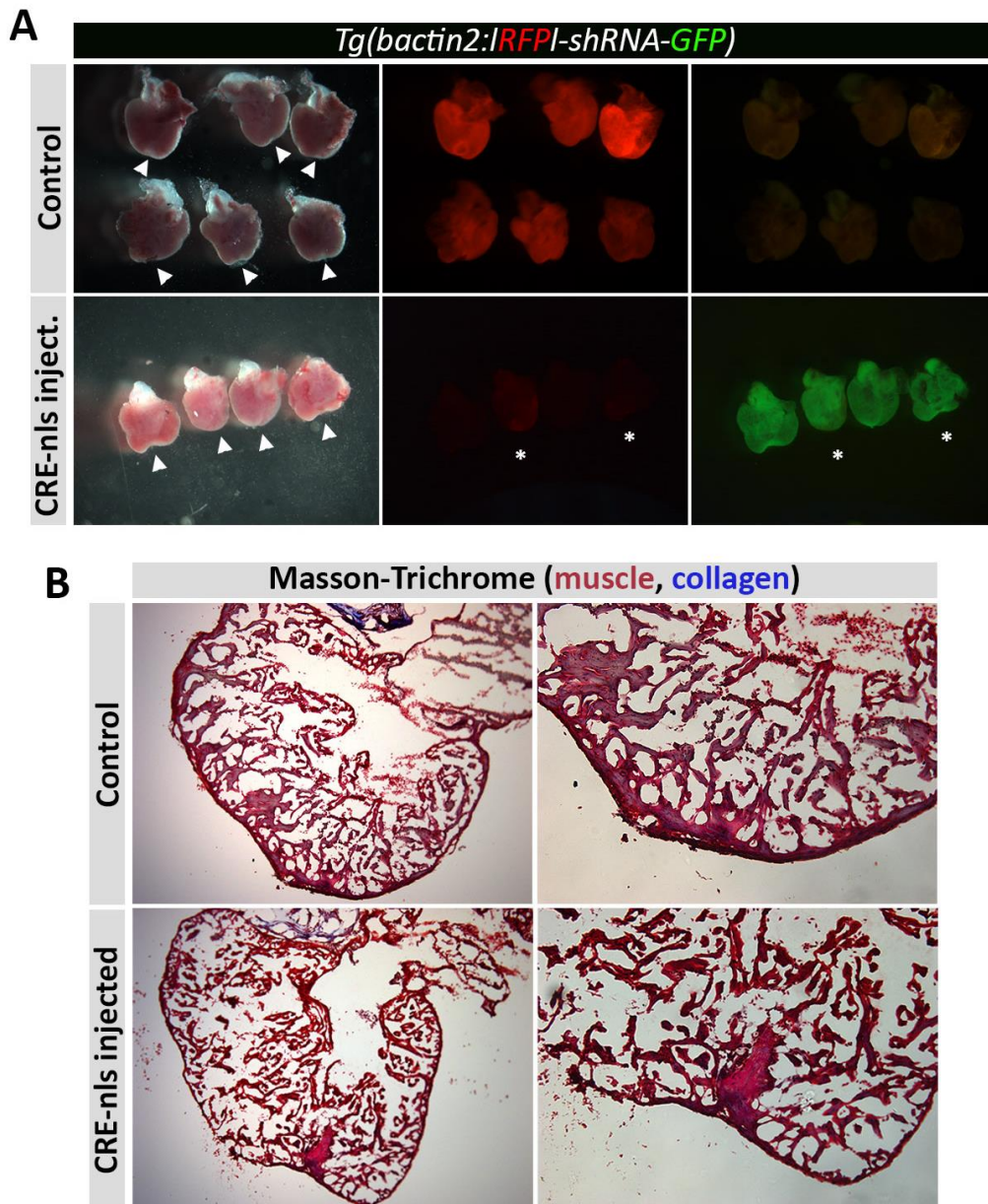
**Figure R 14 | Embryonic *postnb* protein expression in the shRNA line and after recombination. (A)** *postnb* and actin western blot of WT, shRNA line (shAB) and shRNA line after recombination with CRE-nls injection at 1 cell-stage. Samples are embryos at 4 days post-fertilization. **(B)** Quantification of the western blot band intensity corrected by actin band intensity.

Consistent with shRNA-mediated targeting, an ~88% reduction of *postnb* protein levels were also detected by western blot in embryos when compared with WT or the transgenic line without recombination (Figure R 14). Following shRNA induction by 4OH-tamoxifen treatment or CRE-nls, transgenic embryos did not display any apparent morphological alteration nor swimming defect as reported upon morpholino injection against periostin (Kudo et al., 2004). *postnb* expression levels were also evaluated in adult zebrafish at 7dpa, since *postnb* expression in adult hearts is low and 7dpa is the expression peak of *postnb* in cardiac regeneration. Adult fish injected with CRE-nls at 1-cell stage did not display any detectable alterations in general nor in cardiac development. These animals were amputated (Figure R 15A) and at 7dpa *postnb*, as well as GFP, RFP and *postna*, RNA expression levels were evaluated, resulting in a reduction of ~44% of *postnb* expression (Figure R 15B). In terms of RFP RNA levels, a ~88% and ~99% reduction was found in partially recombined and completely recombined adult hearts, respectively. Moreover, an increase of >100-fold in GFP expression in recombined hearts was detected (Figure R 15A and B). This RNA level reduction resulted in a 32.8% decrease of *postnb* protein levels, assessed by Western Blot (Figure R 15C and D). Recombination by tamoxifen treatment in adult individuals was evaluated without success. Hearts were unable to successfully recombine, although the offspring of the treated adult animals recombined upon embryonic tamoxifen treatment (Supplementary Figure 3 in appendix III). Same tamoxifen treatment was evaluated in

## 4. RESULTS



**Figure R 15| Adult *postnb* reduction by shRNA at 7dpa. (A)** Zebrafish hearts at 7dpa of not recombined (control) and recombined hearts by CRE-nls injection at 1 cell-stage. Arrowheads mark the wound. Asterisk marks those hearts not completely recombined. **(B)** RFP, GFP, *postna* and *postnb* RNA expression by qRT-PCR. Animals were separated in mid recombination when some RFP was detected under the microscope or high recombination when no RFP fluorescence was observed. Control stands out for not recombined hearts. **(C)** *postnb* and actin western blot of shRNA line (shAB) and shRNA line after recombination with CRE-nls injection at 1 cell-stage. Samples are hearts at 7dpa. **(D)** Quantification of the western blot band intensity corrected by actin band intensity. Mann-Whitney analysis was used to assess for statistical significance. \*,  $p < 0.05$ ; \*\*,  $p < 0.01$ .



**Figure R 16| Cardiac regeneration difficulty by *postnb* knock-down.** (A) Zebrafish hearts at 30dpa of not recombined (control) and recombined hearts by CRE-nls injection at 1 cell-stage. Arrowheads mark the wound. Asterisk marks those hearts not completely recombined. (B) Masson Trichrome staining of not recombined (control) and recombined hearts by CRE-nls injection at 1 cell-stage at 30dpa.

other transgenic lines available in our group, which recombined satisfactorily (Supplementary Figure 4 in appendix III).

Ventricles of Cre-nls injected animals were also extracted at 30dpa in order to evaluate their regeneration capability. Recombined hearts appeared to have bigger wounds compared to non-recombined clutchmates (Figure R 16A). Masson trichrome

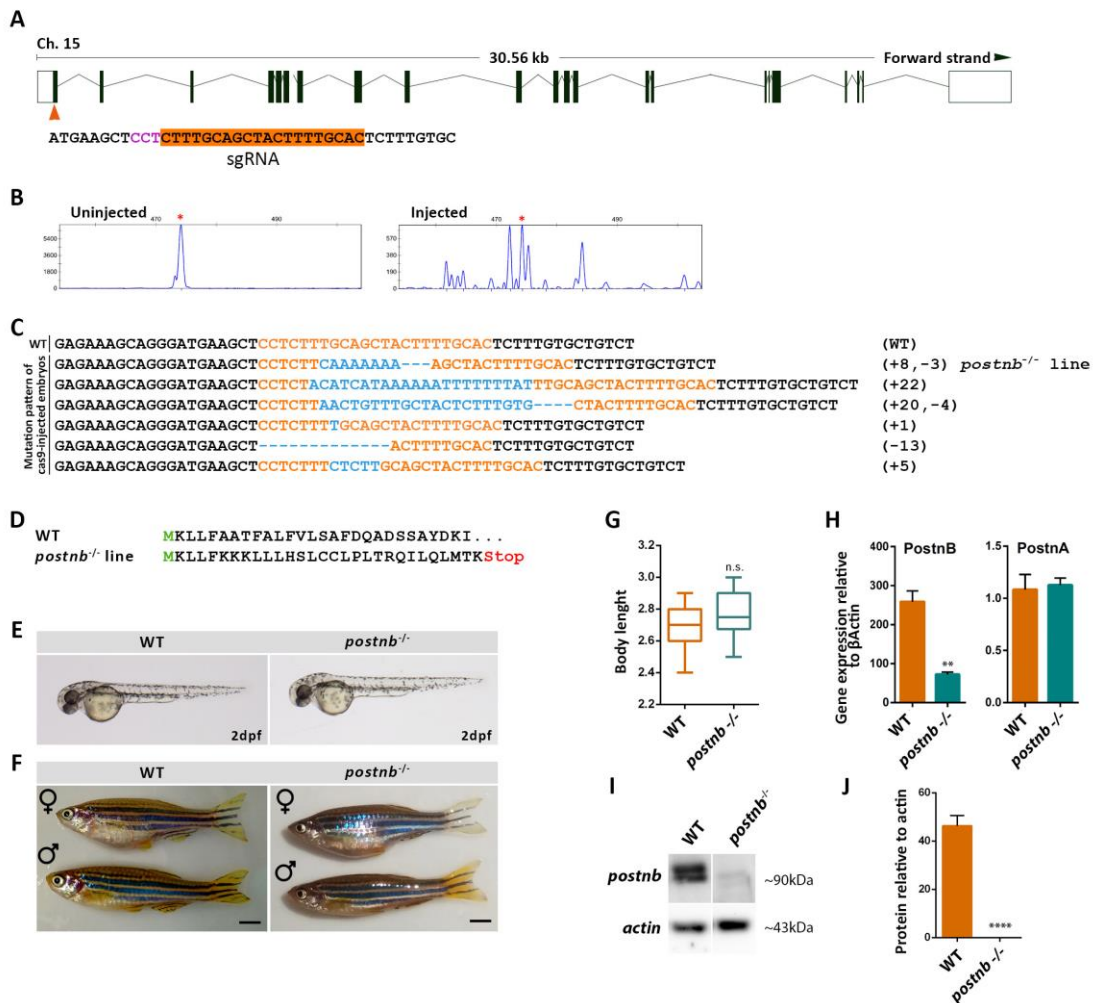
## 4. RESULTS

staining confirmed this result, where shRNA expressing hearts had not appropriately grown the myocardium after 30dpa (Figure R 16B). Even so, we were not sure that the protein reduction accomplished by this knock-down line would be enough to assess the possible role of *postnb* during zebrafish heart regeneration process. This fact together with the lack of increased embryonic or adult mortality in 1 cell-stage recombined fishes, we decided to generate a genomic knock-out.

### 4.1.7. Generation of a knock-out *postnb* line using CRISPR-Cas9 technology to study cardiac regeneration

CRISPR/Cas9 has been recently a great tool for genome editing and knock-out (KO) generation (Gonzales and Joanna Yeh, 2014). Thus, in order to know which is the role of *postnb* during zebrafish heart regeneration, we decided to generate a KO line with CRISPR/Cas9 technology. We designed 4 different sgRNAs targeting the first intron of the *postnb* gene (data not shown) and after analyzing the cutting efficiency of them we chose the one starting 9bp downstream the ATG of the gene (Figure R 17A). The chosen sgRNA was able to cut the *postnb* genomic region with good efficiency (Figure R 17B) generating different indels in the *postnb* locus (Figure R 17C). We only considered acceptable, those indels that changed the reading frame, having the likelihood to generate an early stop codon and truncate the protein as a result. We chose the (+8, -3) indel in order to generate our transgenic line. This indel was predicted to generate a protein of 29 amino acids with a premature stop codon (Figure R 17D).

While generating the stable *postnb*<sup>-/-</sup> line with the selected mutation, we decided to obtain compound *postnb*<sup>-/-</sup> fishes incrossing the F0 (those that the sgRNA and the Cas9 were injected) in order to perform the first regeneration experiments. To select the KO fishes, all the F1 was genotyped to characterize both *postnb* alleles. All the alleles selected during the genotyping (Figure R 17C) generated an early stop codon. Biallelic KO embryos and adult fishes did not display any detectable phenotype nor developmental defect (Figure R 17E, F and G). Moreover, adult *postnb*<sup>-/-</sup> fishes had a normal growth having no effect on body length (Figure R 17G). These animals showed a



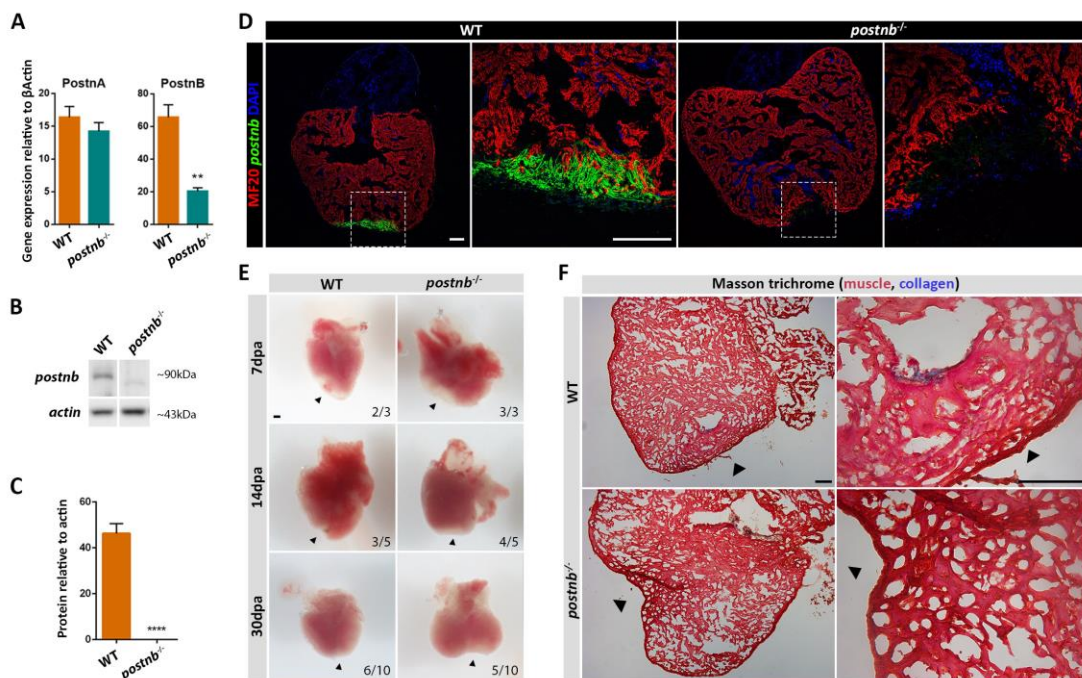
**Figure R 17 | *postnb*<sup>-/-</sup> line by CRISPR/Cas9.** (A) Design of the sgRNA against *postnb* targeting the 1st exon. Target sequence is highlighted in orange, and PAM region is shown in purple letters. (B) Comparison of an uninjected embryo and an embryo where sgRNA+Cas9 was injected into the cell at one-cell stage. Red asterisk marks the WT peak at 474bp, the other peaks in the injected embryo are indicative of the activity of the sgRNA. (C) Mutation pattern of sgRNA and Cas9 protein coinjected embryos. Numbers in the brackets show the number of nucleotides that were deleted (-) or inserted (+). Inserted nucleotides are shown in blue, while orange indicate the original nucleotides of the sgRNA target site. (D) Prosite predicted protein sequences from WT and the KO allele (+8,-3). (E) Images of 2dpf WT and *postnb*<sup>-/-</sup> embryos. (F) Images of an adult male and a female of WT and *postnb*<sup>-/-</sup> zebrafish. (G) Boxplot of the body length from head to tail-base of WT and *postnb*<sup>-/-</sup> zebrafish. (H) qRT-PCR of *postna* and *postnb* gene expression of 2dpf WT and *postnb*<sup>-/-</sup> embryos. Expression relative to β-actin. (I) Western Blot for *postnb* and actin in 4dpf WT and *postnb*<sup>-/-</sup> embryos. (J) Western blot quantification of band intensity corrected by actin. Three biological replicates were quantified. WT, wild-type; dpf, days post-fertilization. Two-tailed T-test was used to assess for statistical significance. \*\*, *p*<0.01; n.s., non-significant. Scale bars 5mm.

reduction in *postnb* RNA levels of ~80%, while no effect on *postna* expression (Figure R 17H), and a complete absence of the *postnb* protein (Figure R 17I and J). Same results were observed in regenerating adult hearts assessed at 7dpa, where a reduction of ~65% *postnb* RNA and no effect on *postna* expression (Figure R 18A), as well as no *postnb* protein were observed (Figure R 18B and C). The reminiscent presence of some RNA

#### 4. RESULTS

content may be due to the fact of the non-sense mediated decay effect. The presence of *postnb* protein was corroborated with an immunohistochemistry at 7dpa, where *postnb* presence in the wound was observed in WT but not in *postnb*<sup>-/-</sup> hearts (Figure R 18D).

We injured adult *postnb*<sup>-/-</sup> and WT clutchmates and assessed regeneration. During all the regeneration process, *postnb*<sup>-/-</sup> fishes had a bigger and withier wound in comparison to WT clutchmates (Figure R 18E). After 30dpa, *postnb*<sup>-/-</sup> fish were less frequently able to regenerate a contiguous wall of new muscle. Moreover, no collagen was observed in *postnb*<sup>-/-</sup> wounds in comparison to WT at 30dpa with Masson trichrome staining (Figure R 18F). Same results were observed at 7dpa, where a bigger wound was seen in *postnb*<sup>-/-</sup> ventricles (Figure R 18D). Based on these data, we conclude that *postnb* is required for correct heart regeneration.



**Figure R 18| Cardiac regeneration is impaired in *postnb*<sup>-/-</sup> zebrafish.** (A) qRT-PCR of *postna* and *postnb* gene expression of 7dpa WT and *postnb*<sup>-/-</sup> hearts. Expression relative to  $\beta$ -actin. (B) Western Blot for *postnb* and *actin* of 7dpa WT and *postnb*<sup>-/-</sup> hearts. (C) Western blot quantification of band intensity corrected by actin. Three biological replicates were quantified. (D) Immunohistochemistry of *postnb* and myosin heavy-chain (MF20) of WT and *postnb*<sup>-/-</sup> hearts at 7dpa. White squares indicate the magnification site. (E) Representative regenerating hearts of WT and *postnb*<sup>-/-</sup> zebrafish. The time points pictured are: 7dpa, 14dpa and 30dpa. (F) Masson Trichrome staining of ventricles at 30dpa of WT and *postnb*<sup>-/-</sup> hearts. Black arrows in E and F indicate the injury site. dpa, days post-amputation; WT, wild-type. Two-tailed T-test was used to assess for statistical significance. \*\*,  $p < 0.01$ ; \*\*\*\*,  $p < 0.0001$ . Scale bars 100 $\mu$ m.

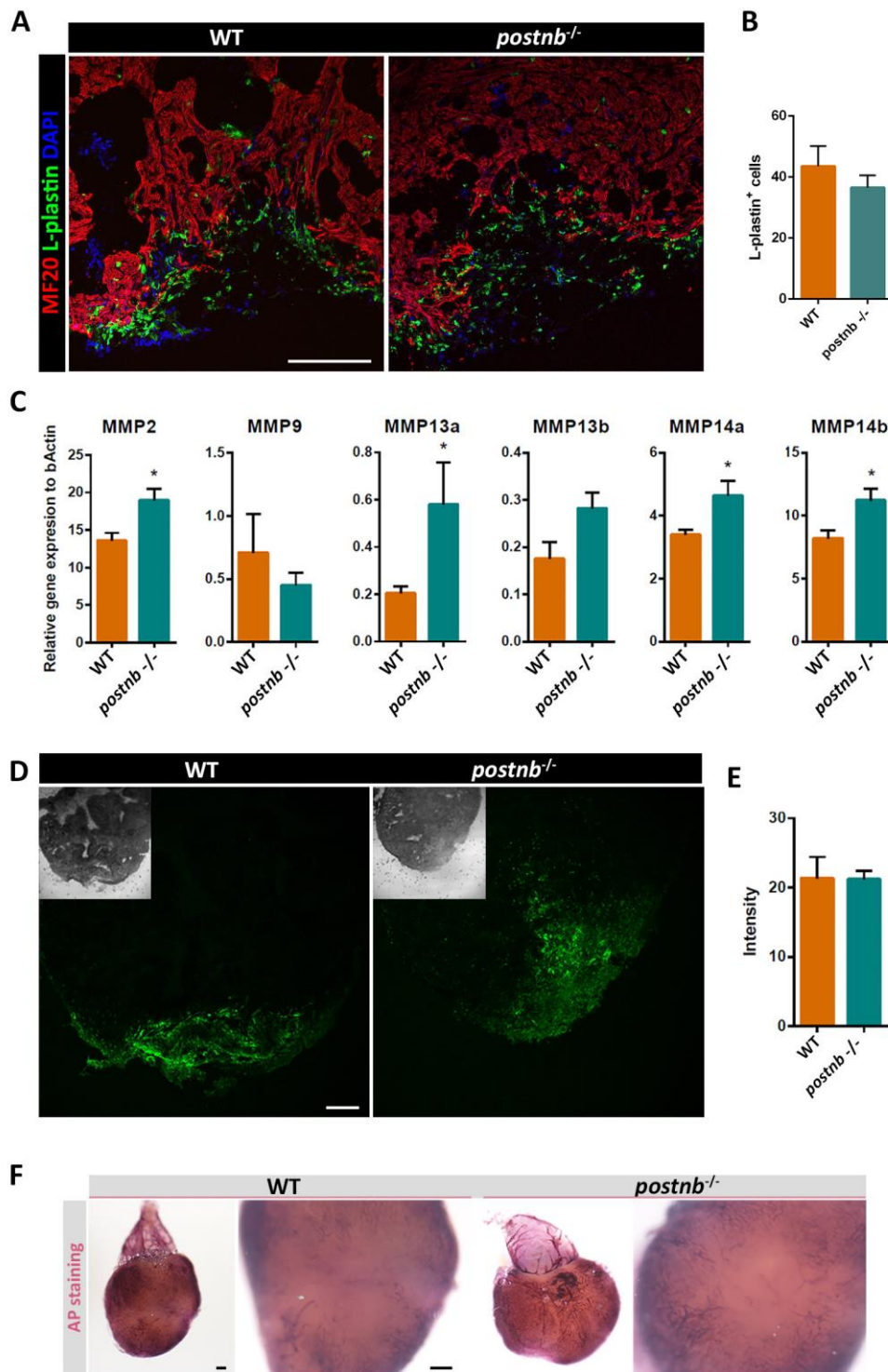
#### 4.1.8. Macrophage recruitment, matrix metalloproteinase activity and revascularization are not affected in *postnb*<sup>-/-</sup> regenerating zebrafish

In the literature, the processes where periostin is involved are numerous and its effects too. One of the described periostin activities, is its role on promoting macrophage recruitment in the injury in after spinal cord injury, or the recruitment of macrophages in a glioma (Guo et al., 2016; Yokota et al., 2017). Then we pursued to check for macrophage infiltration with the leukocyte marker L-plastin (LCP1). We did not observe any difference in macrophage infiltration between WT and *postnb*<sup>-/-</sup> ventricles at 7dpa (Figure R 19A and B). Quantification of L-plastin<sup>+</sup> cells per field in the wound site revealed no differences between WT and *postnb*<sup>-/-</sup> (Figure R 19B).

Another role is the induction of active matrix metalloproteases (MMPs) secretion by periostin (Hakuno et al., 2010). It is also known that, during zebrafish heart regeneration, matrix metalloproteinases are expressed on the injured tissue (Xu et al., 2018). For this reason, we looked at the capacity of *postnb* to induce the expression of different MMPs. We analysed RNA expression of different MMPs by qRT-PCR, and found that *postnb*<sup>-/-</sup> hearts at 7dpa had a significant increase in *mmp2*, *mmp13a*, *mmp14a* and *mmp14b* transcription in comparison to WT hearts (Figure R 19C). Thus, by *in situ* zymography we profiled the level of MMP enzymatic activity at 7dpa of WT and *postnb*<sup>-/-</sup> hearts (Figure R 19D and E). We could not visualize any MMP activity differences in the injured area between WT and *postnb*<sup>-/-</sup> hearts (Figure R 19D). Moreover, after quantification of the signal intensity no changes on MMP activity were still detected (Figure R 19E).

It has been recently determined that periostin has also an effect on revascularization after myocardial infarction in mice models (Chen et al., 2017). Thus, we checked for revascularization after amputation at 10dpa by alkaline phosphatase staining of coronary vasculature. No differences were seen in the revascularization

#### 4. RESULTS



**Figure R 19** *postnb*<sup>-/-</sup> does not have any effect on macrophage recruitment, MMPs activation or revascularization of coronary vasculature. (A) Immunohistochemistry of L-plastin (green) and myosin heavy-chain (Red) of 7dpa WT and *postnb*<sup>-/-</sup> hearts. (B) Quantification of L-plastin positive cells per field of view of WT and *postnb*<sup>-/-</sup> hearts. (C) Expression of different matrix metalloproteinases (MMPs) by qRT-PCR. N=6 (D) MMPs activity by *in situ* zymography of 7dpa WT and *postnb*<sup>-/-</sup> hearts. (E) Intensity quantification of *in situ* zymography signal of 7dpa WT and *postnb*<sup>-/-</sup> hearts. Intensity values were corrected by ROI size. (F) Revascularization assessment by Alkaline phosphatase staining of 10dpa WT and *postnb*<sup>-/-</sup> hearts. Mann-Whitney analysis was used to assess for statistical significance. \*,  $p < 0.05$ . Scale bars 100 $\mu$ m.



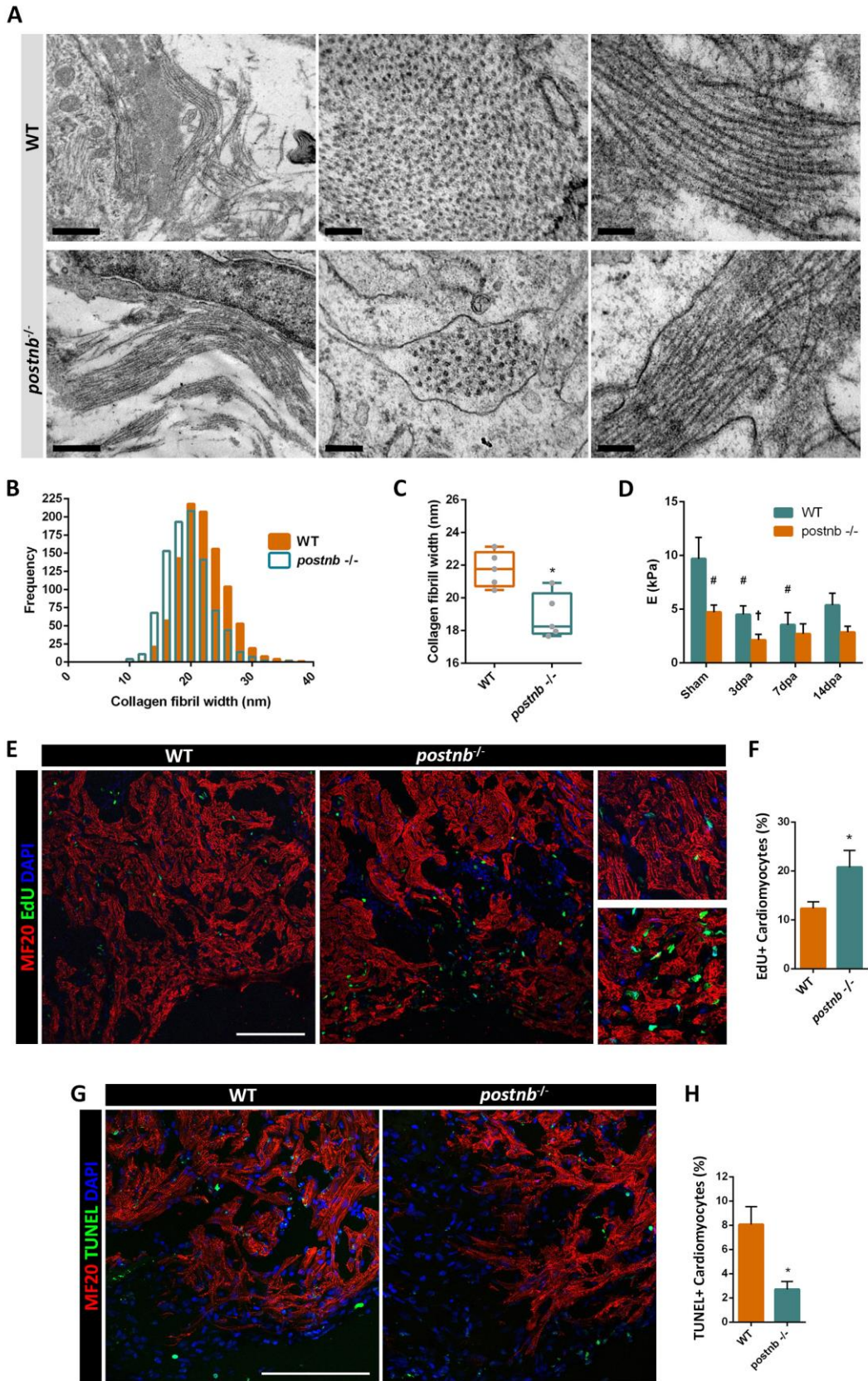
capacities of WT and KO hearts, observing in both cases coronary vasculature in the injury site (Figure R 19F).

#### **4.1.9. *postnb*<sup>-/-</sup> had decreased collagen cross-linking and a softer ECM.**

One of the most studied effects of periostin, is its effect on promoting collagen cross-linking (Kudo, 2017; Maruhashi et al., 2010; Norris et al., 2007). In the masson trichrome staining at 30dpa, we observed absence of collagen staining in *postnb*<sup>-/-</sup> hearts, thus we believe that collagen deposition is being altered. To further investigate this fact, we histologically analyzed 7dpa regenerating ventricles by transmission electron microscopy (TEM), and detected collagen fibers in both WT and KO regenerating hearts (Figure R 20A). After measuring the collagen fiber diameter, we found that the collagen fiber width histogram was shifted to smaller values in *postnb*<sup>-/-</sup> fishes (Figure R 20B), resulting in an average collagen fiber width significantly thinner (Figure R 20C). Thus, *postnb* is required for correct collagen cross-linking in regenerating zebrafish hearts.

It is known that changes in collagen crosslinking or concentration have an impact on ECM stiffness, obtaining stiffer matrices in more cross-linked collagens, and vice versa (Brower et al., 2006; Mujumdar et al., 2001). Thus, we analyzed, weather the effects observed in collagen cross-linking had any impact on ECM stiffness. By Atomic Force Microscopy (AFM), we measured the stiffness of control and regenerating (3, 7 and 14 dpa) WT and *postnb*<sup>-/-</sup> hearts (Figure R 20D). Already from the beginning, we found that ECM from *postnb*<sup>-/-</sup> hearts had half the stiffness of WT hearts, indicating that periostin had an effect on ECM stiffness. When studying the regeneration process at different time points (3, 7 and 14 dpa), we observed that, as already seen in previous experiments, the ECM stiffness from WT hearts decreased during the first days of regeneration (3dpa and 7dpa) and started to recover by 14dpa. This dynamic effect on ECM stiffness was not appreciated in *postnb*<sup>-/-</sup> hearts, where a stiffness decrease was observed at 3dpa but it was maintained low during the other time points analyzed. At

## 4. RESULTS



**Figure R 20** | Collagen cross-linking and ECM stiffness are reduced in *postnb*<sup>-/-</sup> zebrafish while cardiomyocyte proliferation increases. (A) Transmission electron microscope images from collagen rich areas of WT and *postnb*<sup>-/-</sup> hearts at 7dpa. Longitudinal and transversal collagen fibers can be

observed. (B) Histogram representation of the collagen fibril width of WT and *postnb*<sup>-/-</sup> hearts at 7dpa. (C) Boxplot representation of the mean values of the fibril width of each heart (N=5) of WT and *postnb*<sup>-/-</sup> hearts at 7dpa. (D) ECM Stiffness measuring by Atomic Force Microscopy of WT and *postnb*<sup>-/-</sup> hearts at 7dpa. (E) Immunohistochemistry of EdU (green) and myosin heavy-chain (Red) of 14dpa WT and *postnb*<sup>-/-</sup> hearts. (F) Quantification of the percentage of EdU positive cardiomyocytes in WT and *postnb*<sup>-/-</sup> hearts at 14dpa. (G) Immunohistochemistry of TUNEL (green) and myosin heavy-chain (Red) of 7dpa WT and *postnb*<sup>-/-</sup> hearts. (H) Quantification of the percentage of TUNEL positive cardiomyocytes in WT and *postnb*<sup>-/-</sup> hearts at 7dpa. Mann-Whitney analysis was used to assess for statistical significance. \*, p<0.05; #, p<0.05 in comparison to WT sham values; †, p<0.05 in comparison to *postnb*<sup>-/-</sup> sham values. Scale bars (A) 200µm, and (E and G) 100µm.

14dpa the stiffness was not increasing to recover control values, as observed in WT hearts (Figure R 20D). This proves the importance of periostin to regulate cardiac ECM stiffness both in physiologic conditions and during regeneration.

Periostin is known not only to have effects at ECM level, but also to act at cellular level promoting migration or proliferation (Kühn et al., 2007; Oka et al., 2007; Shimazaki et al., 2008; Yokota et al., 2017). Then, we examined whether *postnb* would have any effect on cardiomyocyte proliferation. We compared the cardiomyocyte proliferation at 14dpa of WT and *postnb*<sup>-/-</sup> hearts. Fishes were amputated and EdU was daily injected in the abdominal cavity between 7dpa and 14dpa. Proliferation was calculated counting the percentage of EdU positive cardiomyocytes in the wound area of regenerating hearts at 14dpa. Compared to WT, *postnb*<sup>-/-</sup> hearts experienced an increase of EdU positive cardiomyocytes in the injury site (Figure R 20E and F). In addition, cellular death was also assessed by TUNEL assay (Figure R 20G and H). WT and *postnb*<sup>-/-</sup> hearts at 7dpa were immunostained and TUNEL positive cardiomyocytes were calculated. A reduction of TUNEL positive cardiomyocytes in *postnb*<sup>-/-</sup> hearts was observed when compared to WT hearts (Figure R 20H).



## **5. DISCUSSION**



Extracellular matrix (ECM) remodeling is a critical step in development, wound healing and regeneration (Bayomy et al., 2012; Bonnans et al., 2014; Dobaczewski et al., 2010; Jessen, 2015; Wang et al., 2013). The present thesis characterized the ECM composition and its changes during zebrafish regeneration, as well as determined the need of *postnb* for a complete regeneration. We have developed a decellularization protocol for zebrafish ventricles that results in ECM enrichment, as well as facilitating the analysis of the proteomic profile of the zebrafish ventricle ECM. Moreover, we have analyzed the ECM changes during heart regeneration and assessed the stiffness of the ECM at different time points of this process. Finally, we have also studied the importance of the matricellular protein *postnb* in the context of zebrafish heart regeneration. Altogether, the results from our studies should help better understanding the role of the ECM in zebrafish heart regeneration.

The ECM composition has not been fully studied and described in the specific context of the zebrafish cardiac regeneration. Few are the studies done to analyze the ECM in the zebrafish heart. The proteome of different zebrafish organs, including the heart, were analyzed by Abramsson and colleagues and only 4 collagen proteins were detected in the heart proteome (Abramsson et al., 2010). In the present study, we have described the presence of 7 additional collagens (*col1a2*, *col1a1b*, *col6a2*, *col4a1*, *col4a2*, *col5a2a*, and *col6a6*) in control samples, corroborating that they are the main structural element of the zebrafish heart ECM. Collagens provide tensile strength, regulate cell adhesion, support chemotaxis and migration, and direct tissue development (Frantz et al., 2010). Recently Chen and colleagues analyzed the decellularized ECM of zebrafish heart using a mechanical decellularizing approach (Chen et al., 2016). They qualitatively described the presence of 4 ECM proteins, of which we detect 3 as well as 21 new ones. Thus, our decellularization process followed by LC-MS/MS analysis provided a more comprehensive, as well as quantitative, method to define the ventricular ECM of the zebrafish.

In terms of the cardiac regeneration process, there was no study to our knowledge that analyzed the importance of the ECM itself in the zebrafish cardiac

## 5. Discussion

regeneration model. Transcriptomic and proteomic approaches have sought to profile the whole gene expression and protein changes during zebrafish heart regeneration. The former identified gene expression changes during regeneration process and described an increase of transcripts related with secreted molecules, cathepsins and metalloproteinases, and wound response/inflammatory factors (Lien et al., 2006; Sleep et al., 2010). Also, transcripts coding for ECM and adhesion molecules were detected to be commonly and differentially expressed when comparing the transcriptomes of zebrafish regenerating hearts and fins (Sleep et al., 2010). On the other hand, proteomic studies have been mainly done on native cardiac samples without decellularization prior to protein detection, where ECM proteins could be masked by the large amount of intracellular proteins (Chen et al., 2016; Ma et al., 2018; Missinato et al., 2015; Wang et al., 2013). Moreover, these previous proteomic studies have focused on early regenerating time points and do not provide an overview of the proteomic changes during the entire regenerating process (Chen et al., 2016; Missinato et al., 2015).

It is also worth noting that, in our studies, ECM proteins were overrepresented among those that showed significant changes in abundance during heart regeneration. Thus, enrichment analysis using Enrichr tool on all proteins that showed significant changes during regeneration identified Biological Process GO terms related with ECM as the most represented (Supplementary Figure 1A in Appendix II). In contrast, a similar analysis of published proteomic data (Ma et al., 2018) only identified enrichment of the ECM-related GO terms fibrinolysis (GO:0042730) and plasminogen activation (GO:0031639), and not among the most enriched in that dataset. A summary of the 10 most-enriched Biological Process GO terms during zebrafish heart regeneration identified in our studies and in those of Ma and colleagues (Ma et al., 2018) is presented in Supplementary Figure 1B in Appendix II.

Both transcriptomic and proteomic studies have identified some ECM proteins important during regeneration. Wang and colleagues described the importance of fibronectin during regeneration after ventricular resection, suggesting a positive effect on cardiomyocyte migration (Wang et al., 2013). Also, tenascin C (*tnc*) has been found



to be expressed at the border zone, and suggested to mediate loosening of cardiomyocyte attachment to the substrate, thereby facilitating cardiomyocyte migration (Chablais et al., 2011). Another proteomic study identified the hyaluronic acid receptor (Hmnr) to be important for the epicardium EMT migration towards the injury (Missinato et al., 2015). All these suggest that tissue remodeling and ECM dynamics are important factors during zebrafish heart regeneration.

The fact that our analysis did not detect changes in some ECM proteins found in previous studies, such as *tnc*, may be due to technical limitations. In LC-MS/MS-based analyses, signals of abundant proteins such as collagens and structural proteins can mask the signals of low-abundance proteins. Also, new proteomic analytical tools have been developed, but we strongly believe that proteomic analyses of ECM enriched samples is a powerful approach to study the ECM components in heart regeneration. In this study, we have identified the main changes in ECM protein composition during zebrafish heart regeneration. Decreased amounts of collagen IV, collagen V, and fibrillin 2b, as well as increased amounts of fibrinogens, fibronectin 1b and periostin b comprise the initial regenerating ECM. We have been also able to detect proteins that were not previously detected in any transcriptomic or proteomic study, such as *col4a2* and *fn2b*. Two groups of proteins appear to be regulated differently. In the first group, positive correlation between protein abundance and gene expression in the case of *fn1b* and *postnb*, indicates a transcriptional regulation of these genes during heart regeneration (Le A. Trinh and Stainier, 2004; Sleep et al., 2010). In the second group, decreased levels of *col4a2*, *col5a1*, *col5a2a* and *fn2b* proteins inversely correlate with gene expression, which we interpret as a regulatory feedback mechanism in an attempt to recover the protein levels.

Stiffness is itself a mechanical property of the ECM. It is known to be involved in cell processes such as the regulation of cell proliferation (Balestrini et al., 2012; Yahalom-Ronen et al., 2015), dedifferentiation (Yahalom-Ronen et al., 2015), migration (through durotaxis) (Lo et al., 2000) and stem cell differentiation (Wen et al., 2014). We analyzed the stiffness of the regenerating zebrafish ventricle and found a significant

## 5. Discussion

decrease in ECM stiffness at 7dpa. It is known that an increase in collagen concentration or cross-linking is associated with stiffer myocardium (Brower et al., 2006), whereas an extensive degradation of myocardial collagen is associated with a decrease in ventricular stiffness (Brower et al., 2006; Mujumdar et al., 2001). Thus, this result correlates well with the decrease in abundance of several collagens identified in our proteomic analysis suggesting an association between these two evidences. An unexpected finding of our mechanical characterization of the regenerating heart ECM was that we did not detect any conspicuous differences in stiffness between the regenerating area and the non-injured myocardium located far away from the lesion. This suggests that changes in ECM composition result in organ-wide effects at the biomechanical level. Interestingly, recent data from our laboratories have identified a low ECM stiffness as a permissive factor regulating the heart regeneration ability of neonatal mice (Notari et al., 2018). The exact mechanism(s) by which ECM stiffness regulates heart regeneration competence in adult zebrafish and/or neonatal mice require further investigation.

Changes in ECM composition and stiffness are likely to instruct specific cell behaviors, and may also trigger further changes in the properties of the ECM itself. The ability of the zebrafish cardiac ECM to induce mammal heart regeneration has been very recently assessed by Chen and colleagues (Chen et al., 2016). They observed that the zebrafish cardiac ECM exhibited pro-proliferative and chemotactic effects *in vitro* and contributed to a higher cardiac contractile function in mouse. In general, fibrillins are known to play important roles in TGF $\beta$  signaling by controlling the amounts of cytokines and in endocardium morphogenesis (Dietz, 2010; Mellman et al., 2012). Signaling by the TGF $\beta$ /Activin pathway is known to promote cardiomyocyte proliferation and deposition of ECM proteins (Chablais and Jazwinska, 2012). Moreover, fibronectin 1b promotes cardiomyocyte migration during zebrafish cardiac regeneration (Wang et al., 2013). Periostin may stimulate healing after myocardial infarction in mice through induction of cardiomyocyte proliferation, and it is known to be responsible of collagen cross-linking (covalent linkage of collagen fibers) (Norris et al., 2007; Shimazaki et al., 2008). Collagen cross-linking, in turn, increases at the same time the accumulation of collagen, matrix rigidity and resistance to degradation (Badenhorst et al., 2003; Norton et al., 1997).

Further studies to clarify in detail the function of each ECM protein during cardiac regeneration may lead to a better understanding of this process, and to the development of new avenues for therapeutic intervention to promote regeneration of the mammalian heart.

One of the proteins identified in the proteomic analysis was *postnb*. Periostin is a protein that has been studied in the context of regeneration of various tissues such as skin, bone and heart, as well as cancer (Kudo, 2011). However, the role of periostin in cardiac regeneration has been lately controversial. There are studies claiming that periostin is needed for correct healing after myocardial infarction (MI). Oka et al. reported that *Postn*<sup>-/-</sup> mice had less fibrotic response after MI, leading to greater rates of LV rupture and death (Oka et al., 2007). This results were further confirmed by Shimazaki et al. (Shimazaki et al., 2008). Moreover, Cho et al. claimed that periostin promotes myocardial regeneration in the infarcted adult rat heart by administrating mesenchymal stem cells overexpressing periostin (Cho et al., 2012). In contrast, other reports suggest that periostin is not involved in post-infarction regeneration of adult hearts (Lorts et al., 2009; Taniyama et al., 2016), proposing periostin inhibition as a good therapeutics for MI treatment. Similarly, the *in vitro* effects of periostin on neonatal rodent cardiomyocytes disputed the ability of periostin on promoting regeneration (Kühn et al., 2007; Lorts et al., 2009). A recent study by Chen et al. indicated that the ablation of periostin in P2 neonatal mice suppressed post-infarction myocardial regeneration (Chen et al., 2017). Taking into account that cardiac regeneration is absent in the adult mammalian heart, but its existence is confirmed in the neonatal mammalian heart, we believe that the controversies around periostin are normal (Notari et al., 2018; O'Meara et al., 2015; Porrello et al., 2013, 2011). Thus, we consider that studying the contribution of periostin in a regenerating model such as zebrafish could better define its role in myocardial regeneration.

We used two different strategies in order to generate a reduction or a complete deficiency of *postnb* in zebrafish. To avoid developmental defects and perinatal death (Rios et al., 2005), the first strategy aimed to generate a conditional LOF of *postnb* by

## 5. Discussion

the expression of a shRNA controlled by the CRE/loxP system. The shRNA expression accomplished a 32.8% of *postnb* protein reduction, a fact that we considered insufficient to perform functionality experiments. Others have demonstrated that the multiplex shRNA constructs accomplish higher shRNA expression and achieve a higher reduction of the protein of interest (Dong et al., 2009). Still shRNA expression will generate a knock-down of the protein of interest that in some cases won't be enough to evaluate functionality. On the other hand, we have also used the CRISPR/Cas9 technology which allowed us to generate a *postnb* null zebrafish line. We were able to use this system since the shRNAs allowed us to determine that the depletion of *postnb* during development did not confer any detectable developmental defect nor in the adulthood. Others reported that the injection of a morpholino against periostin resulted in morphological and swimming defects (Kudo et al., 2004). However, morpholinos have been proved to cause effects not related with the LOF of the desired gene, but off-target activity (Bedell et al., 2011). Thus, CRISPR/Cas9 technology is a great tool to generate knock-out lines that do not affect any gene important for development.

Our results showed how the deficiency of *postnb* in zebrafish lead to a lack of myocardial wall growth indicating the importance of this protein in zebrafish heart regeneration. Our findings further confirmed the implication of periostin on fibrosis, specifically on collagen cross-linking. Similar results have been observed in MI mice models where the lack of periostin altered the fibrotic response (Oka et al., 2007; Shimazaki et al., 2008), and its overexpression in mice spontaneously developed cardiac fibrosis and hypertrophy with age (Oka et al., 2007). As mentioned above, modifications of collagen cross-linking are known to modulate stiffness, where an increase in collagen concentration or cross-linking is associated with stiffer myocardium (Brower et al., 2006). We analyzed the stiffness of regenerating zebrafish ventricles of WT and *postnb*<sup>-/-</sup> zebrafish, and observed a decrease of ECM stiffness during the regeneration process on WT hearts. This dynamic stiffness changes were not observed on *postnb*<sup>-/-</sup> hearts, where stiffness was lower than in WT, and decreased during regeneration but was maintained low without a tendency to increase at 14dpa. We suggest these stiffness dynamic changes to be important during cardiac regeneration in zebrafish.

Cardiomyocyte proliferation has been one of the actions of periostin not free from controversy. Some studies have claimed that periostin promotes rat cardiomyocyte proliferation by the administration of recombinant protein either *in vitro* or *in vivo* (Kühn et al., 2007). However, *in vitro* overexpression of periostin by infection with a recombinant adenovirus have not reported any effect regarding cardiomyocyte proliferation (Lorts et al., 2009). Moreover, any effects on cardiomyocyte proliferation were observed in *Postn*<sup>-/-</sup> adult mice after MI (Lorts et al., 2009). Similar results were observed in a MI rat model where periostin was inhibited with an antibody (Taniyama et al., 2016). Thus, we assessed for cardiomyocyte proliferation in our *postnb*<sup>-/-</sup> zebrafish model and observed a proliferation increase in *postnb*<sup>-/-</sup> regenerating hearts.

It is not the first time where ECM stiffness has been postulated as an important factor to conduct a proper regeneration process. In muscle regeneration, an appropriate ECM stiffness is needed for satellite cells to regenerate myofibrils. A decrease of ECM stiffness resulted in a decrease in the regeneration properties of satellite cells (Urciuolo et al., 2013). Another example would be mice neonatal cardiac regeneration. Notari et al. also reported that a reduction of the ECM stiffness by BAPN treatment rescued the ability of mice to regenerate heart tissue after apical resection (Notari et al., 2018). Thus, we believe that the ECM stiffening promoted by the presence of *postnb* during zebrafish heart regeneration is needed for a correct progression of cardiac regeneration. Indeed, the expression of *postnb* may be the conductor to drive the shift of ECM stiffness by changing from a softer ECM observed in the first days of regeneration, to a stiffer ECM. We proposed that this stiffness shift is needed for the correct progression of the regenerating process being a key signal for cardiomyocytes to stop proliferating and start the migration to the injury site. Therefore, a determined environment is necessary for biological processes to take pace, and we believe that *postnb* is not only forming part of the regenerative scaffold but also promotes its organization. It has to be taken into account that periostin is not only present in zebrafish cardiac regeneration, but it is also expressed after human myocardial infarction and mice cardiac injury (Chen et al., 2017; Shimazaki et al., 2008). Thus, how can it be possible that in one scenario it promotes regeneration and it does not have any effect in human or mice? We believe that it is the

## 5. Discussion

combination of secreted signals and other ECM proteins that give zebrafish ECM a favorable environment to promote regeneration. Further studies to determine the detailed molecular function of *postnb* may help to better understand its effect to zebrafish ECM organization and stiffness.

## **6. CONCLUSIONS**





1. The detergent based decellularization protocol presented in this thesis allows an enrichment of the ECM protein content without a conspicuous clearance of a determined group of ECM proteins, allowing to better identify the ECM proteins present in the zebrafish heart and its changes during regeneration.
2. During zebrafish cardiac regeneration, the ECM undergoes dynamic changes. There is an early increase of fibrinogen a, b and g (*fga*, *fgb* and *fgg*), fibronectin 1b (*fn1b*), and periostin b (*postnb*). On the other hand, different collagens (*col4a1*, *col5a1* and *col5a2a*) and fibrillin 2b (*fn2b*) experienced a reduction more evident at 7dpa.
3. Dynamic changes of ECM proteins during heart regeneration result in changes of ECM mechanical properties, reducing stiffness at early regeneration time points. However, there are no stiffness differences between the healthy myocardium and the injury site.
4. *postnb* is expressed by fibroblasts in the injured area of zebrafish resected ventricles, and is essential for proper zebrafish heart regeneration, since CRISPR/Cas9 *postnb*<sup>-/-</sup> zebrafish failed to regrow a contiguous wall of myocardial muscle.
5. During regeneration, *postnb* does not have any effect on general MMPs activation, leukocyte migration or revascularization during zebrafish regeneration. However, it is essential for correct collagen cross-linking regeneration.
6. *postnb* controls the stiffness of ventricular ECM, since the absence of *postnb* results in reduced ventricular stiffness. This stiffness control by *postnb* seem to be important to correctly modulate stiffness for a complete cardiac regeneration. Stiffness analysis together with proliferation analysis suggest that *postnb* is needed to increase the stiffness in the injury border to instruct cardiomyocytes to stop proliferating and migrate to the injury site.



## REFERENCES

- Abramsson A, Westman-Brinkmalm A, Pannee J, Gustavsson M, von Otter M, Blennow K, Brinkmalm G, Kettunen P, Zetterberg H. **2010**. Proteomics Profiling of Single Organs from Individual Adult Zebrafish. *Zebrafish* 7:161–168.
- Adler CP, Costabel U. **1975**. Cell number in human heart in atrophy, hypertrophy, and under the influence of cytostatics. *Recent Adv Stud Cardiac Struct Metab* 6:343–55.
- Alibardi L, Toni M. **2005**. Wound keratins in the regenerating epidermis of lizard suggest that the wound reaction is similar in the tail and limb. *J Exp Zool Part A Comp Exp Biol* 303:845–860.
- Amado LC, Saliaris AP, Schuleri KH, St. John M, Xie J-S, Cattaneo S, Durand DJ, Fitton T, Kuang JQ, Stewart G, Lehrke S, Baumgartner WW, Martin BJ, Heldman AW, Hare JM. **2005**. Cardiac repair with intramyocardial injection of allogeneic mesenchymal stem cells after myocardial infarction. *Proc Natl Acad Sci* 102:11474–11479.
- Andersen DCC, Ganesalingam S, Jensen CHH, Sheikh SPP. **2014**. Do neonatal mouse hearts regenerate following heart apex resection? *Stem Cell Reports* 2:406–413.
- Ashburner M, Ball CA, Blake JA, Botstein D, Butler H, Cherry JM, Davis AP, Dolinski K, Dwight SS, Eppig JT, Harris MA, Hill DP, Issel-Tarver L, Kasarskis A, Lewis S, Matese JC, Richardson JE, Ringwald M, Rubin GM, Sherlock G. **2000**. Gene ontology: tool for the unification of biology. The Gene Ontology Consortium. *Nat Genet* 25:25–9.
- Aurora AB, Porrello ER, Tan W, Mahmoud AI, Hill JA, Bassel-Duby R, Sadek HA, Olson EN. **2014**. Macrophages are required for neonatal heart regeneration. *J Clin Invest* 124:1382–92.
- Badenhorst D, Maseko M, Tsotetsi OJ, Naidoo A, Brooksbank R, Norton GR, Woodiwiss AJ. **2003**. Cross-linking influences the impact of quantitative changes in myocardial collagen on cardiac stiffness and remodelling in hypertension in rats. *Cardiovasc Res* 57:632–641.
- Bakkers J. **2011**. Zebrafish as a model to study cardiac development and human cardiac disease. *Cardiovasc Res* 91:279–88.
- Balestrini JL, Chaudhry S, Sarrazy V, Koehler A, Hinz B. **2012**. The mechanical memory of lung myofibroblasts. *Integr Biol (Camb)* 4:410–21.
- Bassett AR, Tibbit C, Ponting CP, Liu JL. **2013**. Highly Efficient Targeted Mutagenesis of *Drosophila* with the CRISPR/Cas9 System. *Cell Rep* 4:220–228.
- Bayomy AF, Bauer M, Qiu Y, Liao R. **2012**. Regeneration in heart disease - Is ECM the key? *Life Sci* 91:823–827.
- Becker CG, Becker T. **2000**. Gradients of ephrin-A2 and ephrin-A5b mRNA during

## References

- retinotopic regeneration of the optic projection in adult zebrafish. *J Comp Neurol* 427:469–483.
- Becker T, Becker CG. **2014**. Axonal regeneration in zebrafish. *Curr Opin Neurobiol* 27:186–191.
- Bedell VM, Westcot SE, Ekker SC. **2011**. Lessons from morpholino-based screening in zebrafish 10:181–188.
- Bednarek D, González-Rosa JM, Guzmán-Martínez G, Gutiérrez-Gutiérrez Ó, Aguado T, Sánchez-Ferrer C, Marques IJ, Galardi-Castilla M, de Diego I, Gómez MJ, Cortés A, Zapata A, Jiménez-Borreguero LJ, Mercader N, Flores I. **2015**. Telomerase Is Essential for Zebrafish Heart Regeneration. *Cell Rep* .
- Beer RL, Parsons MJ, Rovira M. **2016**. Centroacinar cells: At the center of pancreas regeneration. *Dev Biol* 413:8–15.
- Beltrami AP, Barlucchi L, Torella D, Baker M, Limana F, Chimenti S, Kasahara H, Rota M, Musso E, Urbanek K, Leri A, Kajstura J, Nadal-Ginard B. **2003**. Adult Cardiac Stem Cells Are Multipotent and Support Myocardial Regeneration we have documented the existence of cycling ventricu- lar myocytes in the normal and pathologic adult mam. *Cell* 114:763–776.
- Bely AE. **2006**. Distribution of segment regeneration ability in the Annelida. *Integr Comp Biol* 46:508–518.
- Bely AE, Nyberg KG. **2010**. Evolution of animal regeneration: re-emergence of a field. *Trends Ecol Evol* 25:161–170.
- Benjamin EJ, Virani SS, Callaway CW, Chamberlain AM, Chang AR, Cheng S, Chiuve SE, Cushman M, Dellings FN, Deo R, De Ferranti SD, Ferguson JF, Fornage M, Gillespie C, Isasi CR, Jiménez MC, Jordan LC, Judd SE, Lackland D, Lichtman JH, Lisabeth L, Liu S, Longenecker CT, Lutsey PL, MacKey JS, Matchar DB, Matsushita K, Mussolino ME, Nasir K, O'Flaherty M, Palaniappan LP, Pandey A, Pandey DK, Reeves MJ, Ritchey MD, Rodriguez CJ, Roth GA, Rosamond WD, Sampson UKA, Satou GM, Shah SH, Spartano NL, Tirschwell DL, Tsao CW, Voeks JH, Willey JZ, Wilkins JT, Wu JHY, Alger HM, Wong SS, Muntner P. **2018**. Heart disease and stroke statistics - 2018 update: A report from the American Heart Association, Circulation.
- Bergmann O, Bhardwaj RD, Bernard S, Zdunek S, Barnabé-Heider F, Walsh S, Zupicich J, Alkass K, Buchholz BA, Druid H, Jovinge S, Frisén J. **2009**. Evidence for cardiomyocyte renewal in humans. *Science* 324:98–102.
- Bergmann O, Zdunek S, Felker A, Salehpour M, Alkass K, Bernard S, Sjöström SL, Szewczykowska M, Jackowska T, Dos Remedios C, Malm T, Andrä M, Jashari R, Nyengaard JR, Possnert G, Jovinge S, Druid H, Frisén J. **2015**. Dynamics of Cell Generation and Turnover in the Human Heart. *Cell* 161:1566–75.
- Bibikova M, Carroll D, Segal DJ, Trautman JK, Smith J, Kim Y-G, Chandrasegaran S. **2001**. Stimulation of Homologous Recombination through Targeted Cleavage by Chimeric Nucleases. *Mol Cell Biol* 21:289–297.
- Bonnans C, Chou J, Werb Z. **2014**. Remodelling the extracellular matrix in development and disease. *Nat Rev Mol Cell Biol* 15:786–801.

- Borchardt T, Braun T. **2007**. Cardiovascular regeneration in non-mammalian model systems: what are the differences between newts and man? *Thromb Haemost* 98:311–8.
- Borgens RB. **1982**. Mice regrow the tips of their foretoes. *Science* 217:747–50.
- Bozyk PD, Bentley JK, Popova AP, Anyanwu AC, Linn MD, Adam M, Pryhuber GS, Moore BB, Hershenson MB. **2012**. Neonatal Periostin Knockout Mice Are Protected from Hyperoxia-Induced Alveolar Simplification 7:1–10.
- Brockes JP, Gates PB. **2014**. Mechanisms underlying vertebrate limb regeneration: lessons from the salamander. *Biochem Soc Trans* 42:625–630.
- Brockes JP, Kumar A, Velloso CP. **2001**. Regeneration as an evolutionary variable. *J Anat* 199:3–11.
- Brower GL, Gardner JD, Forman MF, Murray DB, Voloshenyuk T, Levick SP, Janicki JS. **2006**. The relationship between myocardial extracellular matrix remodeling and ventricular function. *Eur J Cardio-thoracic Surg* 30:604–610.
- Bryant DM, O’Meara CC, Ho NN, Gannon J, Cai L, Lee RT. **2015**. A systematic analysis of neonatal mouse heart regeneration after apical resection. *J Mol Cell Cardiol* 79:315–318.
- Burton PBJ, Raff MC, Kerr P, Yacoub MH, Barton PJR. **1999**. An intrinsic timer that controls cell-cycle withdrawal in cultured cardiac myocytes. *Dev Biol* 216:659–670.
- Cai CL, Martin JC, Sun Y, Cui L, Wang L, Ouyang K, Yang L, Bu L, Liang X, Zhang X, Stallcup WB, Denton CP, McCulloch A, Chen J, Evans SM. **2008**. A myocardial lineage derives from Tbx18 epicardial cells. *Nature* 454:104–108.
- Cano-Martínez A, Vargas-González A, Guarner-Lans V. **2007**. Temperature effect on contractile activity of the *Ambystoma dumerilii* heart previously treated with isoproterenol. *Comp Biochem Physiol - A Mol Integr Physiol* 147:743–749.
- Cano-Martínez A, Vargas-González A, Guarner-Lans V, Prado-Zayago E, León-Oleda M, Nieto-Lima B. **2010**. Functional and structural regeneration in the axolotl heart (*Ambystoma mexicanum*) after partial ventricular amputation. *Arch Cardiol Mex* 80:79–86.
- Cao J, Wang J, Jackman CP, Cox AH, Trembley MA, Balowski JJ, Cox BD, De Simone A, Dickson AL, Di Talia S, Small EM, Kiehart DP, Bursac N, Poss KD. **2017**. Tension Creates an Endoreplication Wavefront that Leads Regeneration of Epicardial Tissue. *Dev Cell* 42:600–615.e4.
- Carlson BM. **2007**. Chapter 1 – An Introduction to Regeneration. *Princ Regen Biol* 1–29.
- Chablais F, Jazwinska A. **2012**. The regenerative capacity of the zebrafish heart is dependent on TGF $\beta$  signaling. *Development* 139:1921–30.
- Chablais F, Veit J, Rainer G, Jaźwińska A. **2011**. The zebrafish heart regenerates after cryoinjury-induced myocardial infarction. *BMC Dev Biol* 11:21.
- Chen WCW, Wang Z, Missinato MA, Park DW, Long DW, Liu H-J, Zeng X, Yates NA, Kim K, Wang Y. **2016**. Decellularized zebrafish cardiac extracellular matrix induces mammalian heart regeneration. *Sci Adv* 2:e1600844.

## References

- Chen Z, Xie J, Hao H, Lin H, Wang L, Zhang Y, Chen L, Cao S, Huang X, Liao W, Bin J, Liao Y. **2017**. Ablation of periostin inhibits post-infarction myocardial regeneration in neonatal mice mediated by the phosphatidylinositol 3 kinase/glycogen synthase kinase 3 $\beta$ /cyclin D1 signalling pathway. *Cardiovasc Res* 1–13.
- Chimenti I, Smith RR, Li T-S, Gerstenblith G, Messina E, Giacomello A, Marbán E. **2010**. Relative Roles of Direct Regeneration Versus Paracrine Effects of Human Cardiosphere-Derived Cells Transplanted Into Infarcted Mice. *Circ Res* 106:971–980.
- Cho YH, Cha MJ, Song BW, Kim IK, Song H, Chang W, Lim S, Ham O, Lee SY, Choi E, Kwon HM, Hwang KC. **2012**. Enhancement of MSC adhesion and therapeutic efficiency in ischemic heart using lentivirus delivery with periostin. *Biomaterials* 33:1376–1385.
- Choi W-Y, Gemberling M, Wang J, Holdway JE, Shen M-C, Karlstrom RO, Poss KD. **2013**. In vivo monitoring of cardiomyocyte proliferation to identify chemical modifiers of heart regeneration. *Development* 140:660–6.
- Cong L, Ran FA, Cox D, Lin S, Barretto R, Habib N, Hsu PD, Wu X, Jiang W, Marraffini LA, Zhang F. **2013**. Multiplex genome engineering using CRISPR/Cas systems. *Science* 339:819–23.
- Conway SJ, Izuhara K, Kudo Y, Litvin J, Markwald R, Ouyang G, Arron JR, Holweg CTJ, Kudo A. **2014**. The role of periostin in tissue remodeling across health and disease. *Cell Mol Life Sci* 71:1279–88.
- Creaser EP. **1934**. Some notes on north american crayfish. *Science* 79:364.
- Curado S, Anderson RM, Jungblut B, Mumm J, Schroeter E, Stainier D.Y.R. **2007**. Conditional targeted cell ablation in zebrafish: A new tool for regeneration studies. *Dev Dyn* 236:1025–1035.
- Darehzereshki A, Rubin N, Gamba L, Kim J, Fraser J, Huang Y, Billings J, Mohammadzadeh R, Wood J, Warburton D, Kaartinen V, Lien C-LL. **2015**. Differential regenerative capacity of neonatal mouse hearts after cryoinjury. *Dev Biol* 399:91–99.
- de Preux Charles A-S, Bise T, Baier F, Marro J, Jaźwińska A. **2016**. Distinct effects of inflammation on preconditioning and regeneration of the adult zebrafish heart. *Open Biol* 6:160102.
- De Rienzo G, Gutzman JH, Sive H. **2012**. Efficient shRNA-mediated inhibition of gene expression in zebrafish. *Zebrafish* 9:97–107.
- Diep CQ, Ma D, Deo RC, Holm TM, Naylor RW, Arora N, Wingert RA, Bollig F, Djordjevic G, Lichman B, Zhu H, Ikenaga T, Ono F, Englert C, Cowan CA, Hukriede NA, Handin RI, Davidson AJ. **2011**. Identification of adult nephron progenitors capable of kidney regeneration in zebrafish. *Nature* 470:95–101.
- Dietz HC. **2010**. TGF- $\beta$  in the pathogenesis and prevention of disease: a matter of aneurysmic proportions. *J Clin Invest* 120:403–406.
- Dinsmor CE. **1991**. A history of regeneration research.. Cambridge University Press.
- Dobaczewski M, Gonzalez-Quesada C, Frangogiannis NG. **2010**. The extracellular matrix as a modulator of the inflammatory and reparative response following myocardial

- infarction. *J Mol Cell Cardiol* 48:504–511.
- Dong M, Fu Y-F, Du T-T, Jing C-B, Fu C-T, Chen Y, Jin Y, Deng M, Liu TX. **2009**. Heritable and lineage-specific gene knockdown in zebrafish embryo. *PLoS One* 4:e6125.
- Dor Y, Brown J, Martinez OI, Melton DA. **2004**. Adult pancreatic  $\beta$ -cell s are formed by self-duplication rather than ítem-cell differentiation. *Nature* 429:41–46.
- Frangogiannis NG. **2012**. Matricellular proteins in cardiac adaptation and disease. *Physiol Rev* 92:635–88.
- Frangogiannis NG. **2006**. The Mechanistic Basis of Infarct Healing. *Antioxid Redox Signal* 10:1344–1365.
- Frantz C, Stewart KM, Weaver VM. **2010**. The extracellular matrix at a glance. *J Cell Sci* 123:4195–4200.
- Fratz S, Hager A, Schreiber C, Schwaiger M, Hess J, Stern HC. **2011**. Long-term myocardial scarring after operation for anomalous left coronary artery from the pulmonary artery. *Ann Thorac Surg* 92:1761–1765.
- Gagnon JA, Valen E, Thyme SB, Huang P, Ahkmetova L, Pauli A, Montague TG, Zimmerman S, Richter C, Schier AF. **2014**. Efficient Mutagenesis by Cas9 Protein-Mediated Oligonucleotide Insertion and Large-Scale Assessment of Single-Guide RNAs. *PLoS One* 9:e98186.
- Gamba L, Amin-Javaheri A, Kim J, Warburton D, Lien C-L. **2017**. Collagenolytic Activity Is Associated with Scar Resolution in Zebrafish Hearts after Cryoinjury. *J Cardiovasc Dev Dis* 4:2.
- Gawriluk TR, Simkin J, Thompson KL, Biswas SK, Clare-Salzler Z, Kimani JM, Kiama SG, Smith JJ, Ezenwa VO, Seifert AW. **2016**. Comparative analysis of ear-hole closure identifies epimorphic regeneration as a discrete trait in mammals. *Nat Commun* 7:1–16.
- Gemberling M, Karra R, Dickson AL, Poss KD. **2015**. Nrg1 is an injury-induced cardiomyocyte mitogen for the endogenous heart regeneration program in zebrafish. *Elife* 4.
- Gillan L, Matei D, Fishman DA, Gerbin CS, Karlan BY, Chang DD. **2002**. Periostin secreted by epithelial ovarian carcinoma is a ligand for alpha(V)beta(3) and alpha(V)beta(5) integrins and promotes cell motility. *Cancer Res* 62:5358–64.
- Glasauer SMK, Neuhauss SCF. **2014**. Whole-genome duplication in teleost fishes and its evolutionary consequences. *Mol Genet Genomics* 289:1045–60.
- Goldstein MA, Claycomb WC, Schwartz A. **1974**. DNA Synthesis and Mitosis in Well-Differentiated Mammalian Cardiocytes. *Science (80- )* 183:212–213.
- Gonzales APW, Joanna Yeh J-R. **2014**. Cas9-Based Genome Editing in Zebrafish. *Methods Enzymol* 546C:377–413.
- González-Rosa JM, Burns CE, Burns CG. **2017**. Zebrafish heart regeneration: 15 years of discoveries. *Regeneration* 105–123.
- González-Rosa JM, Martín V, Peralta M, Torres M, Mercader N. **2011**. Extensive scar

## References

- formation and regression during heart regeneration after cryoinjury in zebrafish. *Development* 138:1663–74.
- González-Rosa JM, Peralta M, Mercader N. **2012**. Pan-epicardial lineage tracing reveals that epicardium derived cells give rise to myofibroblasts and perivascular cells during zebrafish heart regeneration. *Dev Biol* 370:173–186.
- Goodrich HB. **1929**. Mendelian inheritance of fish. *Q Rev Biol* 4:83–99.
- Goss RJ. **1966**. Hypertrophy versus hyperplasia. *Science* 153:1615–20.
- Gross R. **1969**. Principles of regeneration. Academic Press.
- Guilak F, Cohen DM, Estes BT, Gimble JM, Liedtke W, Chen CS. **2009**. Control of Stem Cell Fate by Physical Interactions with the Extracellular Matrix. *Cell Stem Cell* 5:17–26.
- Guo X, Xue H, Shao Q, Wang J, Guo X, Chen X, Zhang J, Xu S, Li T, Zhang P, Gao X, Qiu W, Liu Q, Li G. **2016**. Hypoxia promotes glioma-associated macrophage infiltration via periostin and subsequent M2 polarization by upregulating TGF-beta and M-CSFR. *Oncotarget* 7:80521–80542.
- Gupta V, Gemberling M, Karra R, Rosenfeld GE, Evans T, Poss KD. **2013**. An injury-responsive *gata4* program shapes the zebrafish cardiac ventricle. *Curr Biol* 23:1221–7.
- Gupta V, Poss KD. **2012**. Clonally dominant cardiomyocytes direct heart morphogenesis. *Nature* 484:479–84.
- Hakuno D, Kimura N, Yoshioka M, Mukai M, Kimura T, Okada Y, Yozu R, Shukunami C, Hiraki Y, Kudo A, Ogawa S, Fukuda K. **2010**. Periostin advances atherosclerotic and rheumatic cardiac valve degeneration by inducing angiogenesis and MMP production in humans and rodents. *J Clin Invest* 120:2292–2306.
- Harrison MRM, Bussmann J, Huang Y, Zhao L, Osorio A, Burns CG, Burns CE, Sucov HM, Siekmann AF, Lien CL. **2015**. Chemokine-Guided Angiogenesis Directs Coronary Vasculature Formation in Zebrafish. *Dev Cell* 33:442–454.
- Haubner BJ, Adamowicz-Brice M, Khadayate S, Tiefenthaler V, Metzler B, Aitman T, Penninger JM. **2012**. Complete cardiac regeneration in a mouse model of myocardial infarction. *Aging (Albany NY)* 4:966–977.
- Haubner BJ, Schneider J, Schweigmann U, Schuetz T, Dichtl W, Velik-Salchner C, Stein J-I, Penninger JM. **2016**. Functional Recovery of a Human Neonatal Heart After Severe Myocardial Infarction. *Circ Res* 118:216–21.
- Hein SJ, Lehmann LH, Kossack M, Juergensen L, Fuchs D, Katus HA, Hassel D. **2015**. Advanced echocardiography in adult zebrafish reveals delayed recovery of heart function after myocardial cryoinjury. *PLoS One* 10:1–21.
- Hoersch S, Andrade-Navarro MA. **2010**. Periostin shows increased evolutionary plasticity in its alternatively spliced region. *BMC Evol Biol* 10:30.
- Holtzman NG, Iovine MK, Liang JO, Morris J. **2016**. Learning to Fish with Genetics: A Primer on the Vertebrate Model *Danio rerio*. *Genetics* 203:1069–89.



- Horiguchi M, Inoue T, Ohbayashi T, Hirai M, Noda K, Marmorstein LY, Yabe D, Takagi K, Akama TO, Kita T, Kimura T, Nakamura T. **2009**. Fibulin-4 conducts proper elastogenesis via interaction with cross-linking enzyme lysyl oxidase. *Proc Natl Acad Sci* 106:19029–19034.
- Horiuchi K, Amizuka N, Takeshita S, Takamatsu H, Katsuura M, Ozawa H, Toyama Y, Bonewald LF, Kudo A. **1999**. Identification and Characterization of a Novel Protein, Periostin, with Restricted Expression to Periosteum and Periodontal Ligament and Increased Expression by Transforming Growth Factor  $\beta$ . *J Bone Miner Res* 14:1239–1249.
- Hou J, Wang L, Jiang J, Zhou C, Guo T, Zheng S, Wang T. **2013**. Cardiac Stem Cells and their Roles in Myocardial Infarction. *Stem Cell Rev Reports* 9:326–338.
- Howe K, Clark M, Torroja C, Torrance J, Berthelot C, Muffato M, Collins JE, Humphray S, McLaren K, Matthews L, McLaren S, Sealy I, Caccamo M, Churcher C, Scott C, Barrett JC, Koch R, Al. E. **2013**. The zebrafish reference genome sequence and its relationship to the human genome. *Nature* 496:498–503.
- Hsieh PCH, Segers VFM, Davis ME, MacGillivray C, Gannon J, Molkenstein JD, Robbins J, Lee RT. **2007**. Evidence from a genetic fate-mapping study that stem cells refresh adult mammalian cardiomyocytes after injury. *Nat Med* 13:970–974.
- Hu N, Yost HJ, Clark EB. **2001**. Cardiac morphology and blood pressure in the adult zebrafish. *Anat Rec* 264:1–12.
- Huang W-C, Yang C-C, Chen I-H, Liu Y-ML, Chang S-J, Chuang Y-J. **2013**. Treatment of Glucocorticoids Inhibited Early Immune Responses and Impaired Cardiac Repair in Adult Zebrafish. *PLoS One* 8:e66613.
- Huber W, von Heydebreck A, Sültmann H, Poustka A, Vingron M. **2002**. Variance stabilization applied to microarray data calibration and to the quantification of differential expression. *Bioinformatics* 18 Suppl 1:S96-104.
- Hui SP, Sheng DZ, Sugimoto K, Gonzalez-Rajal A, Nakagawa S, Hesselson D, Kikuchi K. **2017**. Zebrafish Regulatory T Cells Mediate Organ-Specific Regenerative Programs. *Dev Cell* 43:659–672.e5.
- Hyde DR, Godwin AR, Thummel R. **2012**. In vivo electroporation of morpholinos into the regenerating adult zebrafish tail fin. *J Vis Exp* 1–8.
- Hynes RO. **2014**. Stretching the boundaries of extracellular matrix research. *Nat Rev Mol Cell Biol* 15:761–763.
- Illingworth CM. **1974**. Trapped fingers and amputated finger tips in children. *J Pediatr Surg* 9:853–858.
- Ishihara J, Umemoto T, Yamato M, Shiratsuchi Y, Takaki S, Petrich BG, Nakauchi H, Eto K, Kitamura T, Okano T. **2014**. Nov/CCN3 regulates long-term repopulating activity of murine hematopoietic stem cells via integrin  $\alpha\beta 3$ . *Int J Hematol* 99:393–406.
- Ishikawa K, Yoshida S, Nakao S, Nakama T, Kita T, Asato R, Sassa Y, Arita R, Miyazaki M, Enaida H, Oshima Y, Murakami N, Niuro H, Ono J, Matsuda A, Goto Y, Akashi K, Izuhara K, Kudo A, Kono T, Hafezi-Moghadam A, Ishibashi T. **2014**. Periostin promotes the generation of fibrous membranes in proliferative vitreoretinopathy.

## References

- FASEB J* 28:131–142.
- Ito K, Morioka M, Kimura S, Tasaki M, Inohaya K, Kudo A. **2014**. Differential reparative phenotypes between zebrafish and medaka after cardiac injury. *Dev Dyn* 243:1106–15.
- Ito J, Akiyama R, Pehoski S, Yu X, Kawakami H, Kawakami Y. **2014**. Regenerative responses after mild heart injuries for cardiomyocyte proliferation in zebrafish. *Dev Dyn* 1–10.
- Ito J, Oishi I, Kawakami H, Glass TJ, Richter J, Johnson A, Lund TC, Kawakami Y. **2012**. Migration of cardiomyocytes is essential for heart regeneration in zebrafish. *Development* 139:4133–42.
- Jao L-E, Wente SR, Chen W. **2013**. Efficient multiplex biallelic zebrafish genome editing using a CRISPR nuclease system. *Proc Natl Acad Sci* 110:13904–13909.
- Jaźwińska A, Sallin P. **2016**. Regeneration versus scarring in vertebrate appendages and heart. *J Pathol* 238:233–246.
- Jessen JR. **2015**. Recent advances in the study of zebrafish extracellular matrix proteins. *Dev Biol* 401:110–121.
- Jesty S a, Steffey M a, Lee FK, Breitbach M, Hesse M, Reining S, Lee JC, Doran RM, Nikitin AY, Fleischmann BK, Kotlikoff MI. **2012**. c-kit<sup>+</sup> precursors support postinfarction myogenesis in the neonatal, but not adult, heart. *Proc Natl Acad Sci* 109:13380–13385.
- Jopling C, Boue S, Belmonte JCI. **2011**. Dedifferentiation, transdifferentiation and reprogramming: Three routes to regeneration. *Nat Rev Mol Cell Biol* 12:79–89.
- Jopling C, Sleep E, Raya M, Martí M, Raya A, Izpisua Belmonte JC. **2010**. Zebrafish heart regeneration occurs by cardiomyocyte dedifferentiation and proliferation. *Nature* 464:606–9.
- Jorba I, Uriarte JJ, Campillo N, Farré R, Navajas D. **2017**. Probing Micromechanical Properties of the Extracellular Matrix of Soft Tissues by Atomic Force Microscopy. *J Cell Physiol* 232:19–26.
- Kajstura J, Urbanek K, Perl S. **2010**. Cardiomyogenesis in the Adult Human Heart. *Circ ...* 107:305–315.
- Karra R, Knecht AK, Kikuchi K, Poss KD. **2015**. Myocardial NF-κB activation is essential for zebrafish heart regeneration. *Proc Natl Acad Sci U S A* 112:13255–60.
- Katz TC, Singh MK, Degenhardt K, Rivera-Feliciano J, Johnson RL, Epstein JA, Tabin CJ. **2012**. Distinct Compartments of the Proepicardial Organ Give Rise to Coronary Vascular Endothelial Cells. *Dev Cell* 22:639–650.
- Keller A, Nesvizhskii AI, Kolker E, Aebersold R. **2002**. Empirical statistical model to estimate the accuracy of peptide identifications made by MS/MS and database search. *Anal Chem* 74:5383–92.
- Kettleborough RNW, Busch-nentwich EM, Harvey SA, Dooley CM, Bruijn E De, Eeden F Van, Sealy I, White RJ, Herd C, Nijman IJ, Fényes F, Mehroke S, Scahill C, Gibbons R, Wali N, Carruthers S, Hall A, Yen J, Stemple DL. **2013**. A systematic genome-wide

- analysis of zebrafish protein-coding gene function 496:494–497.
- Khurana S, Schouteden S, Manesia JK, Santamaria-Martínez A, Huelsken J, Lacy-Hulbert A, Verfaillie CM. **2016**. Outside-in integrin signalling regulates haematopoietic stem cell function via Periostin-Itgav axis. *Nat Commun* 7.
- Kii I, Nishiyama T, Kudo A. **2016**. Periostin promotes secretion of fibronectin from the endoplasmic reticulum. *Biochem Biophys Res Commun* 470:888–893.
- Kii I, Nishiyama T, Li M, Matsumoto K -i. K-I, Saito M, Amizuka N, Kudo A. **2009**. Incorporation of Tenascin-C into the Extracellular Matrix by Periostin Underlies an Extracellular Meshwork Architecture. *J Biol Chem* 285:2028–39.
- Kikuchi K, Gupta V, Wang J, Holdway JE, Wills AA, Fang Y, Poss KD. **2011a**. tcf21+ epicardial cells adopt non-myocardial fates during zebrafish heart development and regeneration. *Development* 138:2895–902.
- Kikuchi K, Holdway JE, Major RJ, Blum N, Dahn RD, Begemann G, Poss KD. **2011b**. Retinoic acid production by endocardium and epicardium is an injury response essential for zebrafish heart regeneration. *Dev Cell* 20:397–404.
- Kikuchi K, Holdway JE, Werdich AA, Anderson RM, Fang Y, Egnaczyk GF, Evans T, Macrae CA, Stainier DYS, Poss KD. **2010**. Primary contribution to zebrafish heart regeneration by gata4(+) cardiomyocytes. *Nature* 464:601–5.
- Kim J, Wu Q, Zhang Y, Wiens KM, Huang Y, Rubin N, Shimada H, Handin RI, Chao MY, Tuan T-L, Starnes VA, Lien C-L. **2010**. PDGF signaling is required for epicardial function and blood vessel formation in regenerating zebrafish hearts. *Proc Natl Acad Sci U S A* 107:17206–10.
- Kim S-H, Turnbull J, Guimond S. **2011**. Extracellular matrix and cell signalling: the dynamic cooperation of integrin, proteoglycan and growth factor receptor. *J Endocrinol* 209:139–51.
- Kimmel CB. **1993**. Patterning the brain of the zebrafish embryo. *Annu Rev Neurosci* 16:707–32.
- Kimmel CB, Kane DA, Walker C, Warga RM, Rothman MB. **1989**. A mutation that changes cell movement and cell fate in the zebrafish embryo. *Nature* 337:358–62.
- Kizil C, Iltzsche A, Kaslin J, Brand M. **2013**. Micromanipulation of Gene Expression in the Adult Zebrafish Brain Using Cerebroventricular Microinjection of Morpholino Oligonucleotides. *J Vis Exp* 1–6.
- Kondoh H, Nishiyama T, Kikuchi Y, Fukayama M, Saito M, Kii I, Kudo A. **2016**. Periostin Deficiency Causes Severe and Lethal Lung Injury in Mice With Bleomycin Administration. *J Histochem Cytochem* 64:441–453.
- Kroehne V, Freudenreich D, Hans S, Kaslin J, Brand M. **2011**. Regeneration of the adult zebrafish brain from neurogenic radial glia-type progenitors. *Development* 138:4831–4841.
- Kruzynska-Freitag A, Machnicki M, Rogers R, Markwald RR, Conway SJ. **2001**. Periostin (an osteoblast-specific factor) is expressed within the embryonic mouse heart during valve formation. *Mech Dev* 103:183–8.

## References

- Kudo A. **2017**. Introductory review: periostin—gene and protein structure. *Cell Mol Life Sci* .
- Kudo A. **2011**. Periostin in fibrillogenesis for tissue regeneration: periostin actions inside and outside the cell. *Cell Mol Life Sci* 68:3201–3207.
- Kudo H, Amizuka N, Araki K, Inohaya K, Kudo A. **2004**. Zebrafish periostin is required for the adhesion of muscle fiber bundles to the myoseptum and for the differentiation of muscle fibers. *Dev Biol* 267:473–87.
- Kühn B, del Monte F, Hajjar RJ, Chang Y-S, Lebeche D, Arab S, Keating MT. **2007**. Periostin induces proliferation of differentiated cardiomyocytes and promotes cardiac repair. *Nat Med* 13:962–9.
- Kwan KM, Fujimoto E, Grabher C, Mangum BD, Hardy ME, Campbell DS, Parant JM, Yost HJ, Kanki JP, Chien C-B. **2007**. The Tol2kit: a multisite gateway-based construction kit for Tol2 transposon transgenesis constructs. *Dev Dyn* 236:3088–99.
- Laflamme MA, Murry CE. **2011**. Heart regeneration. *Nature* 473:326–335.
- Lai S-L, Marín-Juez R, Moura PL, Kuenne C, Lai JKH, Tsekeke AT, Guenther S, Looso M, Stainier DYR. **2017**. Reciprocal analyses in zebrafish and medaka reveal that harnessing the immune response promotes cardiac regeneration. *Elife* 6:1–20.
- Laube F, Heister M, Scholz C, Borchardt T, Braun T. **2006**. Re-programming of newt cardiomyocytes is induced by tissue regeneration. *J Cell Sci* 119:4719–4729.
- Lauridsen H, Pedersen M. **2014**. Rebuilding a heart: complete regeneration after myocardial infarction in the axolotl. *FASEB* 28.
- Lavine KJ, Epelman S, Uchida K, Weber KJ, Nichols CG, Schilling JD, Ornitz DM, Randolph GJ, Mann DL. **2014**. Distinct macrophage lineages contribute to disparate patterns of cardiac recovery and remodeling in the neonatal and adult heart. *Proc Natl Acad Sci U S A* 111:16029–34.
- Le A, Trinh, Stainier DY. **2004**. Fibronectin Regulates Epithelial Organization during Myocardial Migration in Zebrafish. *Dev Cell* 6:371–382.
- Leach JP, Martin JF. **2018**. Cardiomyocyte Proliferation for Therapeutic Regeneration. *Curr Cardiol Rep* 20:1–8.
- Lepilina A, Coon AN, Kikuchi K, Holdway JE, Roberts RW, Burns CG, Poss KD. **2006**. A dynamic epicardial injury response supports progenitor cell activity during zebrafish heart regeneration. *Cell* 127:607–19.
- Li F, Wang X, Capasso J, Gerdes A. **1996**. Rapid Transition of Cardiac Myocytes from Hyperplasia to Hypertrophy During Postnatal Development. *J Mol Cell Cardiol* 28:1737–1746.
- Lien C-L, Harrison MR, Tuan T-L, Starnes VA. **2012**. Heart repair and regeneration: recent insights from zebrafish studies. *Wound Repair Regen* 20:638–46.
- Lien C-L, Schebesta M, Makino S, Weber GJ, Keating MT. **2006**. Gene expression analysis of zebrafish heart regeneration. *PLoS Biol* 4:e260.
- Lo C-M, Wang H-B, Dembo M, Wang Y. **2000**. Cell Movement Is Guided by the Rigidity

- of the Substrate. *Biophys J* 79:144–152.
- Looso M, Preussner J, Sousounis K, Bruckskotten M, Michel CS, Lignelli E, Reinhardt R, Höffner S, Krüger M, Tsonis PA, Borchardt T, Braun T. **2013**. A de novo assembly of the newt transcriptome combined with proteomic validation identifies new protein families expressed during tissue regeneration. *Genome Biol* 14:R16.
- Lorts A, Schwanekamp JA, Elrod JW, Sargent MA, Molkentin JD. **2009**. Genetic manipulation of periostin expression in the heart does not affect myocyte content, cell cycle activity, or cardiac repair. *Circ Res* 104:e1-7.
- Lu P, Takai K, Weaver VM, Werb Z. **2011**. Extracellular matrix degradation and remodeling in development and disease. *Cold Spring Harb Perspect Biol* 3:a005058–a005058.
- Lu P, Weaver VM, Werb Z. **2012**. The extracellular matrix: a dynamic niche in cancer progression. *J Cell Biol* 196:395–406.
- Ma D, Tu C, Sheng Q, Yang Y, Kan Z, Guo Y, Shyr Y, Scott IC, Lou X. **2018**. Dynamics of zebrafish heart regeneration using an HPLC-ESI-MS/MS approach. *J Proteome Res* acs.jproteome.7b00915.
- Mahmoud Ali, O’Meara CCC, Gemberling M, Zhao L, Bryant DMM, Zheng R, Gannon JBB, Cai L, Choi W-Y, Egnaczyk GFF, Burns CGGCEE, Burns CGGCEE, MacRae CAA, Poss KDD, Lee RTT. **2015**. Nerves Regulate Cardiomyocyte Proliferation and Heart Regeneration. *Dev Cell* 34:387–399.
- Marín-Juez R, Marass M, Gauvrit S, Rossi A, Lai S-L, Materna SC, Black BL, Stainier DYR. **2016**. Fast revascularization of the injured area is essential to support zebrafish heart regeneration. *Proc Natl Acad Sci* 113:11237–11242.
- Marro J, Pfefferli C, de Preux Charles A-S, Bise T, Jaźwińska A. **2016**. Collagen XII Contributes to Epicardial and Connective Tissues in the Zebrafish Heart during Ontogenesis and Regeneration. *PLoS One* 11:e0165497.
- Maruhashi T, Kii I, Saito M, Kudo A. **2010**. Interaction between Periostin and BMP-1 Promotes Proteolytic Activation of Lysyl Oxidase. *J Biol Chem* 285:13294–13303.
- Mellman K, Huisken J, Dinsmore C, Hoppe C, Stainier DY. **2012**. Fibrillin-2b regulates endocardial morphogenesis in zebrafish. *Dev Biol* 372:111–119.
- Mendis S, Puska P, Norrving B. **2011**. Global Atlas on cardiovascular disease prevention and control. *World Heal Organ Geneva* 164.
- Mercer SE, Cheng CH, Atkinson DL, Krcmery J, Guzman CE, Kent DT, Zukor K, Marx KA, Odelberg SJ, Simon HG. **2012**. Multi-Tissue Microarray Analysis Identifies a Molecular Signature of Regeneration. *PLoS One* 7.
- Mercer SE, Odelberg SJ, Simon H-G. **2013**. A dynamic spatiotemporal extracellular matrix facilitates epicardial-mediated vertebrate heart regeneration. *Dev Biol* 382:457–69.
- Missinato MA, Tobita K, Romano N, Carroll JA, Tsang M. **2015**. Extracellular component hyaluronic acid and its receptor Hmmer are required for epicardial EMT during heart regeneration. *Cardiovasc Res* cvv190–1. Missinato MA, Tobita K, Romano N, Carrol.

## References

- Morgan TH. **1901**. Regeneration. New York, Macmillan.
- Mozaffarian D, Benjamin EJ, Go AS, Arnett DK, Blaha MJ, Cushman M, Das SR, de Ferranti S, Després J-P, Fullerton HJ, Howard VJ, Huffman MD, Isasi CR, Jiménez MC, Judd SE, Kissela BM, Lichtman JH, Lisabeth LD, Liu S, Mackey RH, Magid DJ, McGuire DK, Mohler ER, Moy CS, Muntner P, Mussolino ME, Nasir K, Neumar RW, Nichol G, Palaniappan L, Pandey DK, Reeves MJ, Rodriguez CJ, Rosamond W, Sorlie PD, Stein J, Towfighi A, Turan TN, Virani SS, Woo D, Yeh RW, Turner MB, Committee AHAS, Stroke Statistics Subcommittee. **2016**. Heart Disease and Stroke Statistics-2016 Update: A Report From the American Heart Association. *Circulation* 133:e38-360.
- Mujumdar VS, Smiley LM, Tyagi SC. **2001**. Activation of matrix metalloproteinase dilates and decreases cardiac tensile strength. *Int J Cardiol* 79:277–286.
- Münch J, Grivas D, González-Rajal Á, Torregrosa-Carrión R, de la Pompa JL. **2017**. Notch signalling restricts inflammation and *serpine1* expression in the dynamic endocardium of the regenerating zebrafish heart. *Development* 144:1425–1440.
- Murry CE, Reinecke H, Pabon LM. **2006**. Regeneration Gaps. Observations on Stem Cells and Cardiac Repair. *J Am Coll Cardiol* 47:1777–1785.
- Naik PK, Bozyk PD, Bentley JK, Popova AP, Birch CM, Wilke CA, Fry CD, White ES, Sisson TH, Tayob N, Carnemolla B, Orecchia P, Flaherty KR, Hershenson MB, Murray S, Martinez FJ, Moore BB. **2012**. Periostin promotes fibrosis and predicts progression in patients with idiopathic pulmonary fibrosis. *AJP Lung Cell Mol Physiol* 303:L1046–L1056.
- Naqvi N, Li M, Calvert JW, Tejada T, Lambert JP, Wu J, Kesteven SH, Holman SR, Matsuda T, Lovelock JD, Howard WW, Iismaa SE, Chan AY, Crawford BH, Wagner MB, Martin DIK, Lefer DJ, Graham RM, Husain A. **2014**. A Proliferative Burst during Preadolescence Establishes the Final Cardiomyocyte Number. *Cell* 157:795–807.
- Nesvizhskii AI, Keller A, Kolker E, Aebersold R. **2003**. A statistical model for identifying proteins by tandem mass spectrometry. *Anal Chem* 75:4646–58.
- Neufeld DA, Zhao W. **1995**. Bone regrowth after digit tip amputation in mice is equivalent in adults and neonates. *Wound Repair Regen* 3:461–466.
- Nishiyama T, Kii I, Kashima TG, Kikuchi Y, Ohazama A, Shimazaki M, Fukayama M, Kudo A. **2011**. Delayed Re-Epithelialization in Periostin-Deficient Mice during Cutaneous Wound Healing. *PLoS One* 6:e18410.
- Nitsche U, Stangel D, Pan Z, Schlitter AM, Esposito I, Regel I, Raulefs S, Friess H, Kleeff J, Erkan M. **2016**. Periostin and tumor-stroma interactions in non-small cell lung cancer. *Oncol Lett* 12:3804–3810.
- Norris R a., Moreno-Rodriguez R, Hoffman S, Markwald RR. **2009**. The many facets of the matricellular protein periostin during cardiac development, remodeling, and pathophysiology. *J Cell Commun Signal* 3:275–86.
- Norris RA, Damon B, Mironov V, Kasyanov V, Ramamurthi A, Moreno-Rodriguez R, Trusk T, Potts JD, Goodwin RL, Davis J, Hoffman S, Wen X, Sugi Y, Kern CB, Mjaatvedt CH, Turner DK, Oka T, Conway SJ, Molkentin JD, Forgacs G, Markwald RR. **2007**. Periostin regulates collagen fibrillogenesis and the biomechanical properties of

- connective tissues. *J Cell Biochem* 101:695–711.
- Norris RA, Potts JD, Yost MJ, Junor L, Brooks T, Tan H, Hoffman S, Hart MM, Kern MJ, Damon B, Markwald RR, Goodwin RL, Avenue A, E-mail SC. **2009**. Periostin Promotes a Fibroblastic Lineage Pathway in Atrioventricular Valve Progenitor Cells 1052–1063.
- Norton GR, Tsoetsi J, Trifunovic B, Hartford C, Candy GP, Woodiwiss AJ. **1997**. Myocardial stiffness is attributed to alterations in cross-linked collagen rather than total collagen or phenotypes in spontaneously hypertensive rats. *Circulation* 96:1991–1998.
- Notari M, Ventura-Rubio A, Bedford-Guaus SJ, Jorba I, Mulero L, Navajas D, Martí M, Raya Á. **2018**. The local microenvironment limits the regenerative potential of the mouse neonatal heart. *Sci Adv* 4:eao5553.
- O’Meara CC, Wamstad JA, Gladstone RA, Fomovsky GM, Butty VL, Shrikumar A, Gannon JB, Boyer LA, Lee RT. **2015**. Transcriptional Reversion of Cardiac Myocyte Fate During Mammalian Cardiac Regeneration. *Circ Res* 116:804–815.
- Oberpriller, John O.; Oberpriller, Jean C.; Mauro A. **1991**. The Development and Regenerative Potential of Cardiac Muscle. Harwood Academic Publishers.
- Oberpriller J, Oberpriller JC. **1971**. Mitosis in adult newt ventricle. *J Cell Biol* 49:560–563.
- Oberpriller JCJOC, Oberpriller JCJOC. **1974**. Response of the adult newt ventricle to injury. *J Exp Zool* 187:249–53.
- Oka T, Xu J, Kaiser R a., Melendez J, Hambleton M, Sargent M a., Lorts A, Brunskill EW, Dorn GW, Conway SJ, Aronow BJ, Robbins J, Molkentin JD. **2007**. Genetic manipulation of periostin expression reveals a role in cardiac hypertrophy and ventricular remodeling. *Circ Res* 101:313–21.
- Olivetti G, Cigola E, Maestri R, Corradi D, Lagrasta C, Gambert SR, Anversa P. **1996**. Aging, cardiac hypertrophy and ischemic cardiomyopathy do not affect the proportion of mononucleated and multinucleated myocytes in the human heart. *J Mol Cell Cardiol* 28:1463–77.
- Olivetti G, Melissari M, Capasso JM, Anversa P. **1991**. Cardiomyopathy of the aging human heart. Myocyte loss and reactive cellular hypertrophy. *Circ Res* 68:1560–8.
- Ontsuka K, Kotobuki Y, Shiraishi H, Serada S, Ohta S, Tanemura A, Yang L, Fujimoto M, Arima K, Suzuki S, Murota H, Toda S, Kudo A, Conway SJ, Narisawa Y, Katayama I, Izuhara K, Naka T. **2012**. Periostin, a matricellular protein, accelerates cutaneous wound repair by activating dermal fibroblasts. *Exp Dermatol* 21:331–336.
- Parente V, Balasso S, Pompilio G, Verduci L, Colombo GI, Milano G, Guerrini U, Squadroni L, Cotelli F, Pozzoli O, Capogrossi MC. **2013**. Hypoxia/reoxygenation cardiac injury and regeneration in zebrafish adult heart. *PLoS One* 8:e53748.
- Pfefferli C, Jaźwińska A. **2017**. The *careg* element reveals a common regulation of regeneration in the zebrafish myocardium and fin. *Nat Commun* 8.
- Porrello ER, Mahmoud AI, Simpson E, Hill JA, Richardson JA, Olson EN, Sadek HA. **2011**.

## References

- Transient Regenerative Potential of the Neonatal Mouse Heart. *Science* (80-) 331.
- Porrello ER, Mahmoud AI, Simpson E, Johnson BA, Grinsfelder D, Canseco D, Mammen PP, Rothmel BA, Olson EN, Sadek HA. **2013**. Regulation of neonatal and adult mammalian heart regeneration by the miR-15 family. *Proc Natl Acad Sci U S A* 110:187–92.
- Poss KD. **2007**. Getting to the heart of regeneration in zebrafish. *Semin Cell Dev Biol* 18:36–45.
- Poss KD, Keating MT, Nechiporuk A. **2003**. Tales of regeneration in zebrafish. *Dev Dyn* 226:202–210.
- Poss KD, Wilson LG, Keating MT. **2002**. Heart regeneration in zebrafish. *Science* 298:2188–90.
- Qin X, Yan M, Zhang J, Wang X, Shen Z, Lv Z, Li Z, Wei W, Chen W. **2016**. TGF $\beta$ 3-mediated induction of Periostin facilitates head and neck cancer growth and is associated with metastasis. *Sci Rep* 6:20587.
- Raya Á, Consiglio A, Kawakami Y, Rodriguez-esteban C, Izpisúa-belmonte JC. **2004**. The Zebrafish as a Model of Heart Regeneration 6:345–351.
- Raya A, Koth CM, Büscher D, Kawakami Y, Itoh T, Raya RM, Sternik G, Tsai H-J, Rodríguez-Esteban C, Izpisúa-Belmonte JC. **2003**. Activation of Notch signaling pathway precedes heart regeneration in zebrafish. *Proc Natl Acad Sci U S A* 100 Suppl:11889–95.
- Reddien PW, Alvarado AS. **2004**. Fundamentals of Planarian Regeneration. *Annu Rev Cell Dev Biol* 20:725–757.
- Rios H, Koushik S V, Wang H, Wang J, Zhou H-M, Lindsley A, Rogers R, Chen Z, Maeda M, Kruzynska-Frejtag A, Feng JQ, Conway SJ. **2005**. periostin null mice exhibit dwarfism, incisor enamel defects, and an early-onset periodontal disease-like phenotype. *Mol Cell Biol* 25:11131–44.
- Rumyantsev P. **1973**. Post-injury DNA synthesis, mitosis and ultrastructural reorganization of adult frog cardiac myocytes. An electron microscopic- autoradiographic study. *Z Zellforsch Mikrosk Anat* 139:431–450.
- Rumyantsev P. **1961**. Evidence of regeneration of significant parts of myocardial fibers of frogs after trauma. *Arkh Anat Gistol Embriol* 376:65–74.
- Sadek HA, Martin JF, Takeuchi JK, Leor J, Nie Y, Giacca M, Lee RT. **2014**. Erratum: Multi-investigator letter on reproducibility of neonatal heart regeneration following apical resection (Stem Cell Reports (2014) 3 (1)). *Stem Cell Reports* 3:690.
- Sallin P, de Preux Charles A-S, Duruz V, Pfefferli C, Jaźwińska A. **2015**. A dual epimorphic and compensatory mode of heart regeneration in zebrafish. *Dev Biol* 399:27–40.
- Sánchez-Iranzo H, Galardi-Castilla M, Sanz-Morejón A, González-Rosa JM, Costa R, Ernst A, Sainz de Aja J, Langa X, Mercader N. **2018**. Transient fibrosis resolves via fibroblast inactivation in the regenerating zebrafish heart. *Proc Natl Acad Sci U S A* 115:4188–4193.
- Sánchez Alvarado A. **2000**. Regeneration in the metazoans: Why does it happen?



*BioEssays* 22:578–590.

- Schnabel K, Wu C-C, Kurth T, Weidinger G. **2011**. Regeneration of Cryoinjury Induced Necrotic Heart Lesions in Zebrafish Is Associated with Epicardial Activation and Cardiomyocyte Proliferation. *PLoS One* 6:e18503.
- Sedmera D. **2011**. Function and form in the developing cardiovascular system. *Cardiovasc Res* 91:252–259.
- Sen S, Sadek HA. **2015**. Neonatal heart regeneration: Mounting support and need for technical standards. *J Am Heart Assoc* 4:3–5.
- Senyo SE, Steinhauser ML, Pizzimenti CL, Yang VK, Cai L, Wang M, Wu T-D, Guerquin-Kern J-L, Lechene CP, Lee RT. **2013**. Mammalian heart renewal by pre-existing cardiomyocytes. *Nature* 493:433–6.
- Shimazaki M, Nakamura K, Kii I, Kashima T, Amizuka N, Li M, Saito M, Fukuda K, Nishiyama T, Kitajima S, Saga Y, Fukayama M, Sata M, Kudo A. **2008**. Periostin is essential for cardiac healing after acute myocardial infarction. *J Exp Med* 205:295–303.
- Sidhu SS, Yuan S, Innes AL, Kerr S, Woodruff PG, Hou L, Muller SJ, Fahy J V. **2010**. Roles of epithelial cell-derived periostin in TGF-beta activation, collagen production, and collagen gel elasticity in asthma. *Proc Natl Acad Sci U S A* 107:14170–5.
- Simone BW, Martínez-Gálvez G, WareJoncas Z, Ekker SC. **2018**. Fishing for understanding: Unlocking the zebrafish gene editor's toolbox. *Methods* .
- Sleep E, Boué S, Jopling C, Raya M, Raya A, Izpisua Belmonte JC. **2010**. Transcriptomics approach to investigate zebrafish heart regeneration. *J Cardiovasc Med (Hagerstown)* 11:369–80.
- Solnica-Krezel L, Schier AF, Driever W. **1994**. Efficient recovery of ENU-induced mutations from the zebrafish germline. *Genetics* 136:1401–1420.
- Stainier D, Fouquet B, Chen JN, Warren KS, Weinstein BM, Meiler SE, Mohideen MA, Neuhauss SC, Solnica-, Krezel L, Schier AF, Zwartkruis F, Stemple DL, Malicki J, Driever W, Fishman M. **1996**. Mutations affecting the formation and function of the cardiovascular system in the zebrafish embryo. *Development* 123:285–92.
- Stainier D, Lee R, Fishman M. **1993**. Cardiovascular development in the zebrafish. I. Myocardial fate map and heart tube formation. *Development* 119:31–40.
- Stanton LW, Garrard LJ, Damm D, Garrick BL, Lam A, Kapoun AM, Zheng Q, Protter AA, Schreiner GF, White RT. **2000**. Altered patterns of gene expression in response to myocardial infarction. *Circ Res* 86:939–945.
- Stedman's medical dictionary, 28th ed. **2005**. . Stedman's.
- Streisinger G, Walker C, Dower N, Knauber D, Singer F. **1981**. Production of clones of homozygous diploid zebra fish (*Brachydanio rerio*). *Nature* 291:293–6.
- Strungs EG, Ongstad EL, Quinn MPO, Palatinus JA, Jourdan LJ, Gourdie RG. **2013**. Cryoinjury Models of the Adult and Neonatal Mouse Heart for Studies of Scarring and Regeneration 1037:343–353.

## References

- Sturzu AC, Rajarajan K, Passer D, Plonowska K, Riley A, Tan TC, Sharma A, Xu AF, Engels MC, Feistritz R, Li G, Selig MK, Geissler R, Robertson KD, Scherrer-Crosbie M, Domian IJ, Wu SM. **2015**. Fetal Mammalian Heart Generates a Robust Compensatory Response to Cell Loss. *Circulation* 132:109–121.
- Sugiura T, Takamatsu H, Kudo A, Amann E. **1995**. Expression and characterization of murine osteoblast-specific factor 2 (OSF-2) in a baculovirus expression system. *Protein Expr Purif* 6:305–11.
- Summerton J, Weller D. **1997**. Morpholino antisense oligomers: design, preparation, and properties. *Antisense Nucleic Acid Drug Dev* 7:187–95.
- Sung P, Jan Y, Lin S-C, Huang C, Lin H, Wen K, Chao K, Lai C, Wang P, Chuang C, Wu H, Twu N, Yen M, Hsiao M, Huang C-YF. **2016**. Periostin in tumor microenvironment is associated with poor prognosis and platinum resistance in epithelial ovarian carcinoma. *Oncotarget* 7:4036–4047.
- Suzuki H, Amizuka N, Kii I, Kawano Y, Nozawa-inoue K, Suzuki A, Yoshie H, Kudo A, Maeda T. **2004**. Immunohistochemical Localization of Periostin in Tooth and Its Surrounding Tissues in Mouse 1275:1264–1275.
- Suzuki R, Shimodaira H. **2006**. Pvcust: an R package for assessing the uncertainty in hierarchical clustering. *Bioinformatics* 22:1540–2.
- Takayama G, Arima K, Kanaji T, Toda S, Tanaka H, Shoji S, McKenzie ANJ, Nagai H, Hotokebuchi T, Izuhara K. **2006**. Periostin: a novel component of subepithelial fibrosis of bronchial asthma downstream of IL-4 and IL-13 signals. *J Allergy Clin Immunol* 118:98–104.
- Takayama I, Tanabe H, Nishiyama T, Ito H, Amizuka N, Li M, Katsube K-I, Kii I, Kudo A. **2017**. Periostin is required for matricellular localization of CCN3 in periodontal ligament of mice. *J Cell Commun Signal* 11:5–13.
- Tanabe H, Takayama I, Nishiyama T, Shimazaki M, Kii I, Li M, Amizuka N, Katsube K ichi, Kudo A. **2010**. Periostin associates with notch1 precursor to maintain notch1 expression under a stress condition in mouse cells. *PLoS One* 5:1–9.
- Tanaka EM, Ferretti P. **2009**. Considering the evolution of regeneration in the central nervous system. *Nat Rev Neurosci* 10:713–723.
- Tanaka EM, Reddien PW. **2011**. The Cellular Basis for Animal Regeneration. *Dev Cell* 21:172–185.
- Tanaka S, Maekawa A, Matsubara L, Imanishi A, Yano M, Roeder RG, Hasegawa N, Asano S, Ito M. **2016**. Periostin supports hematopoietic progenitor cells and niche-dependent myeloblastoma cells in vitro. *Biochem Biophys Res Commun* 478:1706–1712.
- Taniyama Y, Katsuragi N, Sanada F, Azuma J, Iekushi K, Koibuchi N, Okayama K, Ikeda-Iwababu Y, Muratsu J, Otsu R, Rakugi H, Morishita R. **2016**. Selective Blockade of Periostin Exon 17 Preserves Cardiac Performance in Acute Myocardial Infarction. *Hypertens (Dallas, Tex 1979)* 67:356–61.
- The Gene Ontology Consortium. **2017**. Expansion of the Gene Ontology knowledgebase and resources. *Nucleic Acids Res* 45:D331–D338.

- Thisse B, Pflumio S, Fürthauer M, Loppin B, Heyer V, Degrave A, Woehl R, Lux A, Steffan T, Charbonnier XQ, Thisse C. **2001**. Expression of the zebrafish genome during embryogenesis. *ZFIN* . <http://zfin.org/ZDB-PUB-010810-1>
- Thisse C, Thisse B. **2005**. High Throughput Expression Analysis of ZF-Models Consortium Clones. *ZFIN* . <http://zfin.org/ZDB-PUB-051025-1>
- Thomas B, F. WM, G. BC, R. BR, Melitta S. **1998**. Axonal regrowth after spinal cord transection in adult zebrafish. *J Comp Neurol* 377:577–595.
- Thummel R, Bailey TJ, Hyde DR. **2011**. In vivo electroporation of morpholinos into the adult zebrafish retina. *J Vis Exp* e3603.
- Tian Y, Choi CH, Li QK, Rahmatpanah FB, Chen X, Kim SR, Veltri R, Chia D, Zhang Z, Mercola D, Zhang H. **2015**. Overexpression of Periostin in Stroma Positively Associated with Aggressive Prostate Cancer. *PLoS One* 10:e0121502.
- Tsifaki M, Kelaini S, Caines R, Yang C, Margariti A. **2018**. Regenerating the Cardiovascular System Through Cell Reprogramming; Current Approaches and a Look Into the Future. *Front Cardiovasc Med* 5:1–12.
- Tsonis PA. **2000**. Regeneration in vertebrates. *Dev Biol* 221:273–284.
- Tsonis PA, Madhavan M, Tancous EE, Del Rio-Tsonis K. **2004**. A newt's eye view of lens regeneration. *Int J Dev Biol* 48:975–980.
- Uchida M, Shiraishi H, Ohta S, Arima K, Taniguchi K, Suzuki S, Okamoto M, Ahlfeld SK, Ohshima K, Kato S, Toda S, Sagara H, Aizawa H, Hoshino T, Conway SJ, Hayashi S, Izuhara K. **2012**. Periostin, a Matricellular Protein, Plays a Role in the Induction of Chemokines in Pulmonary Fibrosis. *Am J Respir Cell Mol Biol* 46:677–686.
- Underwood TJ, Hayden AL, Derouet M, Garcia E, Noble F, White MJ, Thirdborough S, Mead A, Clemons N, Mellone M, Uzoho C, Primrose JN, Blaydes JP, Thomas GJ. **2015**. Cancer-associated fibroblasts predict poor outcome and promote periostin-dependent invasion in oesophageal adenocarcinoma. *J Pathol* 235:466–477.
- Urciuolo A, Quarta M, Morbidoni V, Gattazzo F, Molon S, Grumati P, Montemurro F, Tedesco FS, Blaauw B, Cossu G, Vozi G, Rando TA, Bonaldo P. **2013**. Collagen VI regulates satellite cell self-renewal and muscle regeneration. *Nat Commun* 4:1–13.
- Van Berlo JH, Kanisicak O, Maillet M, Vagnozzi RJ, Karch J, Lin SCJ, Middleton RC, Marbán E, Molkentin JD. **2014**. C-kit+ cells minimally contribute cardiomyocytes to the heart. *Nature* 509:337–341.
- Varshney GK, Carrington B, Pei W, Bishop K, Chen Z, Fan C, Xu L, Jones M, LaFave MC, Ledin J, Sood R, Burgess SM. **2016**. A high-throughput functional genomics workflow based on CRISPR/Cas9-mediated targeted mutagenesis in zebrafish. *Nat Protoc* 11:2357–2375.
- Vihtelic TS, Hyde DR. **2000**. Light-induced rod and cone cell death and regeneration in the adult albino zebrafish (*Danio rerio*) retina. *J Neurobiol* 44:289–307.
- Vivien CJ, Hudson JE, Porrello ER. **2016**. Evolution, comparative biology and ontogeny of vertebrate heart regeneration. *npj Regen Med* 1:16012.
- Vizcaino JA, Côté RG, Csordas A, Dianas JA, Fabregat A, Foster JM, Griss J, Alpi E, Birim

## References

- M, Contell J, O'Kelly G, Schoenegger A, Ovelheiro D, Pérez-Riverol Y, Reisinger F, Ríos D, Wang R, Hermjakob H. **2012**. The Proteomics Identifications (PRIDE) database and associated tools: status in 2013. *Nucleic Acids Res* 41:D1063–D1069.
- Vrontosova MA, Vorontsova M, Liosner L, Allen P, Billett F. **1960**. Asexual propagation and regeneration. New York: New York: Pergamon Press.
- Wagers AJ, Weissman IL. **2004**. Plasticity of adult stem cells. *Cell* 116:639–648.
- Wang J, Cao J, Dickson AL, Poss KD. **2015**. Epicardial regeneration is guided by cardiac outflow tract and Hedgehog signalling. *Nature* 522:226–230.
- Wang J, Karra R, Dickson AL, Poss KD. **2013**. Fibronectin is deposited by injury-activated epicardial cells and is necessary for zebrafish heart regeneration. *Dev Biol* 382:427–35.
- Wang J, Panáková D, Kikuchi K, Holdway JE, Gemberling M, Burris JS, Singh SP, Dickson AL, Lin Y-F, Sabeh MK, Werdich AA, Yelon D, Macrae CA, Poss KD. **2011**. The regenerative capacity of zebrafish reverses cardiac failure caused by genetic cardiomyocyte depletion. *Development* 138:3421–30.
- Weissman IL, Anderson DJ, Gage F. **2001**. Stem and progen: Origins , and Transdifferentiations. *Cell Developmental Biol* 387–403.
- Wen JH, Vincent LG, Fuhrmann A, Choi YS, Hribar KC, Taylor-Weiner H, Chen S, Engler AJ. **2014**. Interplay of matrix stiffness and protein tethering in stem cell differentiation. *Nat Mater* 13:979–87.
- Westerfield M. **2000**. The Zebrafish Book. A Guide for the Laboratory Use of Zebrafish (*Danio rerio*), 4th ed. Eugene.
- Williams-Boyce PK, Daniel JC. **1980**. Regeneration of rabbit ear tissue. *J Exp Zool* 212:243–53.
- Witman N, Murtuza B, Davis B, Arner A, Morrison JI. **2011**. Recapitulation of developmental cardiogenesis governs the morphological and functional regeneration of adult newt hearts following injury. *Dev Biol* 354:67–76.
- Wu C-C, Kruse F, Vasudevarao MD, Junker JP, Zebrowski DC, Fischer K, Noël ES, Grün D, Berezikov E, Engel FB, van Oudenaarden A, Weidinger G, Bakkers J. **2016**. Spatially Resolved Genome-wide Transcriptional Profiling Identifies BMP Signaling as Essential Regulator of Zebrafish Cardiomyocyte Regeneration. *Dev Cell* 36:36–49.
- Wyatt C, Bartoszek EM, Yaksi E. **2015**. Methods for studying the zebrafish brain: Past, present and future. *Eur J Neurosci* 42:1746–1763.
- Xiao C, Gao L, Hou Y, Xu C, Chang N, Wang F, Hu K, He A, Luo Y, Wang J, Peng J, Tang F, Zhu X, Xiong J-W. **2016**. Chromatin-remodelling factor Brg1 regulates myocardial proliferation and regeneration in zebrafish. *Nat Commun* 7:13787.
- Xu S, Webb SE, Lau TCK, Cheng SH. **2018**. Matrix metalloproteinases (MMPs) mediate leukocyte recruitment during the inflammatory phase of zebrafish heart regeneration. *Sci Rep* 8:7199.
- Yahalom-Ronen Y, Rajchman D, Sarig R, Geiger B, Tzahor E. **2015**. Reduced matrix rigidity promotes neonatal cardiomyocyte dedifferentiation, proliferation and clonal

expansion. *Elife* 4.

Yanger K, Knigin D, Zong Y, Maggs L, Gu G, Akiyama H, Pikarsky E, Stanger BZ. **2014**. Adult hepatocytes are generated by self-duplication rather than stem cell differentiation. *Cell Stem Cell* 15:340–349.

Yokota K, Kobayakawa K, Saito T, Hara M, Kijima K, Ohkawa Y, Harada A, Okazaki K, Ishihara K, Yoshida S, Kudo A, Iwamoto Y, Okada S. **2017**. Periostin Promotes Scar Formation through the Interaction between Pericytes and Infiltrating Monocytes/Macrophages after Spinal Cord Injury. *Am J Pathol* 187:639–653.

Zhang R, Han P, Yang H, Ouyang K, Lee D, Lin Y-F, Ocorr K, Kang G, Chen J, Stainier DYR, Yelon D, Chi NC. **2013**. In vivo cardiac reprogramming contributes to zebrafish heart regeneration. *Nature* 498:497–501.

Zhou B, Ma Q, Rajagopal S, Wu SM, Domian I, Rivera-Feliciano J, Jiang D, Von Gise A, Ikeda S, Chien KR, Pu WT. **2008**. Epicardial progenitors contribute to the cardiomyocyte lineage in the developing heart. *Nature* 454:109–113.



# APPENDIX I

The qRT-PCR primer sequences used for this thesis can be found in the following table.

**Supplementary Table 1 | qRT-PCR primer sequences.**

Gene Name	Primer (5'-3')
<i>postna</i>	Fw: TGAAGGACCTGATTTCTCAAAG
	Rv: GAACGTCCATCCTTGATGATT
<i>postnb</i>	Fw: CGAAGCGGAGGTGAGAAAT
	Rv: TTAGTGAGGAGACGCTTGTTG
<i>col4a2</i>	Fw: AGGGTGAACATGGTGAAGTATT
	Rv: GCATACCCTCCATACCAAAGT
<i>col5a1</i>	Fw: TCCCATCATCGACACCAAAG
	Rv: CTGGATGTCACCCTCAAACA
<i>col5a2a</i>	Fw: CAAGACGGTGAGGATGAGTTG
	Rv: ATGGCTCAGGTTTCCAGATG
<i>fbn2b</i>	Fw: ATGAATGTGACCTGAACCCTAAT
	Rv: CACTCGTCCACATCTGTACATC
<i>fn1b</i>	Fw: ACCTGATGCTCCAACCAATC
	Rv: CACCACACGATAGCCAGTAAT
<i>elfa</i>	Fw: TTTGCTGTGCGTGACATGAG
	Rv: TGCAGACTTTGTGACCTTGC
<i>βactin</i>	Fw: AACGACAACATTGGCATGGC
	Rv: AACATTGCCGTACCTTCAC
GFP	Fw: GAACCGCATCGAGCTGAA
	Rv: TGCTTGTCGGCCATGATATAG
RFP	Fw: CCCAGACCATGAAGATCAAG
	Rv: GTACATGAAGCTGGTAGCC

Appendix I

<b>Gene Name</b>	<b>Primer (5'-3')</b>
<b><i>mmp2</i></b>	Fw: GAGCTCTATGGAGAACCAACAG
	Rv: ATCTGGGCTACAGCATCAAATA
<b><i>mmp9</i></b>	Fw: CCAGTGAGCTTCTCTTCACATT
	Rv: CGTCCTTCTGTAGTGCATGAAT
<b><i>mmp13a</i></b>	Fw: CATGTATCCCACCTACGTTTAC
	Rv: TCAGTGTTTGGGCCATAAAG
<b><i>mmp13b</i></b>	Fw: CTATCATGCGTTCAATCTGTTC
	Rv: GGAGTAAACCGGGTACATAAG
<b><i>mmp14a</i></b>	Fw: GATGTGGCGTTCCTGATAAA
	Rv: TGTAGTTCTGGATACTGAAAGTG
<b><i>mmp14b</i></b>	Fw: TTCTTGGCCCATGCTTAC
	Rv: ACATCATTACCCAGCAAGTC



## APPENDIX II

Supplementary material from chapter 1.

In order to see the supplementary tables 2-8 please refer to the excel file named “Supplementary Tables 2\_6” in the CD provided with this thesis.

7 Supplementary Tables as individual sheets in attached Excel file:

**Supplementary Table 2| Proteins identified during the decellularization process.**

Native zebrafish hearts, after SDS treatment (half), and at the end of decellularization (fully), were analyzed by LC-MS/MS. Log<sub>2</sub> raw intensities and VSN normalized intensities are given for each replicate of each sample group.

**Supplementary Table 3| Peptides identified in the decellularized samples.** Table of all the entries identified in our samples. The table contains the protein name, accession number, molecular weight and the spectral counts values obtained per each replicate.

**Supplementary Table 4| List of proteins represented with an overall of >5 spectral counts.** The table contains for each protein the gene name, the accession number, the molecular weight (MW), the ANOVA value (F), the p-value, and the adjusted p-value (FDR), the values obtained per each replicate and the average. The ECM proteins are identified with an asterisk.

**Supplementary Table 5| List of proteins represented with an overall of >5 spectral counts, normalized by VSN method.** The table contains for each protein the gene name, the accession number, the molecular weight (MW), the ANOVA value (F), the p-value,

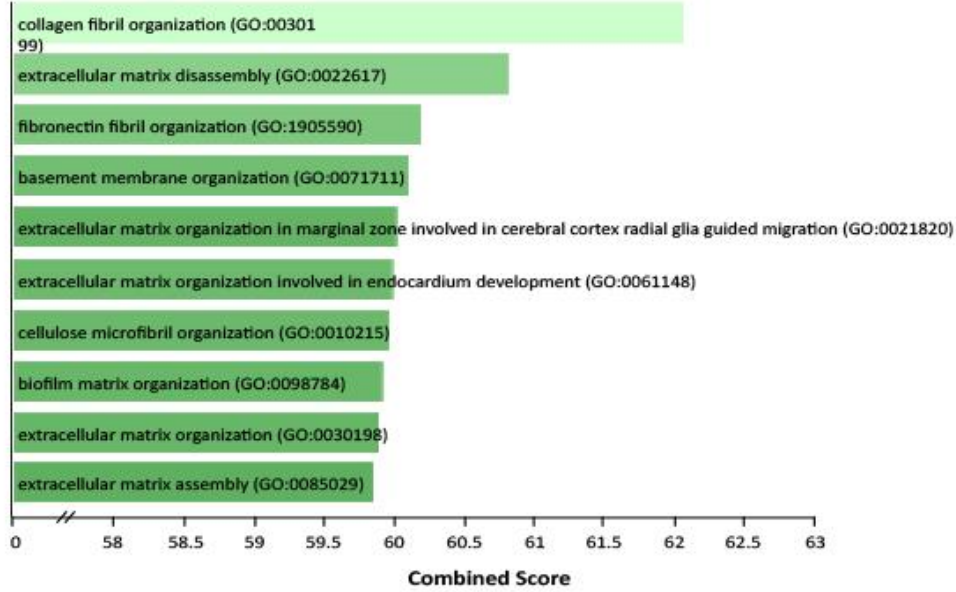
and the adjusted p-value (FDR), the values obtained per each replicate and the average. The ECM proteins are identified with an asterisk.

**Supplementary Table 6| List of proteins differentially expressed during heart regeneration.** The table contains for each protein the gene name, the accession number, the molecular weight (MW), the ANOVA value (F), the p-value, and the adjusted p-value (FDR), the values obtained per each replicate and the average. The ECM proteins are identified with an asterisk. p-value obtained from an ANOVA test of all the samples.

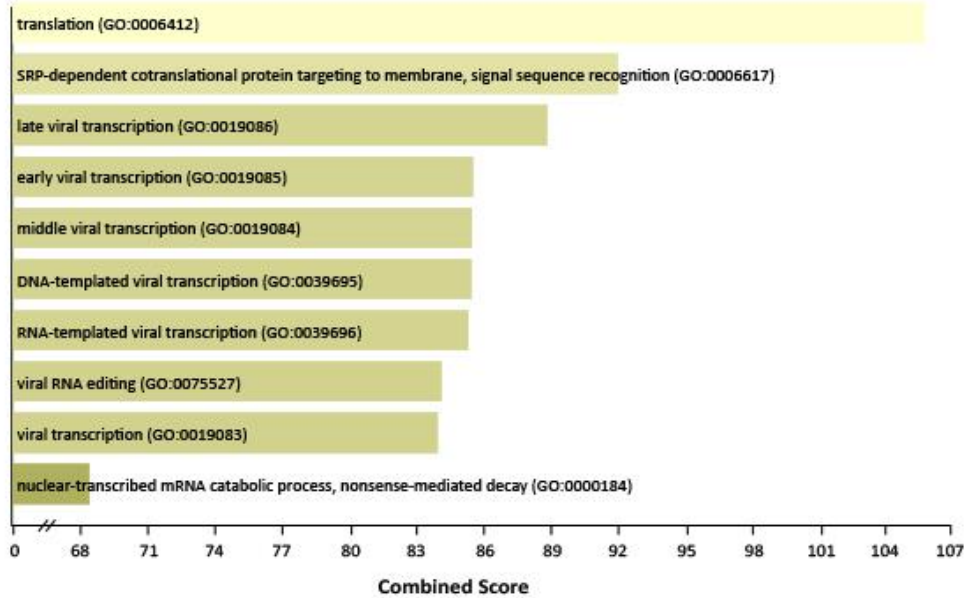
**Supplementary Table 7| List of the peptide identification in LC-MS/MS analysis.**

**Supplementary Table 8| List of protein identifications.**

**A**



**B**

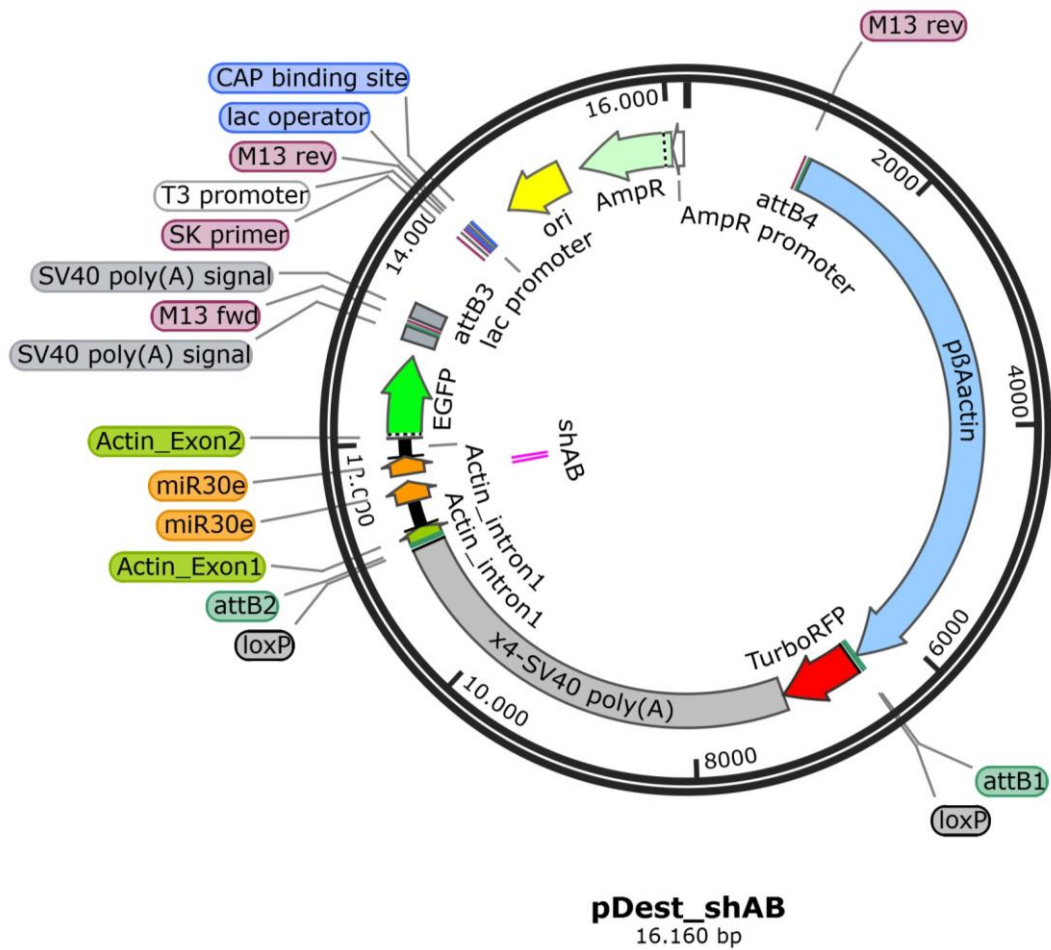


**Supplementary Figure 1 | Biological Process GO enrichment analysis on the differentially-expressed proteins during cardiac regeneration.** Comparison of the enriched Biological Process GO terms on our differentially expressed proteins (A) and the 209 differential protein groups of Ma et al. (Ma et al., 2018) (B).

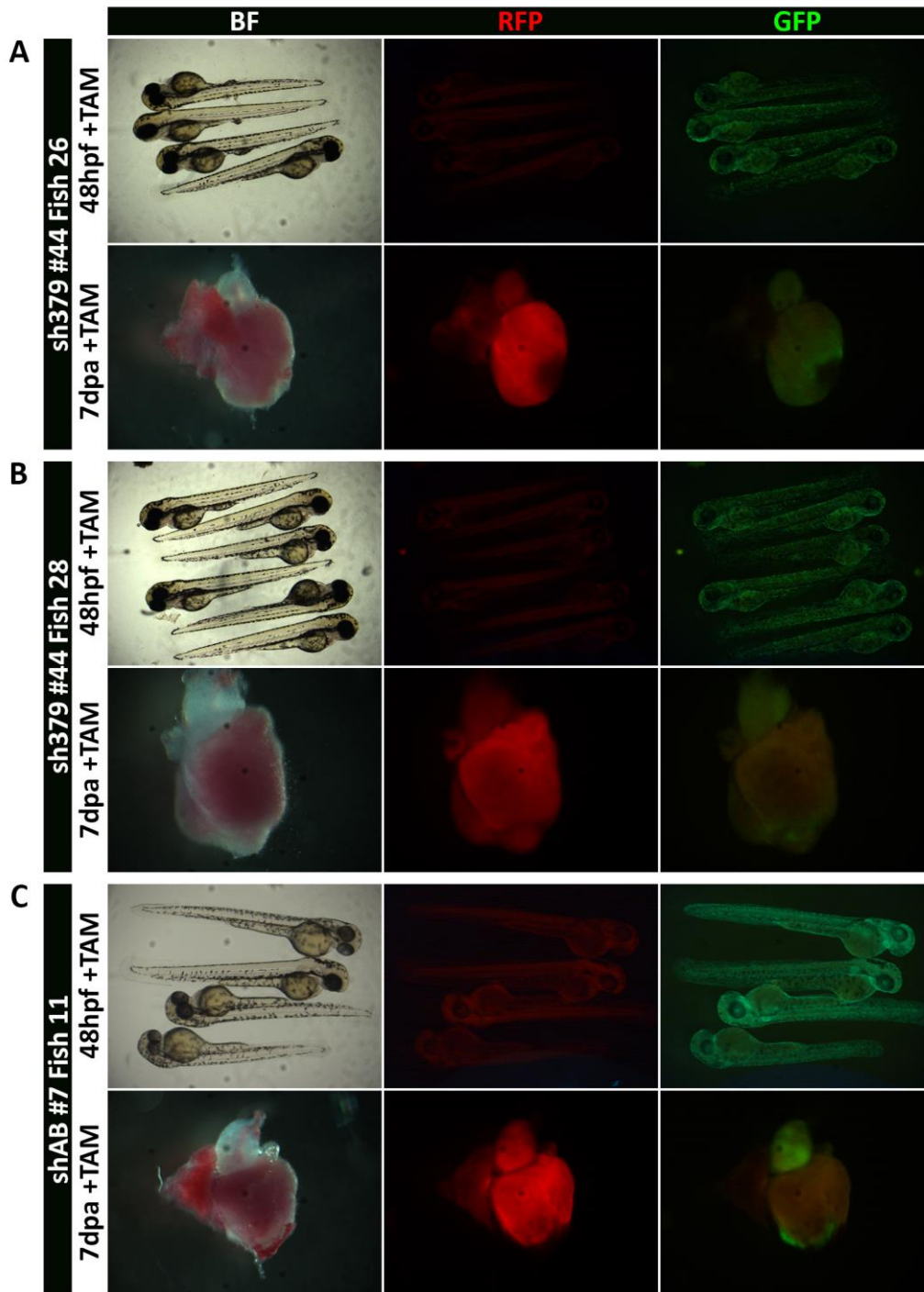


# APPENDIX III

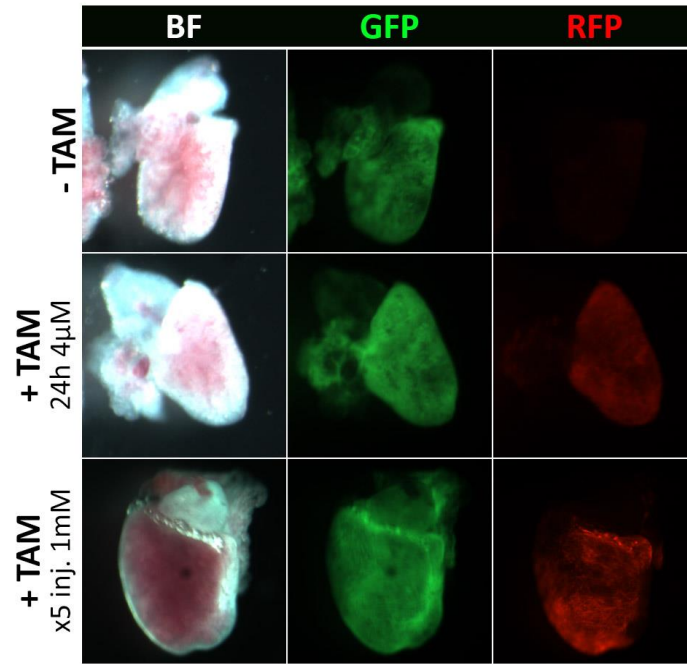
Supplementary figures from chapter 2.



**Supplementary Figure 2 | Map of the construct bactin2:loxP-RFP-STOP-loxP-bactin2-miR30-shRNA-GFP.** Construct for the generation of the conditional shRNA transgenic line.



**Supplementary Figure 3 | Adult tamoxifen treatments of the shRNA lines.** Two different fishes from the sh379 #44 line (A and B) were treated with tamoxifen at adult stage. One fish from the shAB #7 line (C) was treated with tamoxifen at adult stage. Their offspring, prior adult tamoxifen treatment, was also assessed for correct recombination by tamoxifen treatment at 24hpf.



**Supplementary Figure 4 | Adult tamoxifen treatment of dTg ((*eab2:loxP-GFP-loxP-RFP*)(*bactin2:Cre-Ert2*)).** Two different tamoxifen treatments were tested to assess the construct recombination grade.





## APPENDIX IV

Articles, published or under publishing process, written during this thesis:

### **Article 1**

Tekeli, I<sup>†</sup>; Garcia-Puig, A<sup>†</sup>; Notari, M; García-Pastor, C; Aujard, I; Jullien, L; Raya, A. **Fate predetermination of cardiac myocytes during zebrafish heart regeneration.** *Open Biol.* **7**, (2017).

†, These authors contributed equally to this study.

### **Article 2**

**Traction forces at the cytokinetic ring regulate cell division and polyploidy in the migrating zebrafish epicardium**

Authors: Uroz, M; Garcia-Puig, A; Tekeli, I; Elosegui-Artola, A; Albertazzi, L; Roca-Cusachs, P; Raya, A and Trepats, X.

Currently under revision. Submitted to the journal Nature Materials with impact factor (2017): 39.235 on January 24<sup>th</sup>, 2018.

### **Article 3**

**Proteomics analysis of extracellular matrix remodelling during zebrafish heart regeneration**

Authors: Garcia-Puig, A; Mosquera, JL; Jimenez-Delgado, S; Garcia-Pastor, C; Jorba, I; Navajas, D; Canals, F and Raya, A.

Currently under revision. Submitted to the journal Molecular and Cellular Proteomics with impact factor (2017): 5,232 on June 22<sup>nd</sup>, 2018.



# AGRAÏMENTS

Sembla que fos ahir quan vaig començar a l'IBEC sense haver tocat mai un peix zebra. El temps passa volant i, escriure aquestes línies significa que, per fi, he arribat al final d'una etapa molt important a la meua vida. Han sigut uns anys molt intensos, de no parar, ple de bons i no tan bons moments, de mudances de laboratori i de canvis. Durant aquest període, he crescut tant científicament com personalment. Realitzar la tesi doctoral m'ha suposat acceptar tant l'èxit com la frustració. He après també que mai estàs sol, que sempre hi ha algú disposat a donar-te un cop de mà. Que res surt a la primera i que cal perseverança. Ha estat un dels períodes més intensos i durs de la meua vida, però que sempre recordaré amb enyorança. Tot això no hagués estat possible sense el suport i l'ajuda de tota la gent de dins i fora del laboratori que m'ha acompanyat durant tot aquest trajecte.

Primer de tot, agraeixo a l'**Àngel Raya** per donar-me l'oportunitat de poder treballar al seu laboratori. Gràcies per obrir-me les portes al món del peix zebra i confiar que seria capaç d'aportar el meu granet de sorra a l'estudi de la regeneració.

També gràcies a totes les persones que han col·laborat amb el projecte d'aquesta tesi o amb les qui he establert col·laboracions per altres projectes. Al **Francesc Canals**, agraeixo la paciència que ha tingut per ensenyar-me la base per analitzar dades de proteòmica. Gràcies al **Daniel Navajas** i a l'**Ignasi Jorba** per les mesures a l'AFM i les presses que els he demanat els últims moments. Al **Jose Luis Mosquera**, bioinformàtic de l'IDIBELL, amb qui he coincidit poc, però que ha aportat molt a la meua tesi, que m'ha fet considerar que en tot laboratori cal la presència d'un bioinformàtic. Ha estat un privilegi conèixer una persona amb tanta passió per la ciència. I també a la **Marina** amb

qui he vist totes les filigranes que es poden arribar a fer amb explants d'epicardi i que m'han portat tantes visites al IBEC amb "peixolins".

En especial a les *fish girls*, amb qui he compartit molts bons moments, molts somriures i maldecaps amb el peix zebra, animal que totes hem estimat i odiat a la vegada. Gràcies Cristina, Isil i Senda. **Isil**, tu has sigut com la meva germana gran, qui m'ha ensenyat els trucs de com treballar amb el peix zebra, la meva precursora, i alhora una bellíssima amiga. **Cristina**, una ajuda brutal, i a qui he vist créixer més al laboratori, fent-se expertíssima en *zebrafish*. Ara que ja no estic al laboratori, el *lab* deu estar més tranquils sense les nostres converses... ;) Gràcies per tot! I **Senda**, a tu no sé com agrair-t'ho tot. M'has ensenyat tot el que saps (o la petita part que he pogut absorbir), per ser el meu pilar al laboratori, per ser la meva mentora i una mà estesa quan he tingut dificultats, la meva "solucionadora" de problemes. Per ensenyar-me que la biologia molecular "mola" i és com fer màgia (i a vegades una mica frustrant). Sense tu ho hagués tingut tot molt més difícil.

A tots els que han passat pel laboratori de *stem cell potency* de l'IBEC i pel CMRB. De l'IBEC especialment a la **Claudia**, el **Juan**, el **Juanlu**, el **Marcel**, l'**Adriana**, l'**América**. I Claudia, gràcies per les classes de ioga i la teva capacitat per aconseguir que la gent en gaudeixi. I de la darrera etapa al CMRB, agrair als companys que han fet possible que les estones passades al laboratori hagin sigut menys feixugues. Gràcies **Mario**, **Julio**, **Rubén**, **Raquel**, **Yvonne**, **Yannis**, **Olalla**, **Karine**, **Eva**, **Mònica**, **Meritxell** i **Alessandra**. *Yvonne gracias por toda la ayuda y seguro que seguiré acudiendo a ti cuando necesite cualquier gadget. Siempre has encontrado alguna cosa que se adaptaba a las necesidades que tenía en el momento oportuno.*

Als **antoneles**, amb qui també hem compartit molts moments a part dels del laboratori, especialment a l'**Antonella**, el **Roger**, el **Carles**, la **Carla**, l'**Irene**, la **Francesca**, l'**Armida**, l'**Angie**, la **Julia**, la **Neus**, la **Meritxell** i el **Lucas**.

A les plataformes del CMRB, sense la seva experiència no hagués pogut avançar la investigació ni la meitat que ho he fet. En especial a la **Lola**, el **Jose** i la **Carme Casal**. Gràcies per tot el suport, tota l'ajuda i la paciència, sobretot en aquesta darrera etapa. Mai heu tingut un no per resposta, tot i la meva insistència i persistència sense fi.

Vull agrair a les persones que treballen a l'administració del CMRB, i en especial a la **Maria**, per respondre sempre a la meva pregunta persistent: *tiene algun hueco Ángel?*. A l'**Ester**, recent arribada al CMRB però coneguda des del principi, gràcies per ser la meva consciència i ser el corcò que m'ha empès perquè anés escrivint la tesi els últims mesos.

A l'**Elisa**, estudiant d'Erasmus a qui he tingut el plaer de fer de mentora. *You have been those hands that I needed when I most needed them. Thank you for your passion for science and your effort to do things efficiently. Thank you for everything.*

Gràcies també als amics biòlegs de la "uni", amb qui he viscut molts vermutos, grans moments i compartit l'experiència de fer una tesi, gràcies **Esther**, **Iñaki**, **Xabi**, **Sandra**, **Pablo**, **Laura Luque**, **Helena**, **Irene**, **Laura Gaspa** i **Anna Mercé**. En especial, gràcies a la Irene que ha dissenyat i fet realitat la portada d'aquesta tesi. Gràcies pel teu entusiasme i creativitat vers a projectes que combinen art i ciència

Per acabar, agrair el suport als meus admiradors més incondicionals. Als meus pares, la **Marta** i el **Romà**. Gràcies per donar-me força i ensenyar-me que amb perseverança tot es pot aconseguir per més difícil que sembli. També a la meva germana **Clara**, per ser tan bondadosa i oferir-me la seva ajuda incondicional. I per últim, **Carlos**, Gràcies! Has sigut el meu pilar diari i, de fet, qui m'ha acompanyat al llarg de tot aquest viatge, i m'ha ajudat a créixer. Sense el teu suport i la teva confiança tot això no hagués estat possible. Mai podré agrair-te tot el que has fet per mi.

Març de 2019  
Universitat de Barcelona



UNIVERSITAT DE  
BARCELONA

CMR[B]<sup>U</sup>